2016-01-01

Improving The Engineering Properties Of Pla For 3d Printing And Beyond

Carmen R. Rocha
University of Texas at El Paso, carmenrochag@gmail.com

IMPROVING THE ENGINEERING PROPERTIES OF PLA FOR 3D PRINTING AND BEYOND

CARMEN RAQUEL ROCHA GUTIERREZ,

Doctoral Program in Materials Science and Engineering

APPROVED:

David A. Roberson, Ph.D., Chair

Jose Nuñez, Ph.D.

Cristian Botez, Ph.D.

Stephen Stafford, Ph.D.

Charles Ambler, Ph.D.
Dean of the Graduate School

DEDICATION

To God who always gave me the strength to achieve my goals

My humble effort I dedicate to my sweet and loving

Mother

A strong and gentle soul the reason and inspiration of pursuing all those dreams in life

My Father

For earning an honest living for us for supporting and encouraging me to believe in myself and who has been a constant source of knowledge and inspiration

Thanks dear parents for your great support and continuous care

My family

Whose affection, help, love, encouragement and prayers make me be able to success

My friends

The right people that God send me through this path when I need them for guidance

"No one who achieves success does so without the help of others. The wise and confident acknowledge this help with gratitude". Alfred North Withehead

IMPROVING THE ENGINEERING PROPERTIES OF PLA FOR 3D PRINTING AND BEYOND

by

CARMEN RAQUEL ROCHA GUTIERREZ

METALURGICAL AND MATERIALS ENGINEERING MS

CHEMISTRY BS

DISSERTATION

Presented to the Faculty of the Graduate School of

The University of Texas at El Paso

in Partial Fulfillment

of the Requirements

for the Degree of

DOCTOR OF PHILOSOPHY

Materials Science and Engineering

THE UNIVERSITY OF TEXAS AT EL PASO

May 2016

ACKNOWLEDGEMENTS

This dissertation could not have been completed without the great support that I have received from so many people over the years.

Firstly, I would like to sincerely thank Dr. David Roberson for his advice, guidance, understanding, and patience and for his effort and participation in this project. Providing founding for the last several years of my studies was truly helpful but I am far more grateful for his mentorship which was vital in providing a well-rounded experience consistent to my long-term career goals.

I am grateful to Dr. Stafford, for his hands on help on my last Chapter of this dissertation work, Dr. Stafford thank you for your assistance and for sharing your facilities, for you hard work, without your help the last chapter of this dissertation would not be possible.

I am grateful to Dr. Nuñez and Dr. Botez, members of my doctoral committee for their accessibility, guidance, and thank you for keeping your office door open and available for all the times when I needed it.

Dozens of people have helped and taught me immensely at UTEP. Special thanks to my friend Alma Duarte when I had struggled in school and felt stuck in learning in different areas and in a different language, you always help me with your best attitude beyond all your personal problems. We have collaborated on multidisciplinary research, discussed politics and philosophies, religion and shared more than a few beer and wine bottles. To my friend Cesar Terrazas for his guidance and patience for believing in my skills and for his continuous encouragement for his availability for assist me and help me to join to the great community of the W.M Keck Center at UTEP. Brenda Torres you have been a guide and friend for me throughout graduate school, and I would not be here without your help.

Special thanks to all of the members of the Materials Extrusion Lab group, specially Angel Torrado, for his valuable help, for sharing all his knowledge with me, for always being able to help, even when he had his own projects and for is valuable friendship. I would also like to thank Adriana Ramirez for her valuable help and for always being a positive soul in the Polymers Lab. Additionally, I am very grateful for the friendship and help of all of the members of the extrusion research lab Gil Siqueiros, Francisco Andrade and Kevin Schnittker for their friendship and assistance in all the projects in which we have participated, for their availability and commitment.

My deepest gratitude to Nubia Zuverza for being always there for me and for sharing her plastic and life experience, you have become a very special friend to me, for all the conversations, advices, friendship, and fun that we have shared. Thank you Nubia for your help and for taking care of my health when I needed you the most.

To Karina Diaz and Isabel Morales I have always been able to turn to you when I have needed a listening ear, a dissenting opinion, or someone to provide me food. You two are great friends and one of my keys to success. Isabel thank you for your time in reviewing my work and for being my free therapist.

I thank my boyfriend Francisco for his enormous patience for his friendship, for helping me during this path, for always being supportive, for giving psychological and professional advice when I most needed it, for the great conversations and sometimes for taking the responsibility of leading with a graduate woman angry student. Our relationship was strong before, and I hope it will continue to be as strong in the future.

To my friends from Chihuahua who always have been supportive in all possible ways, for your great companionship through difficult times and for always being interested in my studies even though they don’t have any idea of what I was actually doing.

Lastly but most important, I would like to thank my sisters and my parents for all the support and for believing in me. To my Dad who is my academic and personal inspiration you have

encouraged my academic interests from day one, for always supporting me economically and mentally for your unconditional love. Thank you! Gracias papa porque siempre me has impulsado a salir adelante, gracias por toda la ayuda que me has brindado, por ser ese incondicional y amoroso padre. Eres mi ejemplo a seguir, gracias por darme la libertad de ser quien soy y sobre todo por el mejor regalo que me has dado mi mejor amigo y mi mejor compañero mi Coco.

To my mom you are the sunshine of my life. Mamá no existe una mejor amiga que tú, gracias por siempre estar a mi lado, por ser esa luz que ilumina mis pasos, por ser mi mejor consejera, mi mayor cómplice y mi mayor inspiración, por siempre tener la palabra correcta para sanar mi corazón. Dios me premio con unos padres como ustedes, les debo todo lo que soy, muchas gracias.

To my sisters, Elsa and Betty, I have always appreciated the path that you have blazed before me. They are witnesses of my many uncertain moments and constant challenges through this path. Elsa gracias por ser esa incondicional hermana, con la que puedo sentirme segura y protegida, gracias por tus consejos y también por tus regaños, gracias por siempre querer lo mejor para mí y por hacerme sentir tan especial. Betty agradezco que me hayas ayudado y aceptado en tu casa para seguir mis sueños, agradezco tu buen desempeño en UTEP y tu dedicación; me han abierto muchas puertas, agradezco que Noé y tú me hayan abierto las puertas de su casa y que me hayan guiado durante mis inicios en UTEP. Gracias Noé por tu incondicional ayuda durante mis semestres más difíciles en UTEP.

To my nephew's thank you for all the fun, for making me forget about all my responsibilities and make me feel like a child and joy and for your unconditional love.

While I have said the same for others in this list, it is literally true that this dissertation could not have been completed without your participation. Thank you. To anyone that may I have forgotten. I apologize. Thank you as well.

I deeply express my gratitude to my founding sponsors: The Mexican National Council for Science and Technology CONACYT for financing my PhD grade through the scholarship Gobierno

del Estado de Chihuahua- CONACYT 2014. The UTEP ORSP, The department of Metallurgical, Materials and Engineering, the air force of scientific research and the UTEP graduate school.

TABLE OF CONTENTS

LIST OF TABLES

LIST OF FIGURES

CHAPTER 1: INTRODUCTION

1.1. Statement of the problem

Additive manufacturing (AM), now more commonly known as 3D printing, has been classified as efficient, fast, and practical in the prototyping sector of product development. In the work presented here, we will use one of the AM techniques known as Material extrusion 3D printing (ME3DP), which has all the advantages of AM. In ME3DP the material is deposited in successive thin layers on top of each other until a 3D solid object is created. However, one of the biggest challenges facing ME3DP technologies is the limitation of the range of materials used by this technique. Acrylonitrile butadiene styrene (ABS) and poly-lactic acid (PLA) are currently the most common thermoplastics materials used in ME3DP because of their ability to melt and be reprocessed. PLA is rapidly becoming the most widely used material among users of desktop-grade material extrusion 3D printers, due to the perceived health hazards of ABS [1] and the fact that PLA is a biopolymer. PLA is a biodegradable polymer derived from renewable sources such as corn, and sugarcane [2]. The expanded use of this polymer over traditional petroleum-based plastics (ABS) will decrease the demand on petrochemicals, and also lead to less non-biodegradable polymeric waste [3]. While PLA offers an eco-friendly solution for polymeric 3D printing, the mechanical performance is limited by PLA's inherent characteristics (such as moisture absorbance) that may degrade the plastic during processing. PLA novel systems were used through this research maintaining the compatibility with material extrusion 3D printers. The purpose of this investigation is to alter the physical properties of PLA with sustainable additives in order to improve the end use products from this material. Moisture tests were also performed in some of the material systems, to obtain a better understanding of how the mechanical performance of the matrix PLA and the selected materials systems are affected by external moisture conditions. Moreover, a crystalline study was performed in order to understand how the material chain structure interferes in the biodegradability of the material, the possible influences of the additives on the degradation rate of the matrix material

and in to the materials systems and an analysis of the final mechanical and physical properties of PLA and other selected systems after different compostable conditions.

1.2. Background

In 1984 Charles Hull, invented the technology of stereolithography (SL) whose principle was the creation of three- dimensional solids objects by building thin layers of a liquid monomer creating a solid polymer using a laser causing covalent cross-linking at the surface of the photopolymer through a STL file. Hull consolidated a patent collection covering many fundamental aspects of today's additive manufacturing technologies in which the process currently includes 3D printing[4]. The AM process starts with the design of the object using 3D modeling software (Computer Aided Design or CAD), and then the model is generated through a stereolithography file format (STL). This file is processed again with AM software incorporated to an AM machine, which is able to read the CAD file. During these step parameters such as layers, temperatures, diameters, and patterns can be selected to build the layering material until the 3D object is obtained [1]. The technology allows for highly complex structures; it provides a high degree of design freedom. Also, AM or 3D printing industry has been classified as a fast, efficient, and easy technique [2]. The notable growth in additive manufacturing techniques has been made possible by the creation of powerful tools such as 3D printing machines. Additive manufacturing can be classified in different system technologies, discussed on following Table 1.1.

Table 1.1 Additive manufacturing technologies [1]

Classification	Technology	Description	Materials
Binder Jetting	3D Printing Ink-jetting S-Print M-Print	Creates objects by depositing a binding agent to join powdered material.	Metal, Polymer, Ceramic
Direct Energy Deposition	Direct Metal Deposition Laser Deposition Laser Consolidation Electron Beam Direct Melting	Builds parts by using focused thermal energy to fuse materials as they are deposited on a substrate.	Metal: Powder and wire
Material Extrusion	Fused Deposition Modeling	Creates objects by dispensing material through a nozzle to build layers.	Polymer
Material Jetting	Polyjet Ink-jetting Thermojet	Builds parts by depositing small droplets of build material, which are then cured by exposure to light.	Photopolymer, Wax
Powder Bed Fusion	Direct Metal Laser Sintering Selective Lase Melting Electron Beam Melting Selective Laser Sintering	Creates objects by using thermal energy to fuse regions of a powder bed.	Metal, Polymer, Ceramic
Sheet Lamination	Ultrasonic Consolidation Laminated Object Manufacture	Builds a part by trimming sheets of material and binding them together in layers.	Hybrids, Metallic, Ceramic
VAT Photopolymerisation	Stereolithography Digital Light Processing	Builds parts by using light to selectively cure layers of material in a vat of photopolymer	Photopolymer, Ceramic

Additive manufacturing (AM), currently more commonly known as 3D printing, is a process in which a material is deposited in a layer-by-layer manner in the creation of a solid object. The process of 3D printing consists on digital data converted into something tangible by using different techniques and different materials Table 1.1. In the case of Materials Extrusion 3D printing the material or “ink” can be plastic, metal or ceramic [5]. In 2012, 3D printing was predicted to be a profitable area in several markets including industrial manufacturing, the biomedical sector, entrepreneurs, designers and artists wishing to create more complex and high- tech products. The 3D printing industry has had an annual growth rate of 19.9% from 2013 to 2018 [6].

Besides household applications, the emerging demands of these new materials cover a wide range of industry sectors, such as coatings, adhesives, electronics, energy (photovoltaic), aerospace and medical devices (where polymer blends provide innovations in biocompatible materials) [7].

Currently, the most commonly used 3D printing technique is material extrusion 3D printing (ME3DP) which uses a polymeric monofilament in the creation of 3D objects. The process is described in Figure 1.1 below:

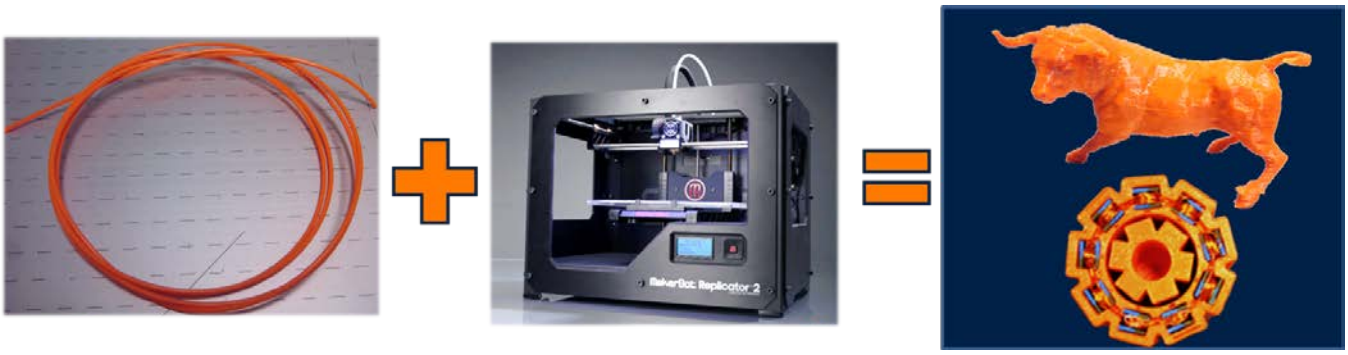

Figure 1.1 Material extrusion based 3D printers use a polymer filament as “ink” to 3D printing objects

1.3. Additive Manufacturing

1.3.1. Materials Extrusion additive manufacturing

Material extrusion 3D printing process (ME3DP) also known as fused deposition modeling (FDM) was developed by S. Scott Crump in the late 1980s and was commercialized by Stratasys [1]. The process consists of the extrusion of thermoplastic through a nozzle to form layers; every time a layer is fully printed, the printer platform is lowered as shown in (Figure 1.2.) This sophisticated technique has allowed users and companies to create any solid objects from a variety of different digital models without the risk of high investments in the actual creation of parts from bad designs. At the same time, any kind of objects will be easier to produce, repair or replace [2].

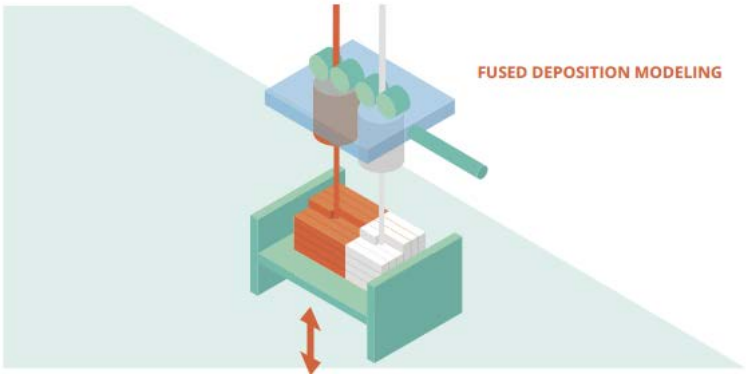

Figure 1.2 Material extrusion 3D printing (ME3DP) or FDM [2]

Recently, most people started to take advantage of the development of the 3D printing technologies, ME3DP has popularized and personalized approach to manufacturing, where the final solid objects can be personalized by the individualized specifications, that is now falling to the point where owning a personal 3D printer is affordable. As a result, the improvement of 3D printer materials has become a necessity, due to the fact that 3D printed objects are less durable than the ones that are traditional manufactured [8].

Many efforts have been done to improve the properties of the materials used in 3D printing, but these improvements are still limited by the strength of the thermoplastic used and the printing orientation. Parameters such as extrusion rate, extrusion temperatures, bed temperatures and sample geometries can be modified for strength improvement during 3D printing. During ME3DP is possible to select the infill density of the desired part, which is the plastic to air ratio. The most common infill percentages for ME3DP are 35 and 100%. When using an infill percentage, a pattern is used to create the desirable strength on the fabricated part. Varying combinations of infill percentage and pattern can influence in parameters such as strength, material used and printing times of the fabricated part [1, 9].

During last decade materials technologies in plastics have been playing a prominent role in the 3D printing industry; plastics commonly used in 3D printing have been growing significantly to widen the range of thermoplastics materials used for this technique as well as the improvement of the materials currently in use. Polymer composite materials and blends can be considered as an option to improve the mechanical, physical and chemical properties of the common substrates used in 3D printing: Acrylonitrile Butadiene Styrene (ABS) and Poly-lactic Acid (PLA) [10].

1.4. Polymers

Many materials we use every day are made of polymers. Polymers are organic materials that can be described as long molecules comprising of repeating structural units. These units are well known as monomers and are connected mainly by covalent chemical bonds. Polymers are also

known as macromolecules, as their chemical properties depend on the size of the molecules that they are composed of, thus short molecular polymers are often weaker in strength [11].

Because of their atomic arrangement, they can be crystalline, amorphous or semi crystalline: Crystalline polymers (Figure 1.3 a) are those whose atomic arrangement is in a regular order this characteristic makes them strong, but also lowers their impact resistance. Amorphous polymers (Figure 1.3 b) are those, whose atomic arrangement are irregular, cannot have an orderly manner to form crystals, and in contrast to crystalline are softer polymers, but they present special toughness properties, such as the ability to twist without breaking. Semi crystalline polymers (Figure 1.3 c) are a mix of crystalline and amorphous polymers; they become low viscosity liquids when exposed to high temperatures, and are the largest group of commercial polymers because they can be strong as crystalline and flexible as amorphous. These provide shaping and molding flexibility provided their viscous liquid state at high temperatures [12].

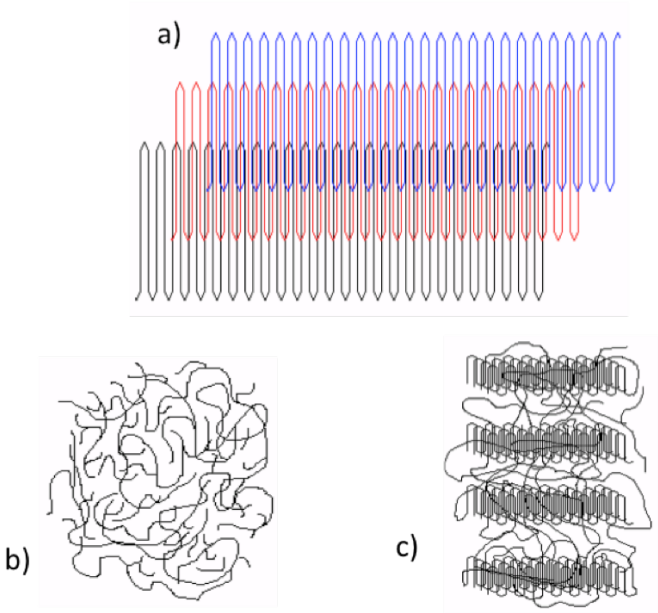

Figure 1.3 Polymer atomic arrangment [12]

It is thought ancient Mesoamericans were the first in the world to use polymers. Based on an article published by Andrady *et al*., 2009 [13]; Mesoamerican people utilized rubber as long as 1600

BC. Several investigations reveal that the Mesoamerican cultures were utilizing rubber and latex in sandal shoes, medicines and to create rubber balls for one of their most important rituals known as the Mesoamerican ballgame. The ancient cultures synthetized the rubber by taking the latex from Castilla elastic trees and mixing with varying concentration of alba vine juices.

The history of rubber usually begins in 1839 when Charles Goodyear discovered vulcanization, mixing sulfur with natural rubber and heating the mixture to a high temperatures resulting in a commercially product used for car tires. Later, in 1907 Leo Baekeland developed the first synthetic polymer known as Bakelite, this material is well recognized for its hardness and high resistivity and its non-conductive properties, for which it is commonly used for electrical components, and also acts as heat and chemical insulator [13, 14].

1.5. Plastics

Plastics are polymers, best defined as larger chains of “mers”. Mers or monomers are basic units commonly made of hydrogen, carbon, oxygen and/or silicon. These individual units are chemically joined together by: polymerization or condensation. Plastics are an important part of our modern society due to their promising properties such as chemical resistance, electrical and insulator properties, lightweight, high strength and highly processable design [15]. Examples of this are the automotive and aerospace industry, which have progressively replaced several metal pieces for plastic materials during the last decades, due to their lighter weight, cheaper price and similar properties that can withstand high temperatures and pressures [16].

Plastics can be divided into two classes: Thermoplastics (TM) and Thermosets (TS). Thermoplastics have high molecular weights, when increasing temperature, the intermolecular chains are weakening and the material tends to soften, this process can be repeated, with the plastic melting and solidifying as the temperature increases above and descents below the melt temperature, respectively. Yet, the material can be increasingly subject to deterioration, so there is a practical limit to the number of times that this reprocessing can take place before material properties undergo [15]. On the other hand, thermosets are described as network polymers that are heavily cross-linked.

Cross-links are formed by the polymerization of a liquid and a hardener; this will make a permanently amorphous structure. Thermosets have properties such as: high thermal stability, high rigidity, high dimensional stability, and lightweight. In addition, they are very resistant to creep and deformation under certain load, and they provide high electrical and thermal insulating properties [17].

1.5.1. Plastics in society

Plastics offer products with handy properties such as good chemical resistance, lightness, and low price, flexibility in thermal and mechanical properties, durability and easy processability. The diversity of polymers and the versatility are used to make an immense amount of products; they have helped to improved technology and replace materials such as metal, ceramic, paper, glass and wood [18].

Plastic production has expanded by approximately 6.8 percent in 2014 compared to the previous year according to a recent data released by the Federal Reserve Board published in Plastics News. This production increment has not only occurred during the last two years, but it has increased since 1993-94. According to the author's prediction, 2015 has been the year with the second highest demand on plastics[19]. Moreover, predictions revealed that the industry of plastics would be increasing in areas such as construction, automotive, electrical and electronics. It is expected that in 2022 the electronic sector will be continuing growing until become the number #1 market consumer sector of plastic industry just in the U.S [20].

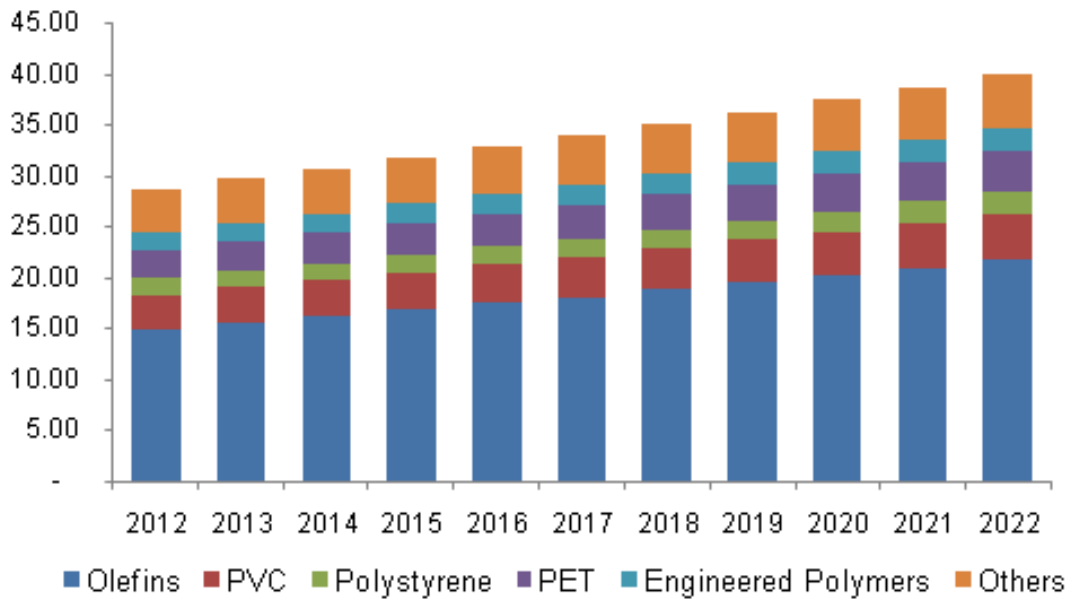

Figure 1.4 U.S Plastic compounding market volume by product in million tons (2012-2022) [20]

Plastics are highly used in all areas of modern society in applications such as biomedical, food packing, automotive, 3D printing, and cosmetics among others [2]. Car industry has been extensively benefited from plastic industry. The transportation industry has been one of the most benefited by plastics. Weight savings accomplished through the use of plastic parts have save fuel consumption over the metal motors; meanwhile the amounts of CO_2 have been reduced due to this light weighting. Textile fibers (nylon, polyester and acrylic), footwear (reducing food waste and prolonging the life of food), communications (disposable cellphones and computer parts), medical technology, cameras, jeweler, high tech and everyday objects have been benefited and improved by plastic materials. Being the packing sector the most demanded industry. However, problems have been arising due to the fact that large quantities of plastics end as waste in the environment and that plastics are commonly petroleum based and not reusable, this ends on pollution and depletion of non-renewable resources [21].

The production and consumption of plastics differs significantly based on the geographic area of each country and their accessibility to the necessary natural resources (Figure 1.5). Plastics contribute the consumption of non-renewable fossil fuels; the production of plastics uses 8% of the

world's oil production where 4% is used as feedstock and 4% during manufacture [22]. On the other hand, plastics are very useful materials that last for a long time. Though, they are usually used once and disposed very easily which ends on landfill producing ocean contamination.

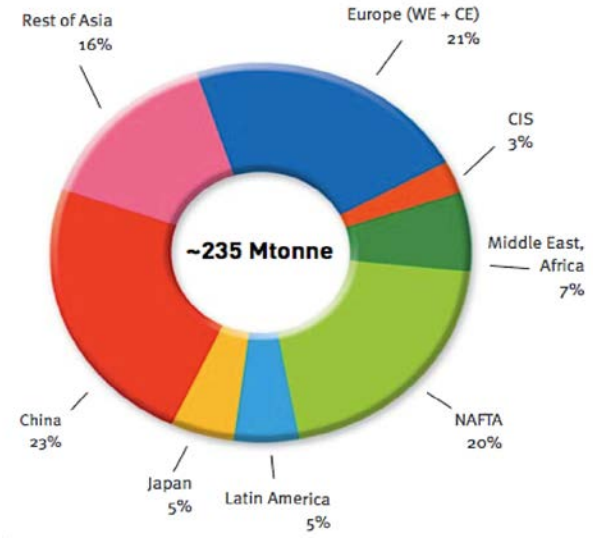

Figure 1.5 World Plastic Production 2011 [23]

1.5.2. Plastics the environment and human health

"One of the most universal and permanent recent changes to the surface of our planet is the accumulation and disintegration of plastics," marked David Barnes, principal author and researcher for The British Antarctic Survey. The report was published on 2009 in a subject issue of Philosophical Transactions of the Royal Society B, a scientific journal [24].

Since the last half-century, discarded synthetic plastics on the urban environment and a wide range of natural terrestrial and marine habitats have become a persistent problem. Plastic is a significant fraction of solid waste mainly composed of food packing and plastics tools that are discarded and replaced easily due to their low cost and lightweight. According to EPA reports around 12% of the municipal solid waste corresponds to household plastic materials such as polystyrene (PS), polypropylene (PP), polyvinyl chloride (PVC) and polyethylene (PE). Some of these materials

waste is readily recycled, while others are not good candidates due to their composition, as they are often obtained from polymer blends and not for the pure resin material [25].

During the disposal of plastics, certain portion is buried on landfills causing a dispersion of harmful chemicals that percolate into the groundwater. Additionally, many single-used plastic products and packaging materials, which account for approximately 50% of all plastics produces, are wrongly disposed of at or near the location where they end their usefulness to the consumer.

The incineration process on waste disposals is another disadvantage of the use of plastics for human health. When plastics are being incinerated they produce emissions of dioxins. Dioxins are insoluble and water and soluble in lipids, this condition allowed them to enter to human body; minimal expositions to these dioxins are crucial to several damaging to human and animal health. As a result, the toxicity of these dioxins can cause several diseases such as: cancer, malformations of fetus, liver damage, declined reproduction and contribute in mental behavioral alterations [26].

According to Plastics Europe, just in 2010 approximately 12 million tons of plastic waste was discarded into the oceans by countries with ocean coastlines. If we take into account that this huge amount of waste is discarded into the ocean each year and that the plastic production is increasing enormously every year we can estimate that up to 80 percent of the world´s marine pollution is plastic debris [27].

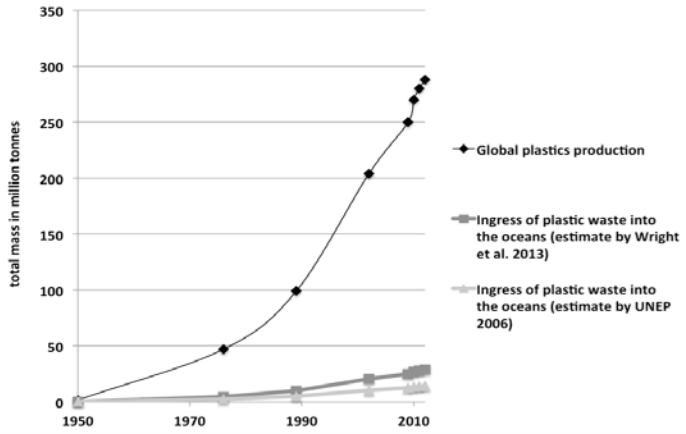

Figure 1.6 Global Plastic Production during 1950 to 2010 and approximate volume of discarded plastics into the oceans. Estimated in different years by different authors [28]

Plastic debris can be defined as persistent solid waste that affects marine environment; this material can float for thousands of years in water acting as transporting devices for invasive species causing a habitat disruption [25]. As a result of this debris accumulation two major ocean vortices have formed, they are better known as ¨garbage patches¨. These debris accumulations consist mostly of plastic materials with an approximate amount of 46, 000 pieces per square mile according to the United Nations Environmental Programme (UNEP).

The Great North Pacific Garbage Patch being the most popular was first revealed to the general public in 1997; and is composed of the Eastern Garbage Patch and the Western Garbage patch. The Eastern extends within the North Pacific subtropical (between California and Hawaii); the second is smaller and is located between Hawaii and Japan. Additionally, there are other waste accumulation sites in areas of the Indian Ocean and the Atlantic Ocean [29, 30].

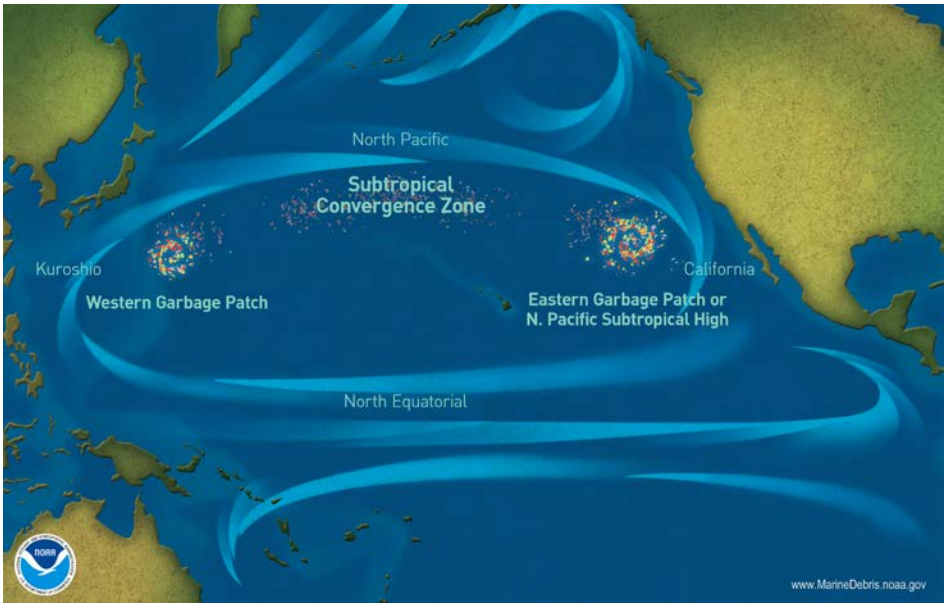

Figure 1.7 Map Marine debris [31]

Land and ocean animals have been the victims of this plastic disposal culture. Numerous marine animals have been harmed or even killed by mistakenly ingesting marine debris. Research conducted in 2006 reported at least 267 marine species have been affected worldwide including sea turtles, sea bird species and of all mammal species not to mention the huge amounts of fish and

crustacean species. Furthermore, plastic debris is affecting the ecosystem by blocking the amount of oxygen necessary for some deeper sea organisms. In addition, there have been assumptions related to the potential transfer toxic substances to the food chain, and subsequently to humans [27].

For these all-aforementioned problems, the work presented here is concerned with making a sustainable engineering polymer that can be reusable and can help to reduce environmental and health effects.

1.5.3. Environmental Alternative

The emergent environmental awareness of the accumulation and the impact of plastic debris in oceans and landfills and moreover the potential chemical impacts of plastic in the ocean have concerned many global organizations around the world to raise awareness of these problems and new rules and regulations are forcing the plastic industry to look for the development of more ecologically friendly plastic materials [32]. Successful management of the aforementioned problems will require the development and implementation of more ecologic plastic materials such as bio-based materials. According to the American Society for Testing and Materials (ASTM) a bio-based material is an organic material in which carbon is derived from renewable source via biological process. Bio-based materials include all plant and animal mass derived from CO_2 recently fixed via photosynthesis, per definition of a renewable resource [33]. The use of bio-plastics promises to be biodegradable, consequently removing those products from the waste stream and saving space in landfills [34]. The use of bio-plastics emerged since 1980. The first bio-plastic utilized was celluloid used for the substitution of ivory in billiards balls [2].

Crops such as corn and soybean have been gaining attraction as a source for sustainable bio-based materials, in order to prevent environmental problems using petroleum, which is the most common, and for typical plastics. Figure 1.8 depicts how different crops can be converted into intermediate chemical products by using different techniques such as gasification, pyrolysis, catalytic conversions, fermentations, extractions, enzymatic conversions among others, to obtain bio-based plastic materials [2].

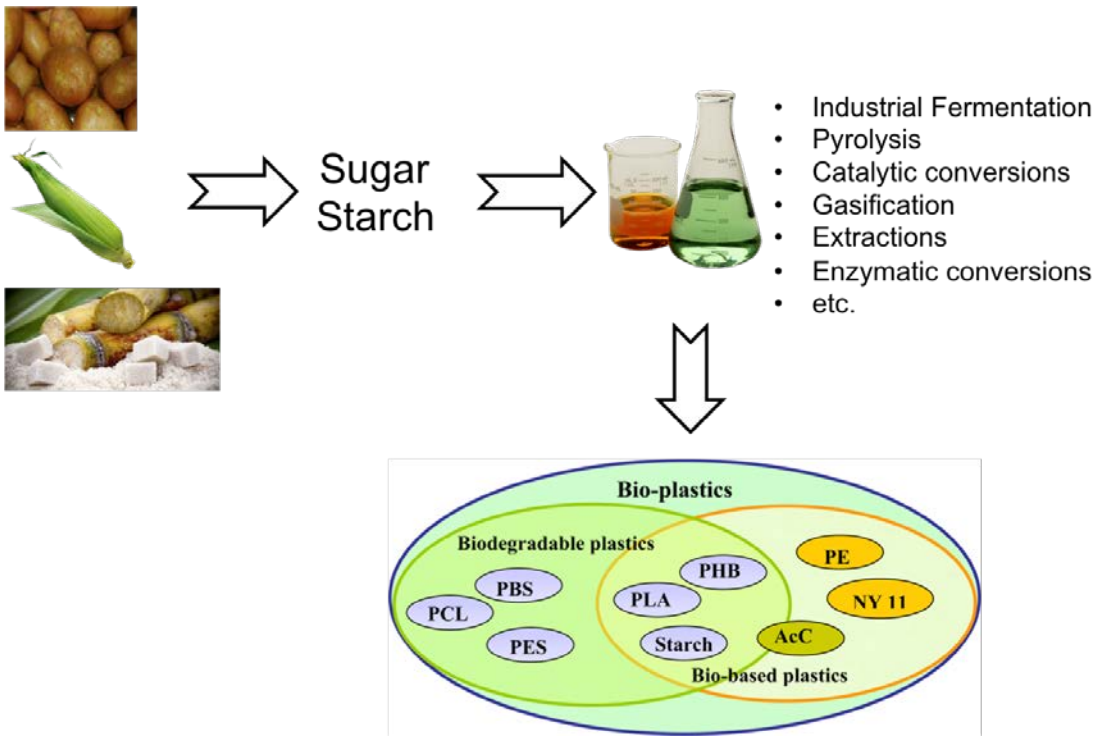

Figure 1.8 Crops to bio-based and bio-plastics conversion [2, 35]

The work presented here will focus on biodegradable and bio-based polymeric systems, it is important to note that not all biopolymers are biodegradable. For example, it is possible to produce polyethylene from corn-based ethanol sources. While the synthesis of polyethylene from a sustainable source decreases demand on fossil fuels, the result is still a non-biodegradable polymer.

Poly-lactic acid (PLA), Poly-hydroxyalkanoate (PHA) are the most common bio-based plastic materials known by researchers because of their potential contribution to sustainable materials development and for the potential to lower the environmental impact caused by conventional fossil-fuel based plastics [36]. In the field of 3D printing ABS and PLA are the most common materials used attributable to their promising properties [2]. PLA has experienced a rapid increase in its use in 3D printing applications particularly in the desktop grade market where several companies such as Maker-Bot Industries are now manufacturing printers specifically intended for the printing of this biopolymer.

1.6. Sustainable Materials for 3D printing

Scientists in the plastic research community are concerned about the negative impacts of the plastic materials on the environment as well as in human health. Therefore, plastic materials have been constant research subject. Various studies have noted that humans are exposed to chemicals daily, and that some are caused by plastic production. Chemicals derived from plastics end up in the human body via ingestion, inhalation or dermal absorption [37-41]. For instance, in the field of 3D printing researchers are exposed to different particles that are toxic during the thermal processing of thermoplastics while using materials such as ABS and PLA.

During the thermal decomposition of the ABS at high temperatures, gases such as carbon monoxide (CO) and hydrogen cyanide (HCN) as well as volatile organics are released. These chemicals have centered the attention of many health researchers into 3D printing community because of the high concentrations of these ultrafine particles that can lead to pulmonary health issues, cardiorespiratory mortality, hospital admission for stroke and asthma symptoms [42, 43]. A recent article published by Stephens *et al.*, [43] concluded that the toxicity among the use of ABS and PLA as well as the emission rate on 3D printing is different depending on the composition of both materials. For instance, the toxicity of ABS has been determined to be higher than the one of PLA, and this is due to the fact that PLA is a bio-based material.

1.6.1. Poly-lactic acid (PLA)

PLA is a linear aliphatic polyester biodegradable obtained from renewable sources such as corn, and sugarcane [1, 44]. Even though, PLA is a bio-based material the process to obtain it goes through a synthetic route [3]. There are two chemicals routes to convert lactic acid to high molecular PLA. One synthesis uses a continuous process and a novel distillation technology with no solvents involved. The second process, converts lactic acid directly to high molecular weight PLA by using solvents in an azeotropic chemical process. The chemical and physical properties of the final product such as biodegradability, crystallinity, and transparency are controlled by the copolymerization of L and D isomer ratios of lactic acid or lactide [45].

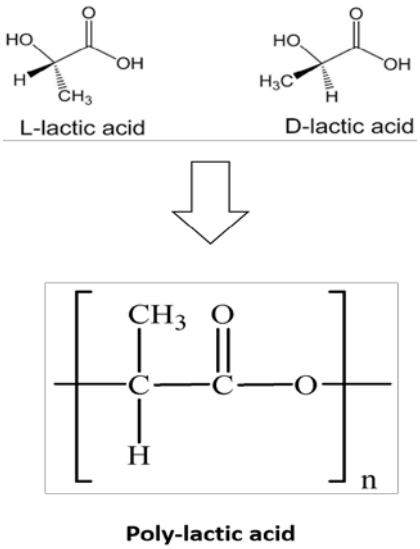

Figure 1.9 Conversion of L and D isomers into high molecular PLA [46]

The future use of this biopolymer over typical petroleum-based plastics will lessen the demand of fossil fuel based polymers as well it will lead less non-biodegradable polymeric solid waste and CO_2 emissions will be reducing [47]. Poly-lactic acid is considered the best biopolymer among the others known because of its mechanical properties such as good stiffness and strength, its recyclability, low toxicity, compostable with the environment and the fact when its produced from renewable resources the CO_2 emissions are eradicated. However, PLA suffers from moisture susceptibility, which contributes to the degradation of the material and reduction of its impact resistance. To improve these undesirable properties many efforts have been made to modify this biomaterial, by making composites, blends, copolymerization processes, plasticization and the use of additives that can optimize the material for particular use applications [3, 48].

PLA has been compared to the most common thermoplastic polymer; polyethylene terephthalate (PET) used in a huge variety of applications such as; plastic bottles, cosmetics holders, storages for cleaners and chemicals, plastic bags, frozen good packing among others [49]. Both PLA and PET share optical, mechanical and physical characteristics (Figure 1.10). Although when compared to PET, the disadvantages of PLA disadvantages arise with brittleness, lower resistance temperatures and higher gas permeability. On the other hand, studies on PET have reported the

presence of inorganic species such as antimony (Sb), traces of metals such as Cobalt (Co), Chromium (Cr), Iron (Fe) and Manganese (Mn) [50].

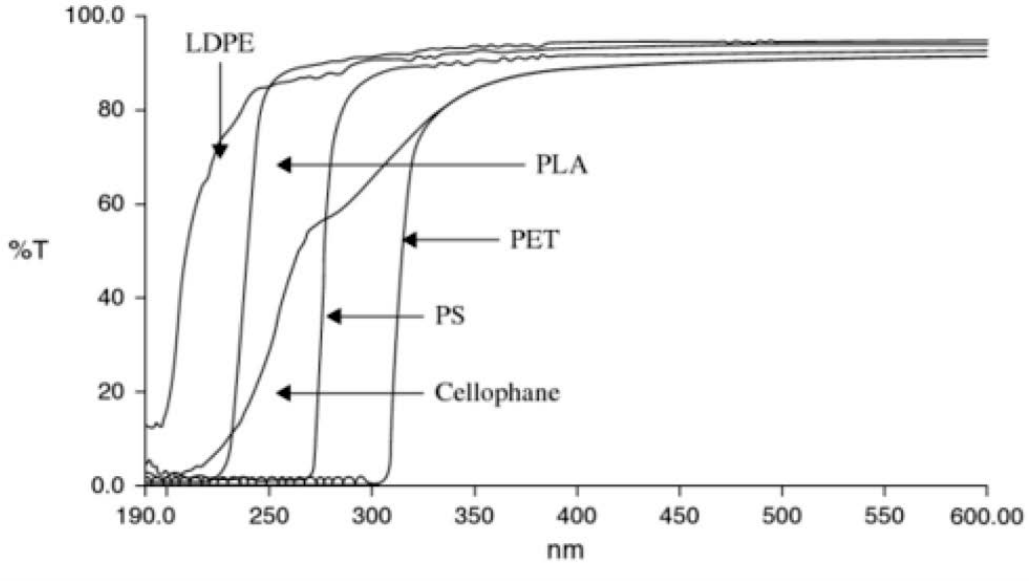

Figure 1.10 Graph comparing the optical properties of some polymers materials [51]

Also the presence of carbonyl compounds such as formaldehyde and acetaldehyde have been reported during the thermo-mechanical and thermo-oxidative degradation of this material. Because of these undesirable properties food- contact packing using PET is strictly regulated. However, according to analytical investigations made by Cristina *et al.*, [50] despite these safety regulations, during the decomposition of PET several toxic chemicals are released produced by the initial reactants and additives [3, 50].

The importance of using PLA has been the center of attention for many plastic industry companies who desire to provide products of improved quality that protect the environment and human health. For this reason, PLA can be used for future developments in biomaterials for 3D printing. Bio-blends can provide a wide range of applications with better properties such as higher stability, giving a whole range of new application and products. As a result, PLA can be modified and adjusted to achieve the desired properties for different industries [2].

In the following image Figure 1.11 different plastics are shown in a pyramid shape. From the top of the peak representing the most dangerous and not eco-friendly plastics can be observed, decreasing to the bottom in terms of hazards such as toxicity, chemical composition and recyclability being the bio-based polymers the most desirable materials [21].

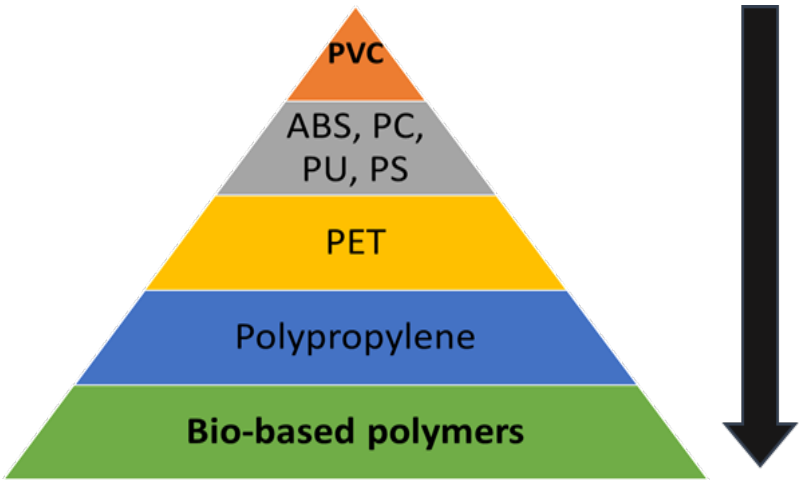

Figure 1.11 Plastic hazardous pyramid [21]

CHAPTER 2: SIGNIFANCE OF STUDY

2.1. Problem statement:

While PLA offers an eco-friendly solution for polymeric 3D printing, the plastic performance is limited by PLA's inherent characteristics (such as moisture absorbance) that may degrade the plastic during processing. There is a huge need to create technology more environmentally sustainable as well as the usage of ME3DP. Overcoming this barrier, the amount of new polymeric material needed by the manufacturing method will be significantly reduced by providing a clear route towards the environmental sustainability of ME3DP.

2.2. Research Goals:

In order to achieve this, novel composite material systems based on PLA will be created with sustainable additives in order to improve the end use products from this material. At the same time a wider range of environmentally sustainable materials would be developed for the ME3DP industry.

- Alter the physical properties of PLA with sustainable additives in order to improve the end use products from this material
- Maintain compatibility with material extrusion 3D printers
- Test the biodegradability of the PLA matrix and the created systems

2.3. The outcomes of this project will:

- Lead to a wider range of materials compatible with material extrusion 3D printing
- Lead to the development of a new class of engineering biopolymers
- Decrease the environmental impact of 3D printing and polymeric materials
- Provide new materials for the 3D printing community avoiding the hazardous fumes that other material such ABS produce

2.4. Research Questions:

- What will be the effect of the fillers recorded on Table 2.1 on the physical properties of PLA?
- Will PLA biodegradability be maintained after the inclusion of additives?
- Which of the created systems will help to improve the mechanical, physical and biodegradable properties of the PLA material?

Table 2.1 Material and filler loadings

Materials	Matrix (wt%)	Filler (wt%)
PLA	400	0
PLA/ SALT 5% NO MILL	400	20
PLA/ SALT 5%	400	40
PLA/ SALT 10%	400	60
PLA/ SALT 15%	400	80
PLA/ SALT 20%	400	20
PLA/ MgCl2	400	20
PLA/BPO4 5%	400	20
PLA/MAYAN YELLOW	400	20
PLA MAYAN BLUE	400	20
PLA/JUTE FIBER 5%	400	20
PLA/ JUTE FIBER FUNCT. W SALT	400	20
PLA/ JUTE FIBER FUNCT. W CHEM SILANE	400	20
PLA- CARBON JUTE FIBER 5%	400	20
PLA/FUNCT.JF W SALT/ MYW 2.5%	400	10
PLA/FUNCT.JF W SALT/ MB 2.5%	400	10

As mentioned before, there are two “great garbage patches” [52-54]: one in the Atlantic Ocean, and the other one in the Pacific Ocean. On every surface of the Earth we can find plastic refuse [55-58]. This is a clear example of the importance for reducing the amount of material type most people use and discard. Additionally, humanity is currently residing on a layer of plastic waste of what is called the “Anthroprocene” geological period.

As an illustrative example we can analyze the large amount of plastic material discarded every time a toothbrush is used up, when the fibers end up their lifetime the hole plastic is thrown away, this ends as other source of plastic waste, other controversial easily disposable materials are straws. Just in America around 500 million of straws are produced every day in order to fulfill the demand of these products. This is the main reason why there is a big need of a model by which 3DP can operate as a sustainable manufacturing process. Awareness has been rising in the 3DP

community about the environmental impact of technology [59], but more effort is still needed in making 3DP more sustainable. Figure 2.1 illustrates discarded toothbrushes and straws and how easy the society discarded them creating a massive amount of polymeric waste.

Figure 2.1 The ease at which society discards polymeric materials presents a need that can be filled by making 3D printing more environmentally sustainable.

CHAPTER 3: METHODOLOGY OF RESEARCH

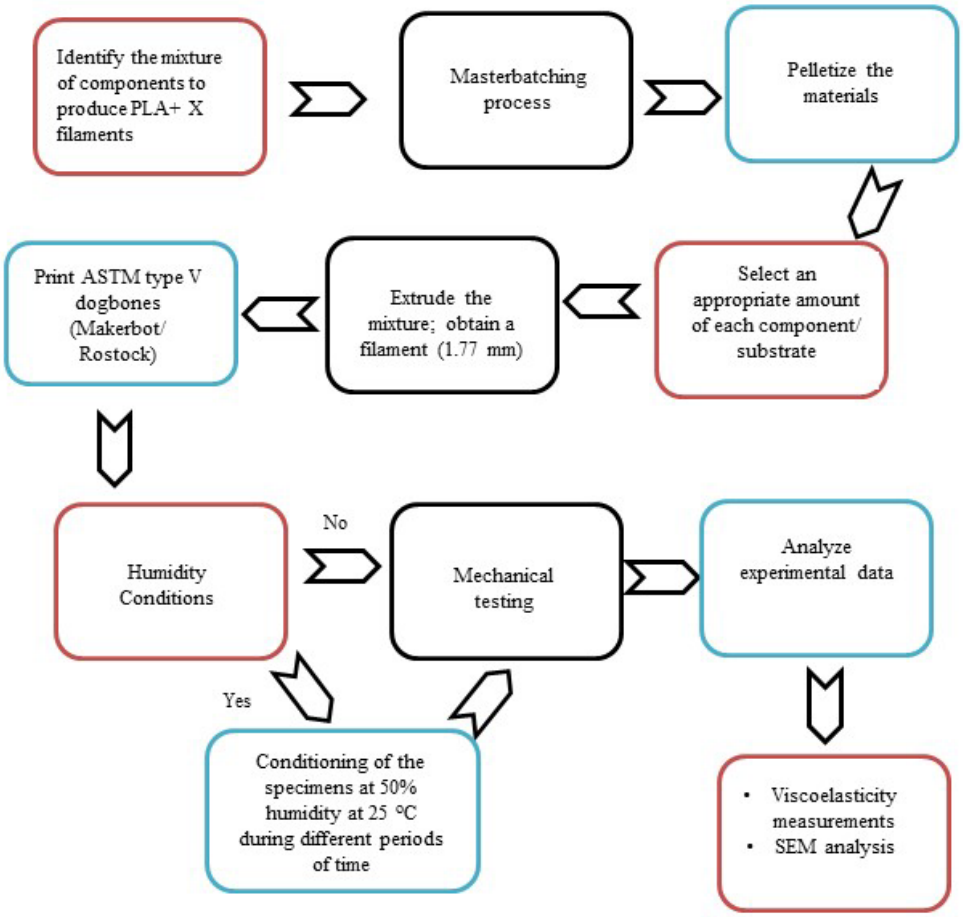

Figure 3.1 Methodology process proposed for the PLA systems

3.1. Selected materials

All materials used in this study will be sustainable/ biodegradable with the intent of imposing minimal environmental impact. The PLA used in this study was Ingeo Biopolymer 4043D PLA (NatureWorks LLC, Minnetonka, MN, USA). This particular grade has been recommended by NatureWorks as the grade to use for 3D printing applications. MayaCrom® Pigments (Mayan Pigments, Inc. El Paso, TX, USA) were also used in this study. These pigments are palygorskite-based pigments originally developed by the Mayan culture of Mesoamerica. The combination of these pigments with polymers such as high-density polyethylene (HDPE) has shown an increase in strength [60]. The sodium chloride (NaCl) was an analytical grade acquired from Sigma- Aldrich.

The Jute Fiber used was obtained from recycled rope originally purchased at Home Depot. The Boron Phosphate (BPO_4) used on these first experiments, was donated from a project previously developed by Dr. Arrowood´s. All the filler materials were incorporated in a 5 wt. % to the baseline material (PLA). Before processing PLA was dried in vacuum oven (80 ºC for 4 hours) while the master batched materials were dried in air circulating oven for 4 hours at 80 ºC.

3.2. Master batching Process

The master batching process consists on the creation of "material sandwiches". The process starts with the creation of PLA sheet films with the help of a hot press. Once the sheet-films of the pure material are ready the filler/fiber is placed in the middle of two films and sealed under temperature and pressure creating the "sandwich". This process was repeated until the material and the filler had a homogenous appearance. The advantage of this process is that the material is partially premixed prior to performing the extrusion process. In this case, the material was melted at a temperature of 180 ^{o} C; the final product was a circular thin sheet. During the master batching for this investigation, several thin sheets of PLA were produced; the filler was then introduced in between two thin PLA sheets. Once the material was master batched the sandwiches were granulated and then diluted with virgin PLA pellets in a certain quantity according to calculations is selected in order to reach the desired weight percent filling. An example of the master batching process can be seen in Figure 3.2.

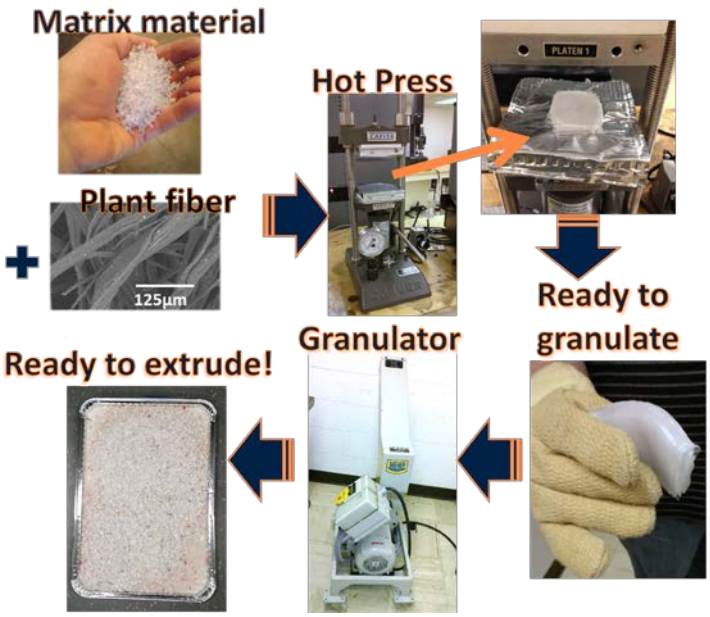

Figure 3.2 The master batching process used in this study.

3.3. Extrusion

The extrusion process was used to produce plastic filaments using a Dr. Collin-Twin-Screw Extruder/ Compounder Model ZK 25T. (Dr. Collin GmbH, Ebersberg, Germany). The extrusion process is critical to the application of 3D printing since robustness of the filament is critical to the printing process. Extrusion is a process in where materials from solid to liquid are comprised into a single component. Everything starts as pellets that are fed from a hopper into a jacketed screw. The screw starts turning on its axis transporting, melting, and pressurizing the material. Then, the material is forced through a die that will shape it into a wire with the desired diameter approximately 1.75 ± 0.05 mm. For this particular research, the filler/fiber materials content was 5 wt. % for all the PLA systems. The final compounded materials were produce in order to be compatible with open source printers such as Maker Bot Replicator (Maker Bot Industries, Brooklyn, NY USA) material extrusion 3D Printer and Rostock Max 2 delta printer (See Me CNC, Goshen, IN). For this work the Rostock Max was primarily used. An example of the extrusion process used to make filaments is exhibited in Figure 3.3.

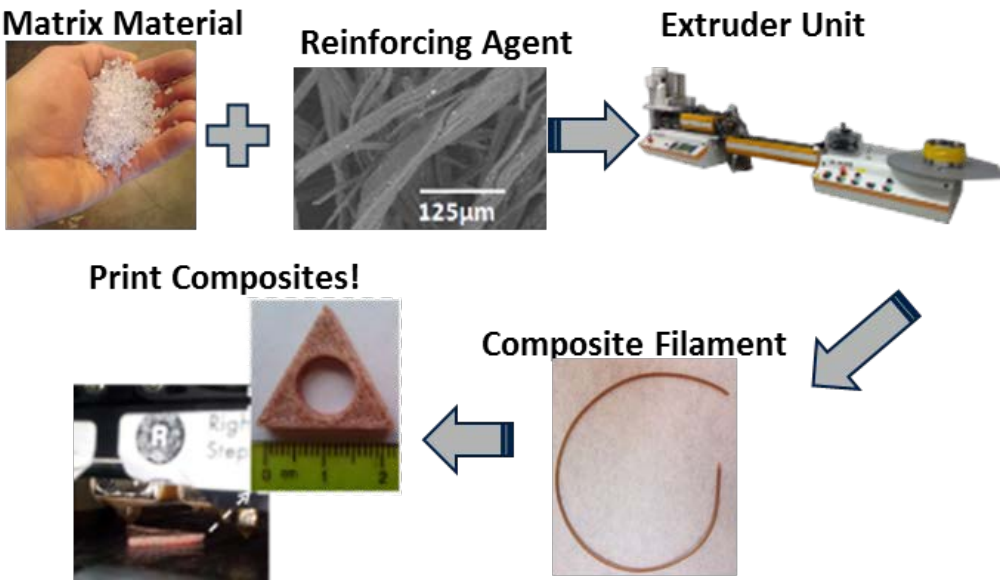

Figure 3.3 Process used to make filaments for 3D printing

The extrusion parameters used for all the PLA systems can be found in Table 3.1

Table 3.1 Extrusion parameters used for the PLA systems

Material	T Zone 1 (ºC)	T Zone 2 (ºC)	T Zone 3 (ºC)	T Zone 4 (ºC)	T Zone 5 (ºC)	Main Screw Speed (RPM)	Feed Screw Speed (% Main)	P Main Screw (bar)	Load (%)
PLA	180	180	182	182	187	32	100	80	72
PLA 5% MayanCrom® Yellow	145	145	142	140	147	35	100	105	72
PLA 5% Jute Fiber	180	180	185	180	185	40	53	90	63
PLA 5% Boron Phosphate	175	175	177	175	183	20	100	75	72
PLA 5% NaCl	180	180	177	180	183	74	40	70	60

3.4. Printing

For this study, the matrix material used was PLA, and the 3D printing process used was material extrusion 3D printing (ME3DP). Some of the parameters considered were: Infill %, layer height and infill pattern, printing directions, temperatures of extrusion and nozzle diameter, as these parameters play an important role on the final mechanical properties of the final fabricated part. Type V specimens were used as described by the American Society for Testing and Materials (ASTM) D638 standard. To verify commercial printability, these samples were printed with a

MakerBot Replicator for the PLA/ NaCl of the compounded materials. All other materials were printed in a Rostock Max 2 delta 3D printer following the parameters presented on Table 3.2 and Table 3.3. The printing directions of the dog-bone structures for this specific study were isotropic in the XYZ directions (Figure 3.4). The raster height of 0.4 mm and a raster width of 0.4 mm for all the blends except for the PLA/ NaCl blend using a 0.8 mm modified nozzle diameter.

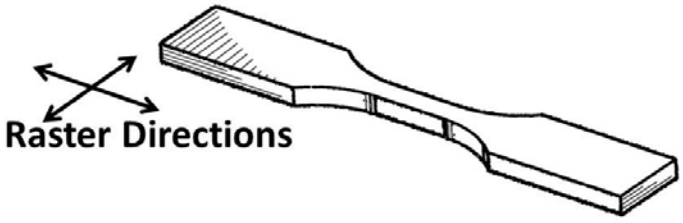

Figure 3.4 ASTM D638 Type V XZY printed directions [10]

Table 3.2 Printing parameters used for the PLA systems using a delta printer at 80ºC

	Object Infill (%)	Layer Height (mm)	Number of Shells	Feedrate (mm/s)	Travel Feedrate (mm/s)	Print Temperature (°C)	Filament Diameter (mm)	G-code Nozzle Diameter (mm)	Actual Nozzle Diameter (mm)	Raft
PLA	100	0.27	1	40	55	220	1.75	0.4	0.4	No
PLA 5% MayaCrom®Yellow	100	0.27	1	40	55	220	1.72	0.4	0.4	No
PLA 5% Jute Fiber	100	0.27	1	40	55	220	1.75	0.4	0.4	No
PLA 5% Boron Phosphate	100	0.27	1	40	55	220	1.77	0.4	0.4	No
PLA 5% NaCl	100	0.27	1	40	55	220	1.8	0.4	0.4	No

Table 3.3 Printing parameters used for one of PLA systems using MakerBot printer at 80 °C

Material	Object Infill (%)	Layer Height (mm)	Number of Shells	Feedrate (mm/s)	Travel Feedrate (mm/s)	Print Temperature (°C)	Filament Diameter (mm)	G-code Nozzle Diameter (mm)	Actual Nozzle Diameter (mm)	Raft
PLA 5% NaCl	100	0.27	1	40	55	220	1.8	0.6	0.8	No

3.5. Moisture analyses

Bio-plastics have gained attention for their contribution to the environment and desirable properties such as recyclability, negligible CO_2 emissions solid waste reduction in landfills and

oceans, reduction in energy fossil-fuel consumption, among other advantages. However, they tend to be hygroscopic materials, defined as the capability of a substance to attract and hold water molecules from the surrounding environment due to the interaction of the water molecules and the polymeric chains [61]. The physical and mechanical properties of bio-plastics are influenced by temperature and relative humidity causing problems such as material degradation, poor mechanical properties, viscosity and dimensional changes among others [62]. Hygroscopic behavior of the PLA systems was tested under moisture conditions established according to the standard procedure ASTM D618. Samples were exposed to 50% humidity at 25 ºC for 48, 96, 192 and 384 hours in a relative humidity chamber VWR model 2375B with the purpose of examine the moisture absorption of the PLA systems.

CHAPTER 4: PRELIMINARY RESULTS

Blends of PLA with the organic-based materials 1) sustainable pigments 2) salt 3) jute fiber and 4) Boron Phosphate have been prepared with the end goal of producing materials with altered mechanical and rheological properties that can be of great benefit to the 3D printing field while retaining the “green” nature of PLA. The reason for the use of 3D printing (3DP) as a test bed is twofold: 1) 3DP is gaining widespread adoption as a manufacturing method necessitating that a culture of environmental sustainability be instilled among users and 2) PLA is currently one of the most common materials used in 3DP meaning that adequate benchmarking exists to test the effects of our efforts.

4.1. Mechanical testing

The tensile testing was performed according to ASTM standard D638-10 using the Type V dimensions. The samples were printed using a Maker Bot Replicator (Maker Bot Industries, Brooklyn, NY) and a Rostock Max 2 type delta printer. Material extrusion test specimens were conditioned during different periods of time in a relative humidity chamber. Before and after different periods of time under moisture conditions previously established, the samples were subjected to loading using an Instron® 5866 (Instron, Norwood, MA) to test the mechanical properties of the different PLA systems. The resulting ultimate tensile strength (UTS) systems data are shown in Figure 4.1.

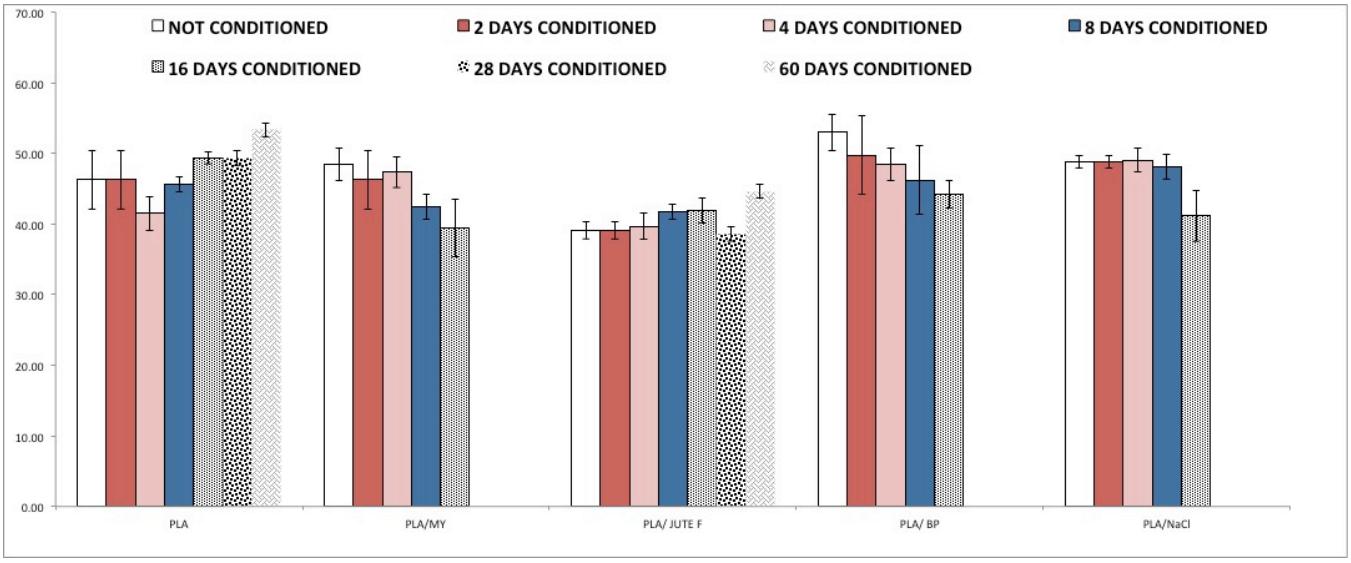

Figure 4.1 Tensile data of the five PLA systems with and without under humidity conditions (Not conditioned, 2, 4, 8, 16, 28 and 60 days conditioned).

The tensile test revealed that all the PLA materials systems with the exception of the PLA/ Jute Fiber blend result in a very small increase of the mechanical properties when are combined with the PLA matrix under non-moisture conditions. After the humidity treatment PLA/ Mayan Yellow, PLA/Boron Phosphate and PLA/NaCl systems showed a decreasing tendency of the UTS after certain period of time (16 days). On the other hand, an increasing tendency of the UTS was observed for the PLA by itself and for the PLA/Jute Fiber system after the same conditions of humidity, temperature, pressure and time at which the systems were exposed. Further moisture analyses were carried out on these two systems for 28 and 60 days. Results depict an important increment on the UTS for the PLA matrix and the PLA/ Jute Fiber system during 60 days under moisture conditions. Surprisingly, increasing the UTS of PLA and the Jute system contradicts the proven fact that moisture affects the mechanical properties of PLA. However, a more detailed study under special establish parameters such as temperatures, moisture percentage and certain atmosphere conditions will help to understand the behavior of the PLA and jute fiber system under the exposed conditions.

4.2. Dynamic mechanic analysis (DMA)

Dynamic Mechanical Analysis (DMA) is an accurate method for measuring the viscoelastic properties of materials (elastic behaviors of materials). The sample is subjected by a controlled

sinusoidal stress known, then the sample will deform after certain amount of stress. How much it deforms is related to its toughness (stiffness). Since we are applying a sinusoidal force, we can express the modulus as a component: the storage modulus, and loss modulus. The storage modulus is the measure of the sample's elastic behavior. The ratio of the loss to the storage modulus is the tan delta, defined as a measure of the energy dissipation of a material. Modulus values change with temperature and transitions in materials can be perceived as changes in the tan delta curves. This includes not only the glass transition and the melt, but also other transitions that occur in the glassy transition (above T_g). These transitions indicate refined changes in the material [63].

The thermo mechanical properties of the different compounded materials were evaluated with a DMA (TA Instruments Q800, TA Instruments, New Castle, DE, USA). The test was performed in order to investigate the changes and improvement of the thermal properties of the PLA matrix with the addition of the different filler/ fiber materials, the highest temperature used for the test was the maximum temperature used for pure PLA. Five materials, PLA, PLA/Mayan Yellow, PLA/Jute Fiber, PLA/ BPO_4, and PLA/ NaCl were tested to find the possible interactions effects between PLA matrix and the filler materials and also to see the changes in thermal properties of the PLA by itself and with the different organic filler materials. DMA was run in the dual cantilever-bending mode with amplitude of 15 µm, the sample dimensions were: thickness 3.14 mm, length 35 mm and width 12.74mm. The temperature range was from room temperature, about 25 ºC to 120 °C with a heating rate of 3-5 °C/min and using a linear frequency of 1 to 100 Hz.

The results of the DMA testing are shown in Table 4.1 and Table 4.2, where it can be seen that pure PLA possesses a glass transition temperature (T_g) of 61.04 °C. The filler/fiber addition of the four composites to the PLA matrix resulted in a lowering of the Max tan delta temperatures for MayaCrom® Yellow and the donated boron phosphate composites compared to one of the PLA matrix. However, after the addition of NaCl and Jute Fiber the glass transition temperature of the materials decreases slightly (compared with baseline PLA samples) and the tan delta increased

significantly, resulting in an increase temperature window of elastic behavior between the onset of viscous behavior determined by the storage modulus curves and the maximum tan delta.

As a result, the main point of this study was that the addition of NaCl and Jute Fiber materials to the PLA matrix. In the case of the jute plant fiber, the temperature of the maximum tan delta was increased from 71.34 to 76.8°C while in the case of NaCl, the max tan delta temperature increased to 73.91°C which indicates the material is absorbing energy. The elastic window increased from 10.3°C to 14.34 and 18.37°C for the NaCl and jute fiber systems respectively, meaning that a wider service temperature range could possibly be used for parts fabricated from this material system as compared to PLA alone.

The temperatures for the five systems start to soften higher than 50°C but the modulus start to increase at 80 °C especially for the PLA/ MayaCrom® Yellow blend affecting the rheological behavior of the material. In the other hand, in the case of the PLA/ NaCl system when 80°C is reached the storage modulus decrease significantly, as a result the sodium chloride increases the ability of PLA matrix to flow. Finally, the incorporation of Jute Fiber into the matrix resulted in an increase of the energy stored (elasticity behavior).

Table 4.1 DMA temperature results

Material	Glass Transition Temperature, * °C	Max ten delta temp, °C	ΔTg to max ten delta, °C
PLA	61.04	71.34	10.3
PLA/ MayaCrom® Yellow	60.74	70.59	9.85
PLA/ Jute Fiber	58.1	76.8	18.7
PLA/ Boron Phospate	61.28	71.21	9.93
PLA/ NaCl	59.57	73.91	14.34

† 1 Hz

*Onset determined from storage modulus curve

Table 4.2 DMA modulus and complex viscosity results

Material	Storage modulus at 40 ° C, MPa	Complex viscosity at 80 ° C, Mpa-sec	Max tan delta
PLA	2683	8.76	1.8
PLA/ MayaCrom® Yellow	2146	3.58	0.8233
PLA/ Jute Fiber	2113	2.307	0.8206
PLA/ Boron Phospate	2199	1.408	1.179
PLA/ NaCl	2302	0.4133	1.797

† 1 Hz

4.3. Fracture analysis

Fracture surfaces of representative from each sample batch were analyzed with a Hitachi TM- 1000 scanning electron microscope (SEM; Hitachi High- Technologies Europe GmbH, Germany) operating at a 15 kV accelerating potential and equipped with a backscatter electron (BSE) detector. SEM imaging allowed fracture surface morphology observations of the matrix and composite structures to identify common failure modes within these material systems [10].

Representative electron micrographs of the fracture surfaces for the five material systems studied showed different fracture behaviors. SEM micrographs of the fracture surfaces of baseline PLA tensile test specimens compared to the other four systems (Figure 4.2). During the SEM

analysis it was observed that each filler/fiber result in a distinct effect on the fracture surface morphology.

The tensile test caused a partial ductile deformation of the PLA matrix. However, PLA mostly revealed a smooth fracture surface (Figure 4.2 a) as a result can be concluded that the PLA matrix behaves as a brittle material. Micrograph analysis of the PLA/Jute Fiber (Figure 4.2 d) shows a good dispersion between the PLA matrix and the fibers. However, when the tensile was performed the fibers pull out apart from the PLA matrix. According to work performed by Wang *et al*., [64] moisture absorption increased linearly with the fiber loading in Polypropylene material (PP) and after their investigations, they concluded that fibers encapsulated into the matrix of the material inhibited the moisture absorption. During Wang's investigation they were working with 20% and 40 wt.% loadings [64]. Comparing these results with our PLA/Jute Fiber system we can deduce that since our loading is lower we had a better dispersion of the fibers through the matrix. The MayaCrom® Yellow fracture surface is shown in (Figure 4.2 b) an observable fracture surface with CO_2 inclusion or voids are observed. Micrograph fracture surface of the PLA/ BPO_4 (Figure 4.2 c) shows that the filler did not attach to the PLA matrix. The fracture surface micrograph for the PLA / sodium chloride system (Figure 4.2 e) shows a good attachment of the salt into the PLA matrix.

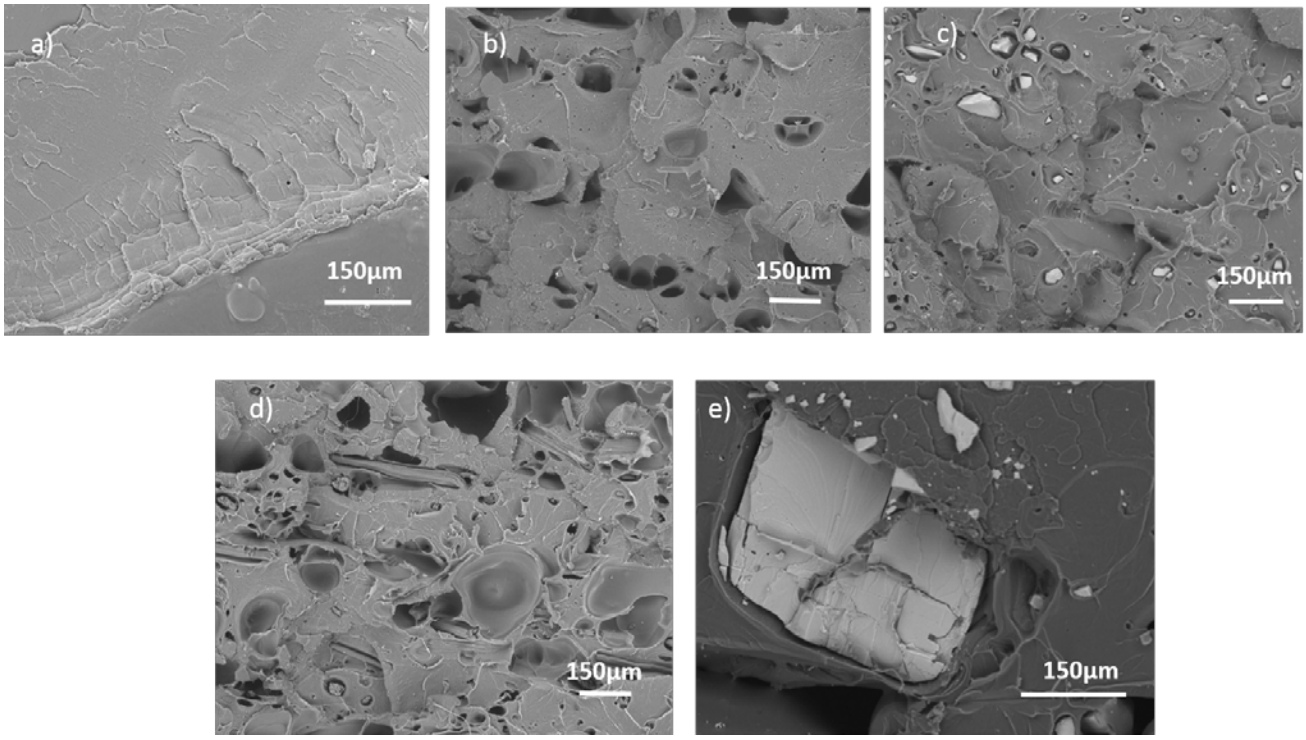

Figure 4.2 From left to right SEM Micrograph: a) PLA matrix, b) PLA/ MayaCrom® Yellow system, c) PLA/BPO_4, d) PLA/ Jute Fiber and e) PLA/ NaCl

4.4. In-soil biodegradability study

Preliminary work combining PLA with jute plant fiber is presented in Figure 4.3, which depicts tensile test data conducted for this project. As can be seen, the jute plant fiber had a detrimental effect on the mechanical strength of the printed test specimen.

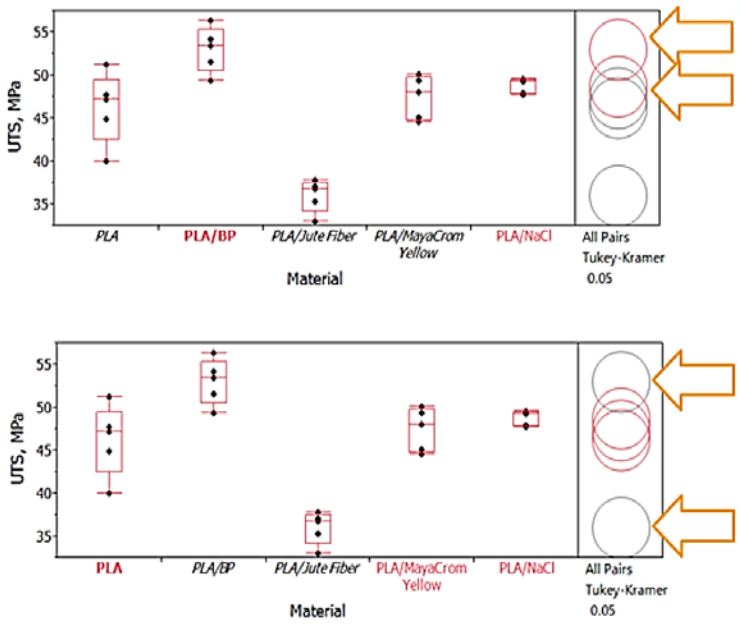

Figure 4.3 Effect on mechanical strength cause on PLA-based polymer matrix composites.

Of the additives tested here, NaCl shows promise in altering the physical properties of PLA. From Figure 4.3 we can see that salt adheres well to the matrix. No observable difference to weight was observed for any of the samples buried in the soil environment for two weeks. However, after 12 weeks, PLA specimens exhibited an increase in weight, while (1.95± 0.02 g increasing to 2.03 ± 0.01 g) the PLA/ NaCl composite exhibited a decrease in weight (2.49 ± 0.03 g decreasing to 2.24 ± 0.12 g).

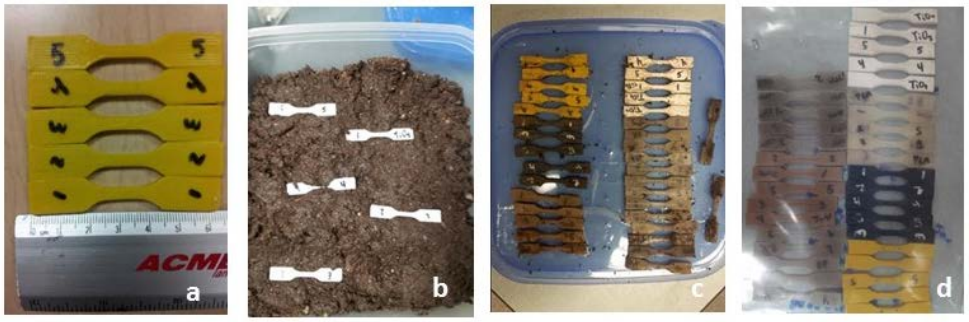

Figure 4.4. In soil- biodegradability study.

4.5. Discussion and Conclusion

Four PLA filler/ fiber systems were created (PLA/ NaCl, PLA/ Jute Fiber, PLA BPO_4 and PLA/MayaCrom® Yellow) and test in order to be able to compared systems' results with the PLA matrix. Preliminary results for the PLA, PLA/NaCl and PLA/Jute Fiber systems showed promising viscoelastic behavior. MayaCrom® Yellow filler DMA results showed an ability to decrease viscosity of PLA which can benefit the 3D printing process. Fracture surface of the four systems determined that NaCl presented the best adhesion to the PLA matrix. In the other hand, the Jute Fiber didn't present a good attachment to the matrix; similar results were observed for the BPO_4 filler. Finally, the MayaCrom® Yellow filler created voids in the PLA matrix. Ultimate tensile strength of all systems showed a decrease in mechanical properties of the systems under moisture conditions, which we can confirm that the materials presented a high moisture percentage, a result a decrease in the mechanical properties. However, the PLA/ Jute system and the PLA matrix by itself presented an increase on the UTS after the humidity treatment. Again PLA/ Jute Fiber came up with interesting results. Future work will be focused in keeping improving the properties of the PLA by using NaCl and Jute Fiber sustainable materials. Results of the in-soil biodegradability study indicated there was no weight loss after 2 weeks. Tensile testing of the buried specimen will be performed to see if mechanical properties were affected. Biodegradability of poly-lactide acid (PLA) plastic tensile test specimens in garden soil will be repeated and the specimens will be buried for a month.

4.6. DMA results

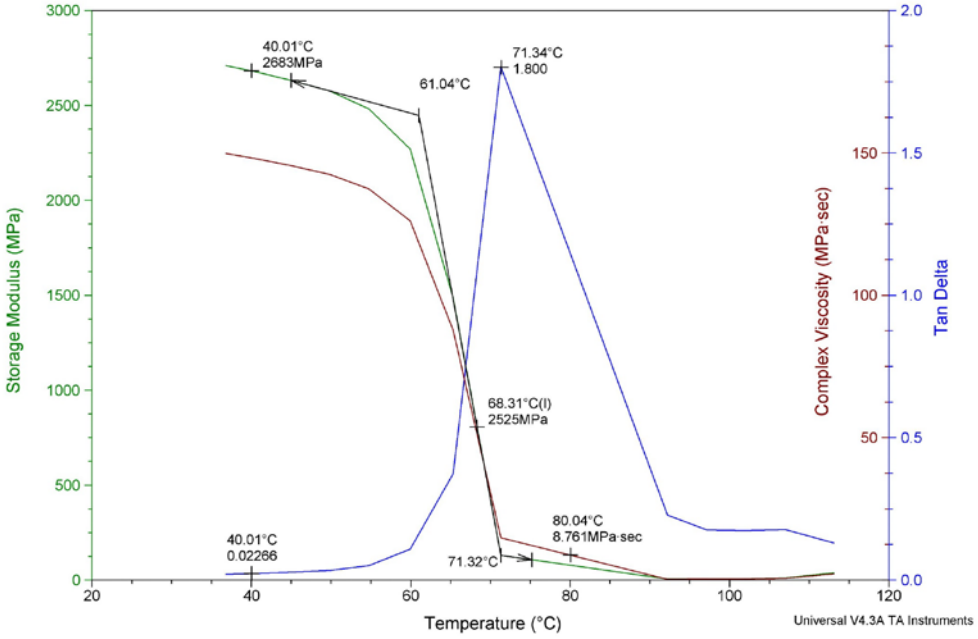

Figure 4.5 PLA BASELINE DMA

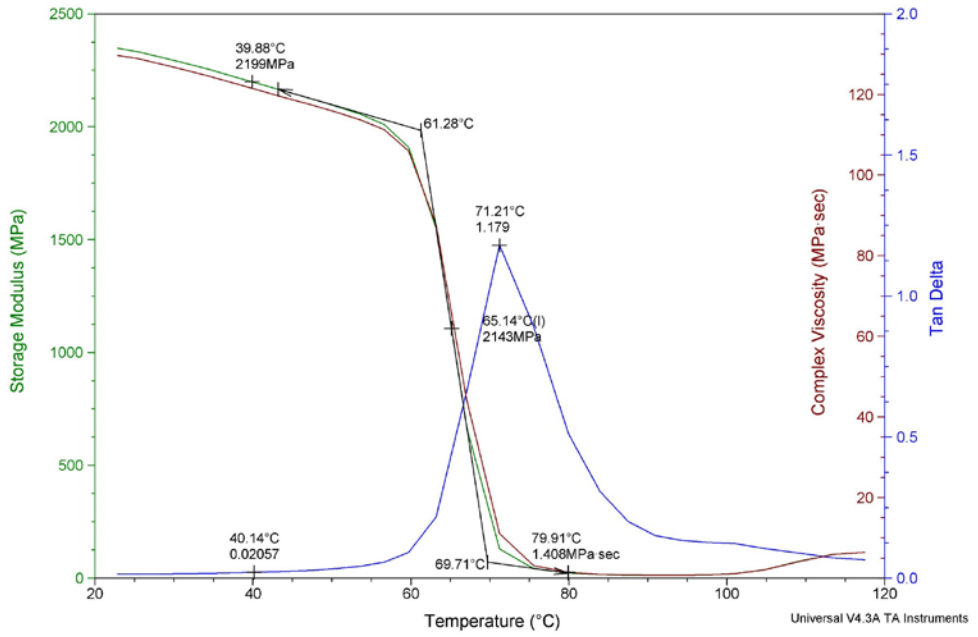

Figure 4.6 PLA BORON PHOSPHATE

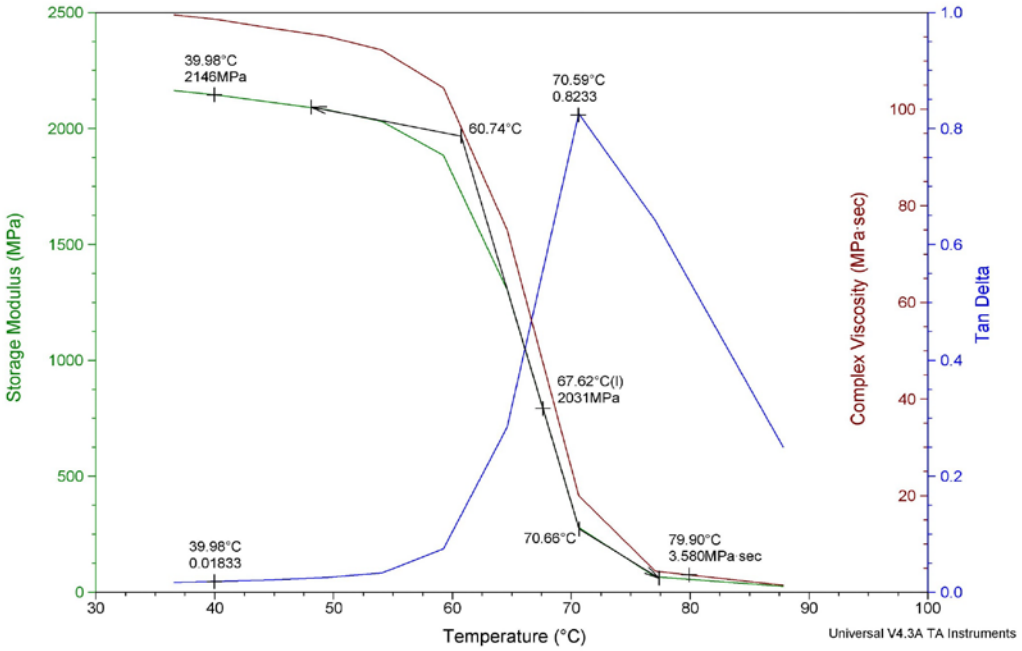

Figure 4.7 PLA/ MAYACROM® YELLOW

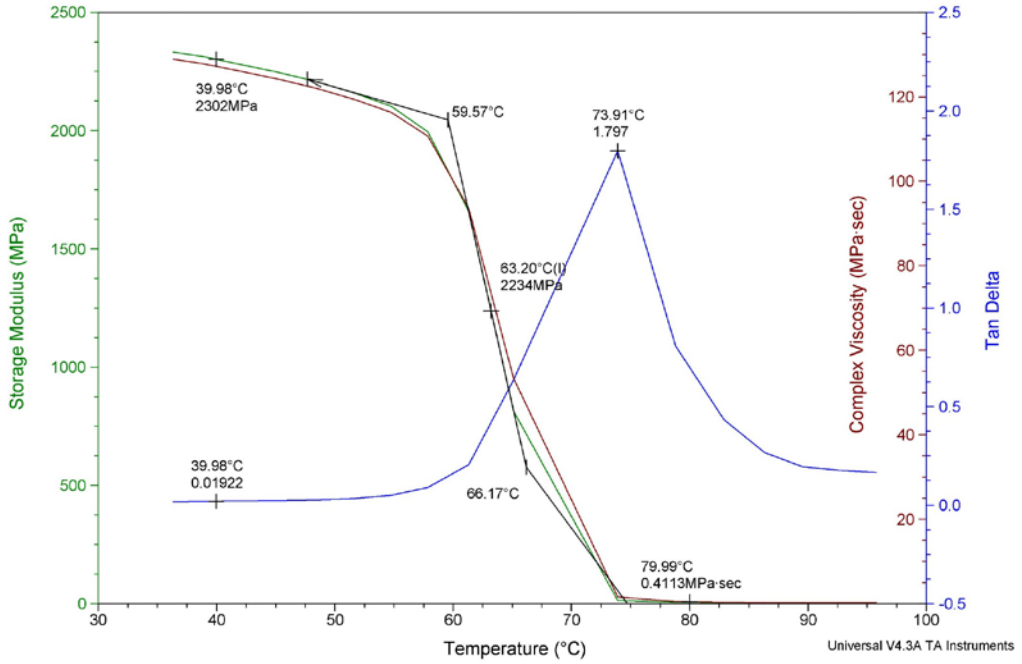

Figure 4.8 PLA/ NaCl

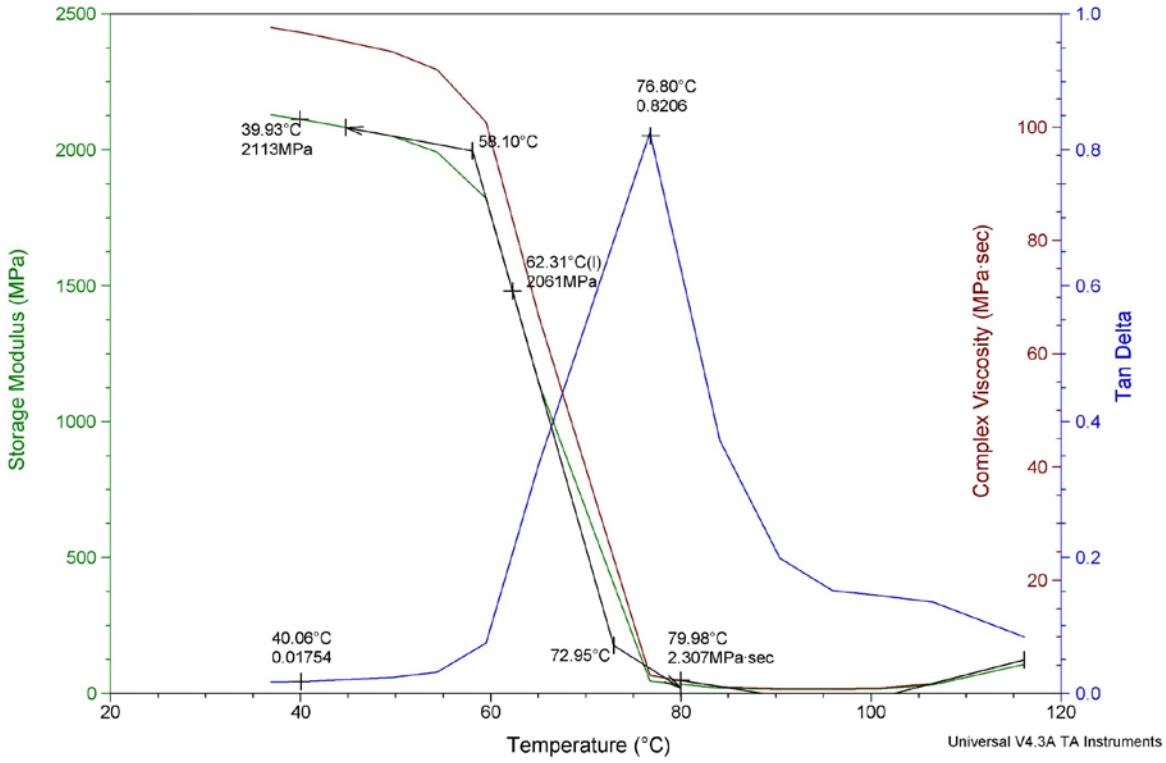

Figure 4.9 PLA/JUTE FIBER

CHAPTER 5: FINAL RESULTS

Results presented here in Chapter 5 represent the main output of this research effort. The initial data for composites of PLA compounded with jute fiber, MayaCrom® Blue, MayaCrom® Yellow and un-milled salt, along with the effect of functionalizing jute fiber in an aqueous solution of NaCl were presented in Chapter 4. That data is intermixed with the data presented in this section for completeness.

Functionalization of fillers is a critical aspect in the successful creation of polymer matrix composites. However, the chemicals typically used to achieve functionalization (silanes) are not environmentally friendly. In order to keep close to the goal of creating environmentally friendly polymer-based materials for 3D printing, it was decided to explore the use of NaCl as a functionalization agent for jute plant fiber. As seen in the previous data in Chapter 4, while jute fiber has a positive effect on the max tan delta, the SEM micrographs indicated poor adhesion to the PLA matrix. On the other hand, NaCl exhibited good adhesion to the polymer matrix. Here, we seek to see if treating the jute fiber with NaCl in an aqueous solution will effectively functionalize the fibers. Comparison to functionalizing jute plant fiber with (3-Glycidyloxypropyl) trimethoxy-silane was also carried out in order to understand the viability of our process.

Monofilaments were produced using a Dr. Collin Twin Screw Extruder/ Compounder Model ZK 25T (Dr. Collin GmbH, Ebserberg, Germany). Several filler materials were combined with PLA in the formation of sustainable 3D printable polymer matrix composites: 1) Sodium chloride (NaCl) (Sigma); 2) jute plant fiber sourced from rope purchased from Home Depot; 3) Carbonized jute fiber; 5) MayaCrom® Blue; 6) MayaCrom® yellow (both from Mayan Pigments. Inc., El Paso, TX, USA); 7) Magnesium Chloride ($MgCl_2$) (Sigma); 8) Boron Phosphate (BPO_4) purchased from Alfa Aesar Company; 9) Jute plant fiber functionalized with (3-Glycidyloxypropyl) trimethoxy-silane purchased from Sigma Aldrich was also carried out in order to understand the viability of our process.

The filler materials evaluated in this study were chosen based on the perceived environmental sustainability. All additives were blend at a 5% by weight ratio to PLA. With the purpose of study, the influence of different particle size in the PLA matrix/ salt filler samples were prepared at 10 min ball milling times in which composites the variation in concentration started from 5 to 20% by weight ratio to PLA. The changes on particle size before and after the ball mill process are reported on the following image (Figure 5.1)

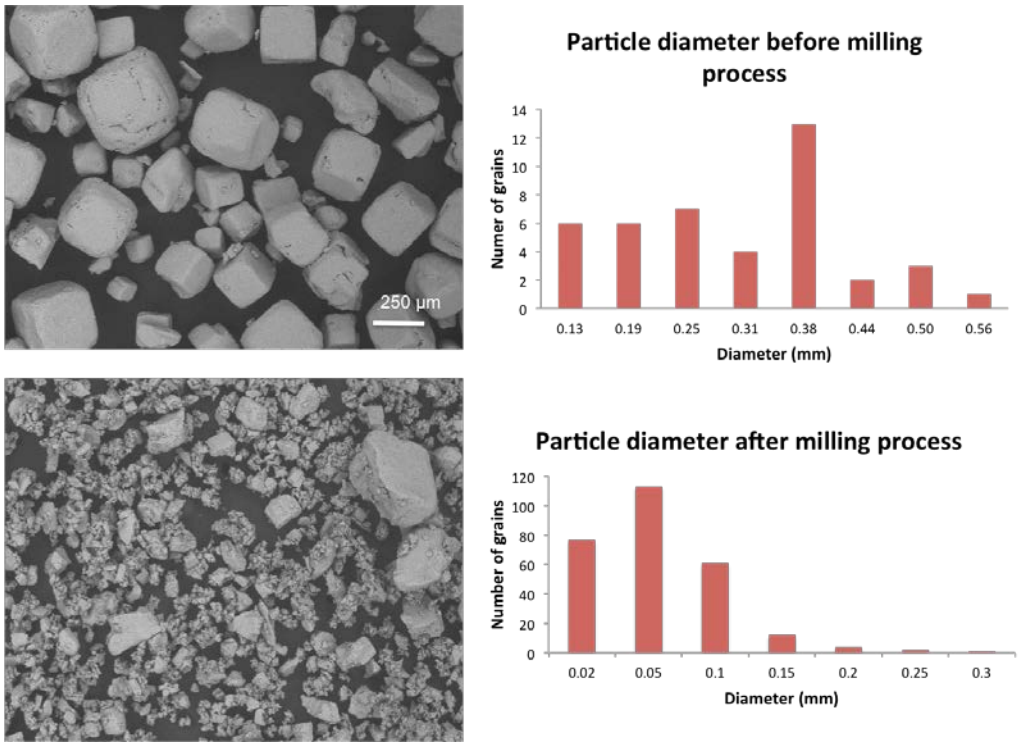

Figure 5.1 Particle size analysis for NaCl before and after the milling process

Hybrid NaCl and Jute-functionalized NaCl MayaCrom® composites were also produced. As seen in Chapter 4, the benefit of the addition of the MayaCrom® pigments was the decrease in viscosity; which could benefit the 3D printing process by allowing a greater level of flow to occur. This has shown to increase surface finish quality and decrease the presence of air gaps between print rasters according to Rocha *et al.*, [10]. Jute plant fiber functionalized with salt, and both Mayan Pigment fillers were combined to produce two new polymer composite materials. The composition of these new materials was 2.5% by weight ratio to PLA.

Initial research performed on desktop 3D printers presented on Chapter 3 was done with the purpose of verifying the commercial printability on the XYZ directions and to test the mechanical properties of the materials' systems following the common dog-bone ASTM D638 standard type V. During tensile testing, the final fabricated specimen is affected by different parameters such as the different additives and the chemical chain structure in the matrix material by itself. Moreover, according to Umetani *et al.*, [65] and [66], parts manufactured by ME3DP usually exhibit mechanical property anisotropy; which means that the properties of the final fabricated part depend on the build orientation and raster pattern. The percentage degree of weakness increases in the Z-direction because the interface between layers is not as strong as in XYZ directions. For this study a transversal raster pattern was used to print layers perpendicular to the length of the specimen on the XYZ directions. In the case of the transversal specimen, there was no edge shell and as previously reported by Torrado *et al.,* [67] the use of transversal or faux vertical fabricated specimens mimics the ZXY print raster pattern and allow to evaluate the anisotropy properties of the material avoiding the typical problems that are present when the specimens are fabricated on the vertical directions.

On this Chapter we evaluated the influence of the fillers in comparison to the PLA matrix as well as the anisotropy of each material system. To evaluate the percentage decrease in strength due to raster sensivity ASTM D638 type V specimens were printed on XYZ directions using the baseline crosshatched pattern print layers alternated by 90° and the faux vertical raster pattern mimics the ZXY directions under the same parameters conditions mentioned on Chapter 3 on Table 3.2 using an open source Rostock Max 2 delta 3D printer.

In order to observe the influence on crystallinity by the filler materials into the PLA matrix, X-Ray Diffraction analyses were performed in a Bruker D8 Discover system employing Cu K-α radiation (1.54Å). XRD analysis has been shown to be a viable method to observe the degree of crystallinity of PLA [68].

5.1. Tensile Results

The mechanical properties' performance for 3D printing materials PLA, revealed that the addition of Boron Phosphate (BPO_4), Sodium Chloride in 5 wt.% un-milled and Mayan Yellow® led to tensile test specimens with slightly higher ultimate tensile strength values than those printed from PLA alone. For the rest of the systems, the addition of Sodium Chloride at higher wt. percentage than 5, Mayan Blue®, jute fiber with all different treatments lead to low ultimate tensile strength values lower than PLA matrix by itself. This decrease in strength may be due to the thermal degradation of the organic components of jute fiber inside of the PLA matrix, resulting in the creation of voids. Yet, the addition of jute plant fiber increased the percentage elongation specimens, an explanation could be that the particles rearrange inside the matrix when the force is applied, in that way they are able to tolerate more plastic deformation than the PLA plastic by itself or the other materials systems as noted in Torrado *et al*., [67]. The created tri-blend composed of MayaCrom® Blue system affects the mechanical properties of the PLA matrix. Moreover, the tri-blend composed using MayaCrom® Yellow did greatly affect the mechanical properties of the PLA matrix material by decreasing the UTS of the material. The results of the tensile strength for all the materials systems are presented on Table 5.1

Table 5.1 UTS for the fabricated horizontal systems

Material	UTS (MPa)		Elongation at break (%)	
HORIZONTAL	**AVG**	**ST. DEV.**	**AVG**	**ST. DEV.**
PLA	51.936	6.276456325	3.608	1.242807306
PLA/ SALT 5% NO MILL	48.228	0.983817056	2.448	0.674625822
PLA/ SALT 5%	43.6	2.376913966	2.652	0.338998525
PLA/ SALT 10%	43.932	2.186873567	3.99	0.597996656
PLA/ SALT 15%	39.358	1.361372837	2.33	0.293001706
PLA/ SALT 20%	35.7	1.752643717	2.988	0.849040635
PLA/ MgCl2	40.384	5.117087453	5.558	0.412698437
PLA/BPO4 5%	48.112	3.59129169	3.778	1.128392662
PLA/MAYAN YELLOW	47.43	2.514507904	2.552	0.112116011
PLA MAYAN BLUE	38.776	0.669256304	15.874	1.128392662
PLA/JUTE FIBER 5%	39.05	1.218667305	4.846	0.234029913
PLA/ JUTE FIBER FUNCT. W SALT	40.96	1.24109629	9.358	3.420814231
PLA/ JUTE FIBER FUNCT. W CHEM SILANE	43.53	3.481970706	1.68	0.636356818
PLA- CARBON JUTE FIBER 5%	42.526	3.784941743	2.848	0.678616239
PLA/FUNCT.JF W SALT/ MYW 2.5%	38.3	5.80436043	2.812	0.449076831
PLA/FUNCT.JF W SALT/ MB 2.5%	40.762	1.772663533	19.81	1.64441479

As expected, overall the specimens fabricated in ZXY exhibited lower strength values than those printed on the XYZ directions. Surprisingly, this was not the case for the parts fabricated on the ZYX directions headed for the tri-blend composed of MayaCrom® Yellow and followed by the inorganic $MgCl_2$ actually presented a highest roughness compared to the other sixteen systems composite materials. Parts fabricated with ionic sodium chloride with a 20 wt. % load and the functionalized jute fiber chemically treated also presented a percentage decrease in strength due to raster sensivity, meaning that these systems can tolerate higher plastic deformations when they are fabricated using the print transversal raster pattern on a 3D printer. The results for the parts fabricated using are recorded on Table 5.2 and Table 5.3

Table 5.2 UTS Results for the fabricated vertical systems

Material	UTS (MPa)		Elongation at break (%)	
FAKE VERTICAL	**AVG**	**ST. DEV.**	**AVG**	**ST. DEV.**
PLA	32.05	1.564544662	1.996	0.326236111
PLA/ SALT 5% NO MILL	40.79	2.928146171	3.3	0.352420204
PLA/ SALT 5%	35.372	1.156397855	2.65	0.311287648
PLA/ SALT 10%	37.426	2.048244126	3.746	0.769304881
PLA/ SALT 15%	33.062	3.366662442	3.66	1.077334674
PLA/ SALT 20%	34.314	2.460435734	3.98	1.158511977
PLA/ MgCl2	42.31	7.054142046	5.71	0.924472823
PLA/BPO4 5%	36.196	4.397574786	2.822	1.080680341
PLA/MAYAN YELLOW	36.296	2.514507904	2.236	0.786625705
PLA MAYAN BLUE	33.408	2.163667257	20.702	5.760357628
PLA/JUTE FIBER 5%	34.59	1.218667305	3.284	0.510715185
PLA/ JUTE FIBER FUNCT. W SALT	26.81	2.587199258	5.776	2.020378677
PLA/ JUTE FIBER FUNCT. W CHEM SILANE	41.442	6.359891194	2.384	0.389846123
PLA- CARBON JUTE FIBER 5%	35.61	2.839436564	4.464	1.330405953
PLA/FUNCT.JF W SALT/ MYW 2.5%	44.968	2.533877661	3.188	0.63903834
PLA/FUNCT.JF W SALT/ MB 2.5%	33.37	5.327216909	7.316	1.798410409

Table 5.3 % Decrease in strength due to raster sensibility

System	% Decrease in strength due to raster sensitivity
PLA	18.93%
PLA/ SALT 5% UNMILLED	13.72%
PLA/ SALT 5%	18.87%
PLA/ SALT 10%	14.81%
PLA/ SALT 15%	16.00%
PLA/ SALT 20%	3.88%
PLA/ MgCl2	-4.77%
PLA/BPO4 5%	24.77%
PLA/MAYAN YELLOW	23.47%
PLA MAYAN BLUE	13.84%
PLA/JUTE FIBER 5%	11.42%
PLA/ JUTE FIBER FUNCT. W SALT	34.55%
PLA/ JUTE FIBER FUNCT. W CHEM SILANE	4.80%
PLA- CARBON JUTE FIBER 5%	16.26%
PLA/FUNCT.JF W SALT/ MYW 2.5%	-17.41%
PLA/FUNCT.JF W SALT/ MB 2.5%	16.66%

5.2. Fracture surface analysis

5.2.1. Fractography of the systems fabricated on XYZ directions

Fractography of tensile test specimens printed on the XYZ directions from the composites tested here, allowed for observations related to the heftiness of the filler/matrix interface as wells the effect of additives to the crack surface morphology induced by exposed stress-strain conditions. Baseline PLA tensile specimens exhibited a fracture surface morphology indicative of a brittle failure mode which correlates with the low percentage elongation at break values recorded for the material. Fracture surface analysis shown NaCl to adhere well to the PLA matrix. Crack propagation is clear on the surfaces (highlighted in Figure 5.2) of the individual particles. There is also no evidence of particles pulling out nor were there any gaps between the particles and the matrix. In contrast, the fracture surface of the PLA/jute plant fiber composite possessed features indicating a poor interface between the fibers and the matrix (in Figure 5.3 i). The addition of MayaCrom® pigments had the effect of prompting voids within the PLA matrix; which influenced the decrease in tensile strength as compared to baseline samples (Figure 5.4 m).

While the addition of jute plant fiber increased the glass transition window, (previously reported on Chapter 4) the poor adhesion to the matrix at room temperature play an important role to the overall performance of this composite. NaCl exhibited characteristics indicating a strong bond with the PLA matrix, for this reason two additional experiments were carried out. One consisted on a particle refinement process to analyze how the particle size affects the blending of the two materials and the mechanical properties of the system. After a refinement particle treatment in the ball mill during 10 min; salt particles were added at different concentrations to the PLA matrix. It was observed that the addition of 5% salt before the particle refinement process was best dispersed and attached to the matrix than the system created after the particle refinement process (Figure 5.2 b and c). Moreover, it was observed that with the increasing concentration of salt in the PLA matrix the adhesion between the matrix and the particles decreased (Figure 5.2 c, d, e and f). These can also be correlated with the obtained tensile-strength results (Table 5.1).

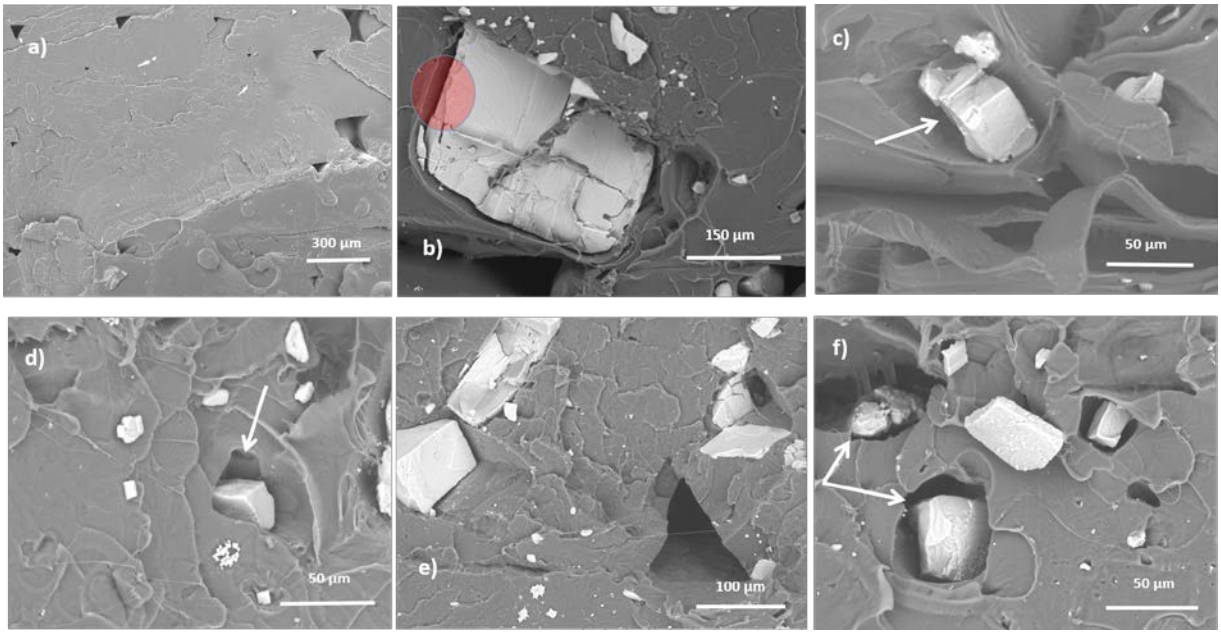

Figure 5.2 SEM fracture analysis of PLA/ NaCl system. From left to right a) Fracture surface PLA baseline, b) PLA/ Salt 5% before the particle refinement, c) PLA/ Salt 5%, d) PLA/ Salt 10%, e) PLA/ Salt 15% and f) PLA/ Salt 20% after particle refinement

The other experiment was performed where the jute plant fiber was first functionalized; in an aqueous NaCl solution previous to the system compounding. The result was a reduction in percentage elongation while the UTS stayed mostly the same (Table 5.1). Supplementary analysis of the fracture surface via SEM (Figure 5.3 i) revealed the presence voids into the PLA matrix that could be air or other volatile substance trapped inside the composites, which formed during the thermal degradation of the fibers during the extrusion or the printing process. According to Hongwei et al., [69] during alkali treatments of jute fibers the hemicelluloses and lignin are partially removed these facilitated to the inter-fibillar region to be less solid and less rigid. This makes the fibrils more capable of rearranging themselves along the direction of tensile deformation (Figure 5.3j). There was a slight increment on the UTS results on the carbonized jute fiber system compared to that one of the non-functionalized jute and the alkali functionalized jute with the inorganic sodium chloride aqueous solution, this could be due some chemical and physical alterations could have occurred on the fibers when were heated at more than 300 ºC such as oxidation, dehydration or decarboxylation [70] (Figure 5.3 l). Jute fibers treated with silanes, shown an improvement on tensile due to the silane chemical effect as a coupling agent to modify fiber surfaces. According to Kabir *et al*., [71] the

composition of silane forms a chemical link between the fiber surface and the matrix through a siloaxane bridge. However, the strength increment was not very notable in comparison to the green-alkali treatment. The percentage elongation at break was notably higher for the alkali treated jute fibers. The increase in ultimate tensile strength for the alkali modify jute fibers compared to the non-functionalized, the carbonized jute fibers and the silane modify jute fibers systems indicates an increase in toughness caused by an increase in the bond strength between the fiber and the matrix.

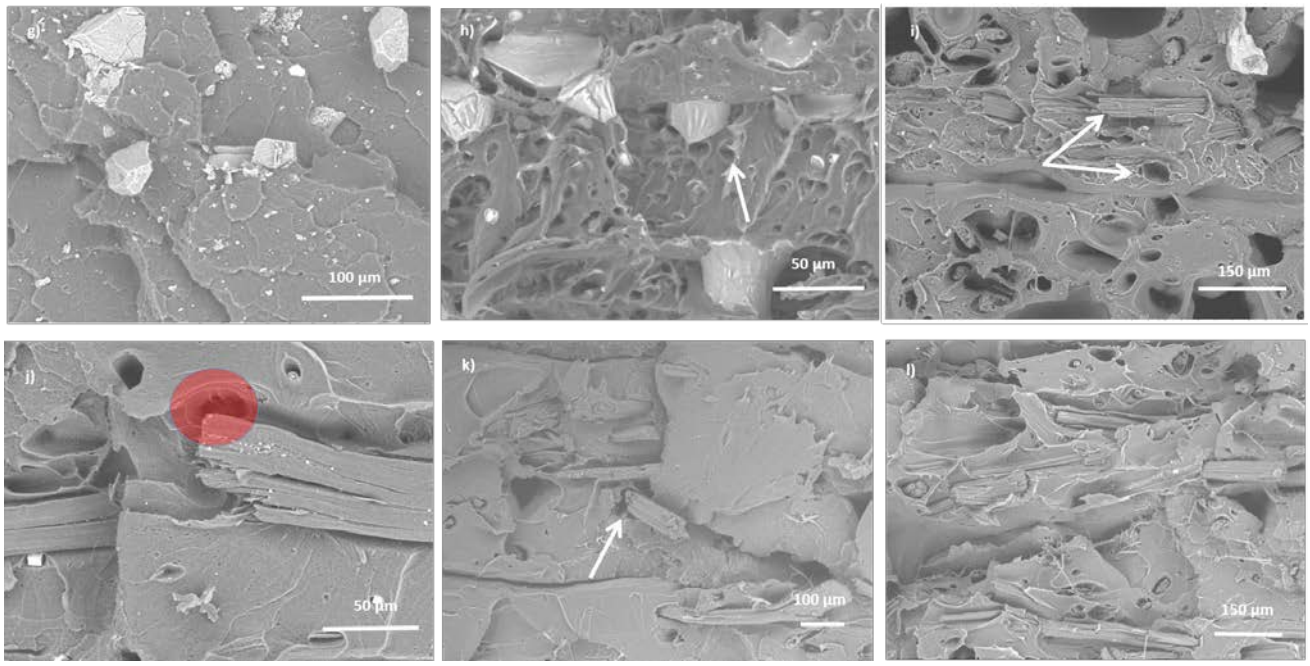

Figure 5.3 Fracture analysis of g) PLA/ BPO_4, h) PLA/ $MgCl_2$, i)PLA/ Jute Fiber 5%, j)PLA/ Functionalized jute fiber with NaCl, k)PLA/ Functionalizes jute fiber with chemical silane and l) PLA/carbonized jute fiber

The result of the addition of all material fillers was a decrease in the mechanical properties as compared to PLA, namely a decrease in the yield strength. However, over all the other systems boron phosphate was the filler that had the lower impact on the UTS recorded results. Fractography of the PLA/ BPO_4 showed a brittle behavior on the surface and features indicating the BPO_4 particles fairly adhere to the PLA matrix. However, the addition of BPO_4 could produce a chemical change between the matrix and the inorganic filler during the different processes used. According to Sharmin *et al.*, [72] boron and the phosphorus are network formers. The inorganic phosphate composed of tetrahedral units (PO_4^{3-}) can highly modify the structure of some materials, if the

inorganic catalyst is in contact with the presence of oxygen bridges, which are present on the PLA molecule.

Magnesium chloride ($MgCl_2$) Figure 5.3b was reported to have a decrease in strain at break. The decreased strength was attributed to the presence of small bubbles; these defects were determinant on propagate the crack along the specimen surface; these small bubbles are very likely to be water vapor since this filler presented a very high hygroscopicity [73]. It is also observable that the inorganic filler had an important impact in the plasticity of the PLA material, which could also be determinant in decreasing the mechanical properties of the material by itself. Magnesium Chloride is a type of metal halide, which forms proton donating solvated constituents that act as solvents for plastics. Under certain environmental conditions these agents promote crazing in polymers under stress conditions, the cracking occurs because the disruption of hydrogen bonding in the plastic as the environment become attracted to either water in the environment or with hydrated metal halide such as magnesium chloride [74].

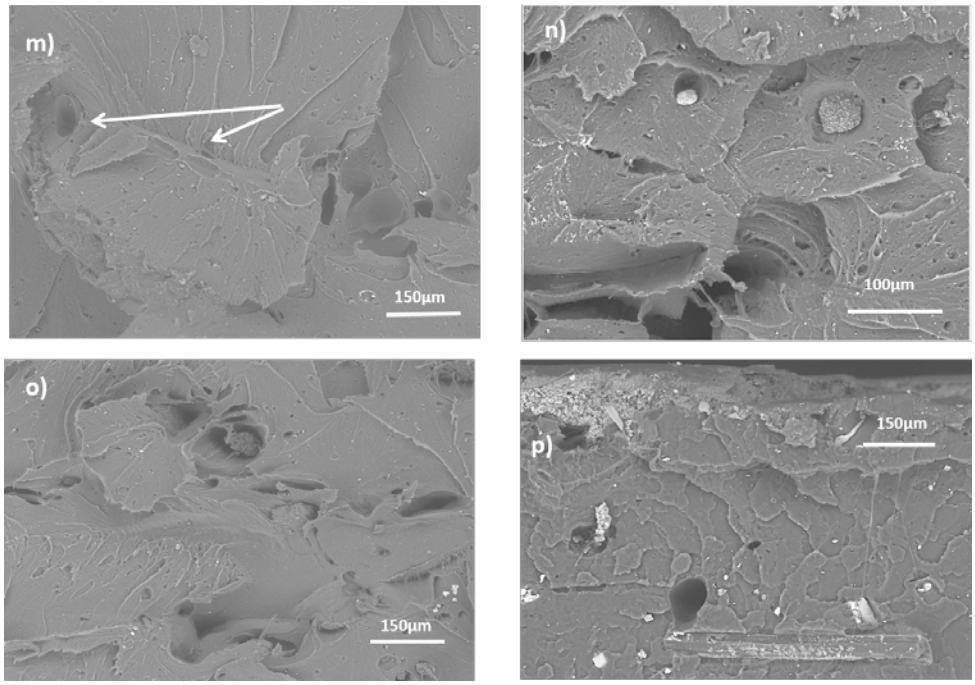

Figure 5.4 Fracture surface analysis of m) PLA/ Mayan Blue®, n) PLA/Functionalized Jute Fiber / Mayan Yellow, o) Mayan Yellow ® and p) PLA/Functionalized Jute Fiber / Mayan Blue systems

Fracture surface analyses of the MayaCrom® PLA blends showed crack propagation in the matrix material indicated by white arrows. According to tensile-strength results there was a much better mechanical bonding between PLA/ MayanCrom® Blue increasing the percentage elongation at break of the PLA material. Opposite to the high percentage in young modulus results for the MayaCrom® Blue, the ultimate tensile strength results benefited the MayaCrom Yellow; results showed a higher UTS for the PLA/ Mayan Yellow® system.

Fracture analyses for the tri-blend based MayaCrom ® pigments and after the incorporation of the incorporation of the functionalized jute plant fiber composite seem to have a good interface between the fibers and the PLA matrix, in presence of Sodium Chloride as a functionalization agent [75]. Results for the mechanical properties of both tri-blends based on the MayaCrom® pigments did not have big changes as compared to the PLA/ MayaCrom® systems. However; according to tensile-strength results there was a much better mechanical bonding between PLA/Functionalized Jute Fiber / MayanCrom® Blue and also an increase on the UTS properties; which was opposite to the UTS previously tested for the PLA/ MayaCrom® Yellow system. Decrease on UTS for the tri-blend based on the MayaCrom® Yellow could occur due to bad printing and the presence of the air gaps on the final fabricated part.

5.2.2. Fractography of systems fabricated on ZXY directions.

SEM fractography analysis showed a preferential failure within the raster interface for the systems with higher percentage decrease due to raster sensivity. The fracture for these two materials was also observed to be smoother with lower plastic deformation as previously observed by Torrado et al., [67]. Relating the sensitivity to raster pattern between PLA and the PLA/$MgCl_2$ (Figure 5.5 a), the tri-blend based Mayan Yellow (Figure 5.5 b) and the PLA/ Salt 20% loading (Figure 5.5 c) composite systems revealed the addition of these fillers to reduce the difference in UTS between the transversal and crosshatched raster pattern.

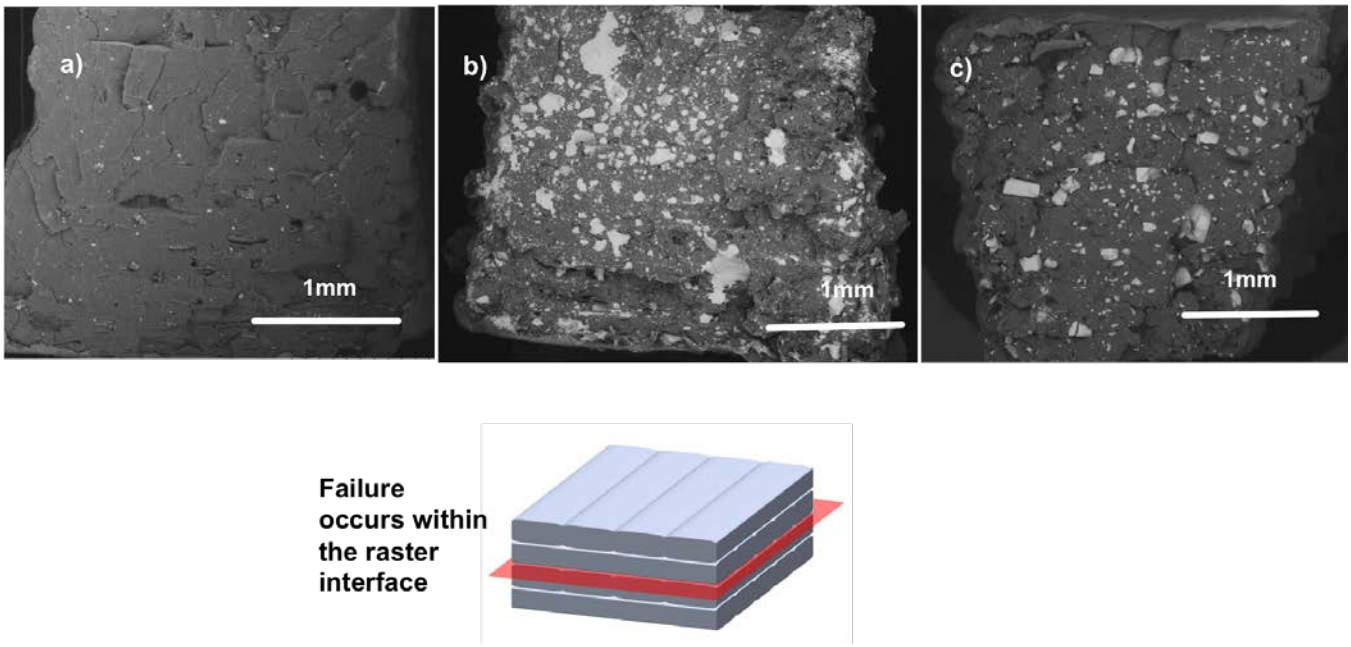

Figure 5.5 Fractography analysis of a) PLA/ $MgCl_2$, b) tri-blend based Mayan Yellow and c) the PLA/ Sodium Chloride at 20% loading. Failure model [1]

More notable is that this decrease in mechanical property anisotropy did not come at the expense of overall yield strength, as has been the case in work related to decreasing the anisotropy of ABS-based ternary polymeric blends as explored in Torrado *et al*., [66].

5.3. Crystallinity Analysis

The normal room temperature XRD analyses were carried out on a Bruker D8 Discover X-Ray diffraction system (XRD). The radiation applied was Cu Kα operating at 40 kV and 40 mA. The samples were measured in air temperature in step-scan mode with a scan speed of 5° locked coupled 2θ and a counting time of 1 s. Data collection and evaluation were performed with EVA software. Profile fitting was applied to extract information in the samples in order to observe the influence of the fillers in the PLA microstructure matrix and the effects of crystallinity on the PLA baseline material and in some of the filler materials (NaCl and BPO_4). To analyze the effect of the different crystalline content PLA specimens, they were annealed at 120°C during 20 min. The Profile Fitting option of the software uses a model that employs intrinsic parameters to describe phase analysis, peak identification and cell parameters among others.

XRD PLA baseline results were fitted with the chemical composition of L-Lactide-poly (ethylene glycol) - (($C_3H_4O_2$) -(C_2H_4O) -($C_3H_4O_2$)) n that is not exactly the same substance of PLA by itself. However, according to Castillo *et al.*, [76] these two substances share similarities; poly (ethylene gycol) (PEG) is synthetized from the same L-lactic acid as the poly (lactic) acid (PLA). Ethylene glycol is used in conjunction with PLA to improve the hygroscopicity of the PLA by itself. Results depict one significant peak was observed at approximately 2θ of 17° for the PLA annealed an un-annealed baseline specimen. Three more peaks belonging to PLA baseline appeared at ± 2θ of 15°, 19.3 and 22.5° were detected. These results can be more noticeable on the annealed samples. These data were also compared with external XRD patterns data in order to verify our analyses [77].

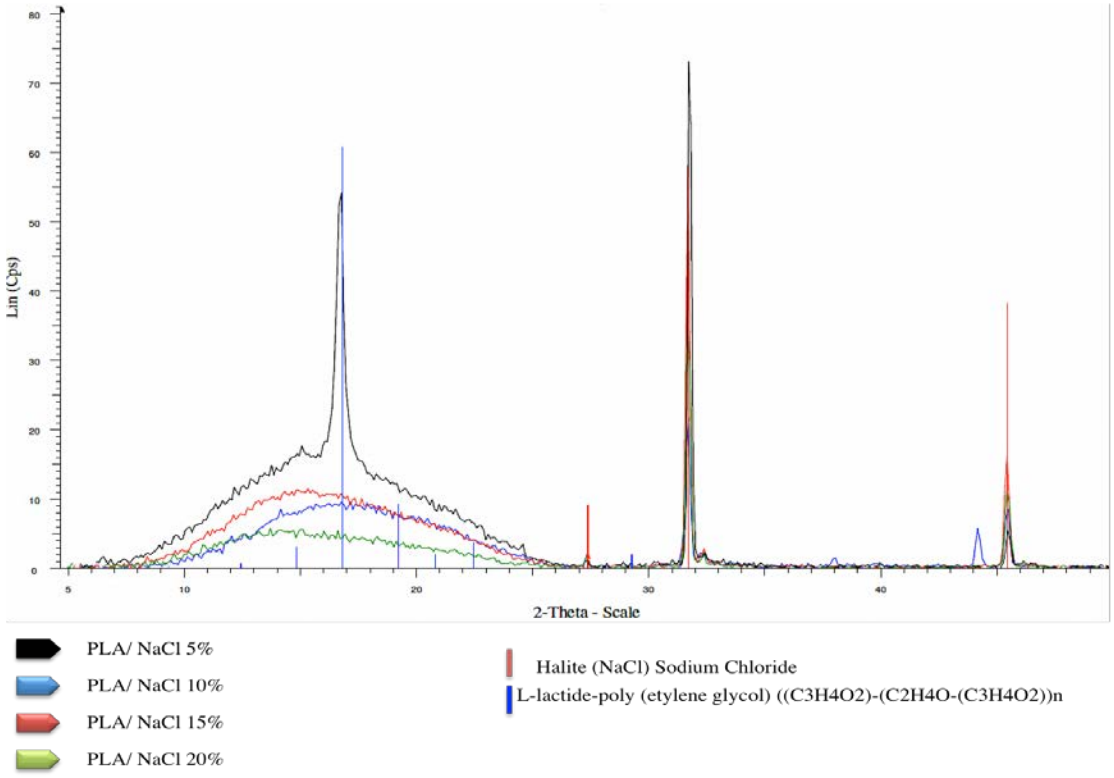

Figure 5.6 XRD analysis for the ionic compound and the degree of crystallinity at different concentrations

Regarding the ionic compound three characteristic peaks were observed during the analyses at ± 2θ of 27.5°, the strongest 31.7° and 45.5°. After heat treatment, it was observed that the intensities of each material in the case of the ionic systems varies depend upon the concentration of

each; it was observed that the percentage of crystallinity is inversely proportional to the concentration in the material; however, the variations were not very noticeable.

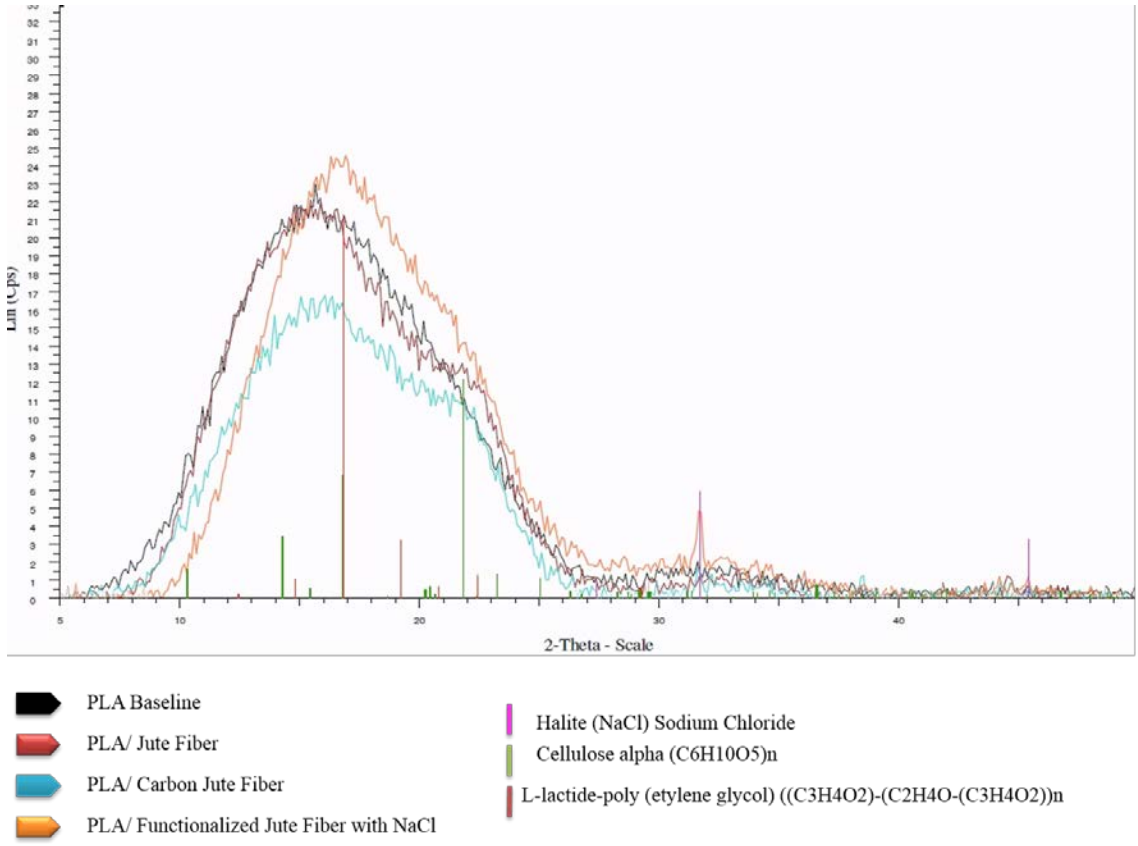

Figure 5.7 X-Ray Diffraction comparison of annealed PLA baseline and systems containing jute fibers

Jute fibers are composed of cellulose, hemicellulose, and lignin. Other components, usually considered as surface impurities, are the pectin and wax substance. Higher cellulose content leads to higher stiffness and, therefore, will be most suitable for plastics reinforcement. The chemical structure of cellulose contains three hydroxyl groups, which in the macromolecular cellulose structure form hydrogen bonds. This makes cellulose the most important of the chemical components of plants fibers, particularly in the manufacture of composites. Two of these hydroxyl groups form intermolecular bonds, while the third one forms intra-molecular hydrogen bonds [78].

XRD analyses were also performed on the PLA/ Jute fiber composites material; results showed that jute fiber did not affect the crystallinity of the PLA material by it. However, two minor peaks were recorded at 15.8 and 22.8 2θ belonging to the hybrid NaCl functionalized jute fiber.

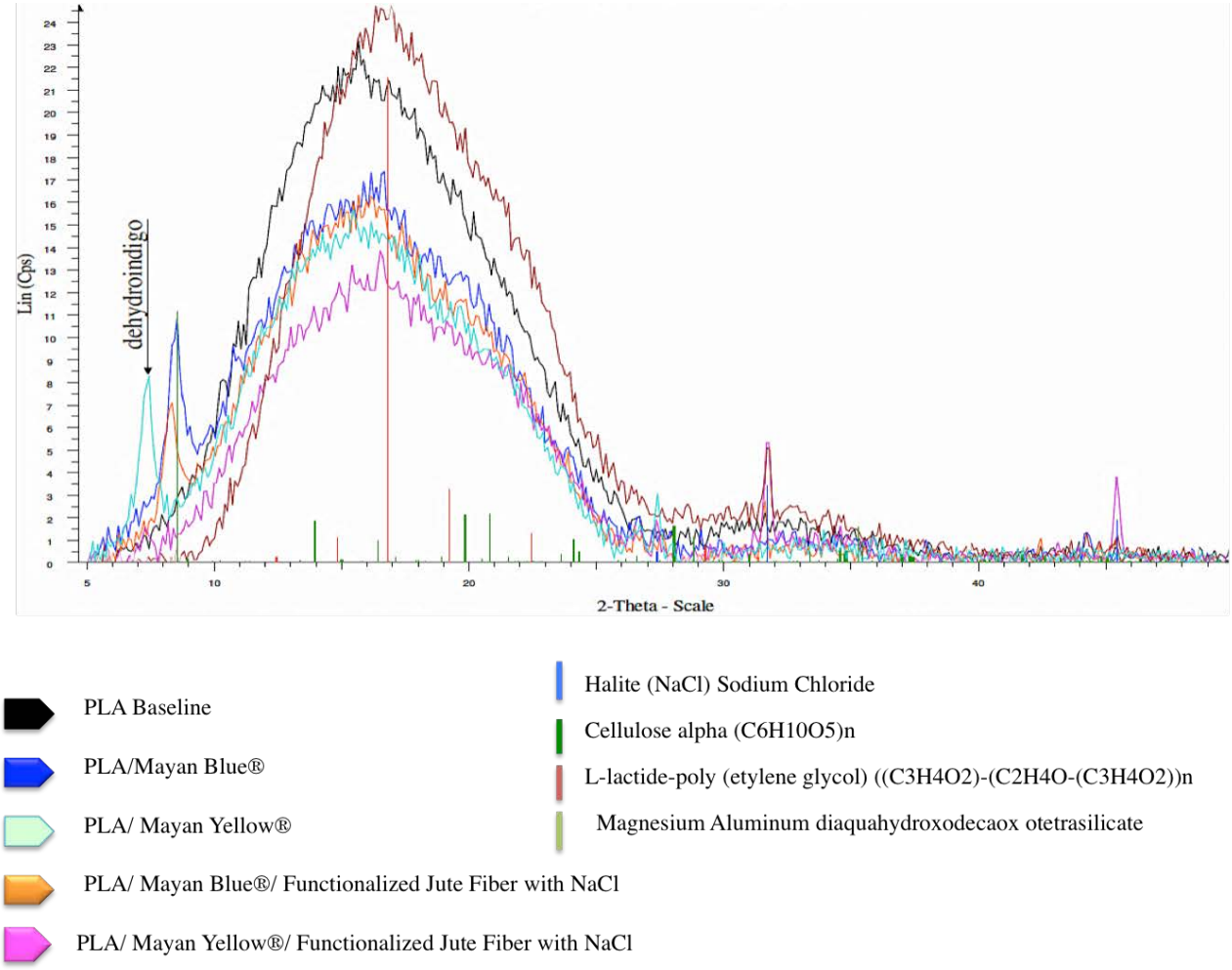

Figure 5.8 X- Ray Diffraction comparison of PLA, the Mayan Pigments and the tri-blends systems

Mayan Pigments were also analyzed using XRD techniques; as was expected the molecule that constitutes de MayaCrom® Yellow (dehydroindigo) was found in the organic range of the spectra, also the presence of palygorskite which is the main ingredient of MayaCrome® Blue was detected, which corresponds to the Magnesium Aluminum silicate patterns at ±2θ of 7 and 8.5°. Again the ionic compound was found at the aforementioned range. Results can prove that our tri-

blend material (Mayan Pigment/ Jute Fiber functionalized with PLA/ NaCl) was successfully blended without losing the microstructure of each material.

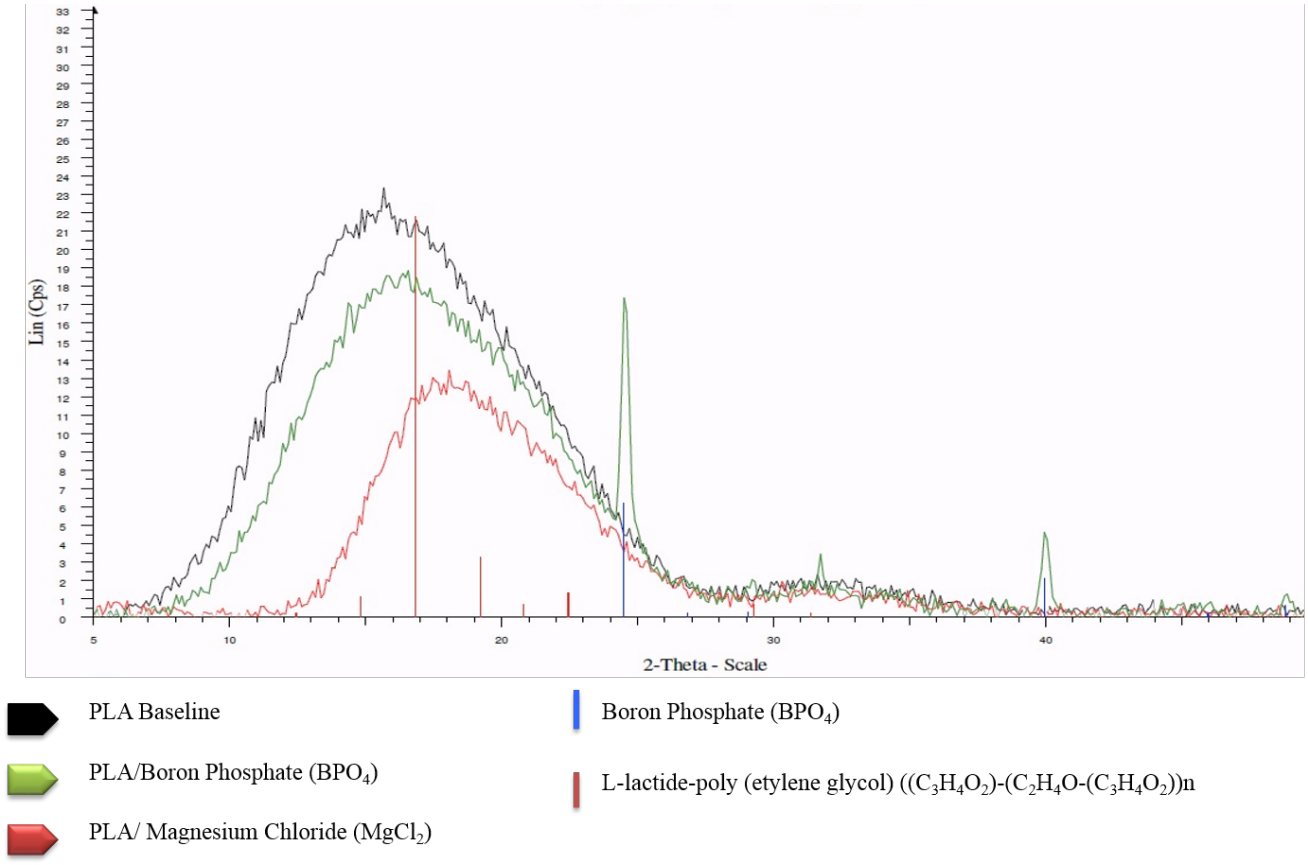

Figure 5.9 X-Ray Diffraction of PLA baseline and the inorganics $MgCl_2$ and BPO_4 filler materials

During the XRD analysis of the PLA/ $MgCl_2$ blend no specific or special procedure was followed, which could be the reason that no peak was found in the XRD spectra of this specific material. Zhang *et al*., has reported a special treatment before taking any lecture of this specific inorganic filler due to elevate material hygroscopocity [79]. Detected patterns for the inorganic BPO_4 were detected at ±2θ of 25 and 40°.

5.4. Melt Flow Index Study

As an additional test to examine the influence of the fillers previously aforementioned on the PLA resin and to evaluate their flow behavior properties of these materials a melt flow test was

performed using a MP1200M Extrusion plastometer melt flow indexer (Tinius Olsen, Horsham, PA, USA). All of the materials were tested following a detailed procedure based on the ASTM D1238 standard. The mass of the resin (≈ 8g) was extruded in 10 minutes the resulting value is commonly called the melt flow rate (MFR), melt index (MI), or melt-flow index (MFI). This test measures the melt viscosity or flow resistance of the polymer at particular shear stress (related to the applied load) and temperature [80].

Table 5.4 Melt flow index test parameters

Material	Melt flow rate (g/ 10 min)	Temperature (°C)	Test Load (Kg)
CONTROL (PLA BASELINE)	**6**	**210**	**2.16**
PLA Baseline	6.7	210	2.16
PLA/ SALT 5%	26	210	2.16
PLA/ SALT 10%	35.5	210	2.16
PLA/ SALT 15%	36	210	2.16
PLA/ SALT 20%	40.7	210	2.16
PLA/ MgCl2 5%	8	150	2.16
PLA/ BPO4 5%	26	210	2.16
PLA/ MAYAN YELLOW 5%	14	210	2.16
PLA/ MAYAN BLUE 5%	28	210	2.16
PLA/ FUNCT WITH SALT JUTE FIBER 5%	15.2	210	2.16
PLA/ FUNCT WITH CHEM SILANE	14.85	210	2.16
PLA/ JUTE FIBER 5%	17.62	210	2.16
PLA/ CARBON. JUTE FIBER 5%	34.5	210	2.16
PLA/ FUNCT. JF WITH SALT/ MB 2.5%	14	210	2.16
PLA/ FUNCT. JF WITH SALT/ MYW 2.5%	27.3	210	2.16

5.5. Discussion and Conclusion

The resulted compounded materials systems were obtained by altering the physical properties of the biopolymer with the addition of sustainable additives. On this Chapter melt compounding was used to combine PLA with fourteen different systems results for all the systems showed an apparent difference in physical properties observed as compared to PLA alone. Explored in deepest detail was the effect of the addition of NaCl to PLA with and without a particle refinement treatment. Results after the particle refinement showed a decrease UTS tendency when the salt concentration increases. Moreover, the incorporation of jute fiber was explored on detailed. Results of the jute fibers systems lead to a slight increment on the UTS for the functionalized jute fiber with

NaCl and slightly higher for the carbonized jute fiber system and even more in the functionalized jute fiber with silane. However, the percentage elongation at break was higher for the non-functionalized jute fiber system. During the addition of all material fillers, the mechanical properties of the PLA material were affected decreasing the yield strength of the material. However, over all the other systems Boron Phosphate was the filler that had the lower impact on the UTS recorded results. Even though, fracture surfaces analyses showed a poor attachment of the filler into the matrix. A possible hypothesis is that the inorganic filler had a chemical effect on the PLA matrix. However, more research is needed to clarify our assumptions and possible evaluations of the filler in the matrix at different wt. percentages.

In respect to both tri-blend systems the combination of these three materials decreases the ultimate strength properties of the biopolymer. Anisotropy studies were performed in order to measure the percentage decrease in strength due to raster sensibility when the tensile specimens were fabricated on the ZXY directions. Results exhibited a negative anisotropy for the PLA/ $MgCl_2$ and the tri-blend based on Mayan Yellow® systems.

Fractography of tensile specimen's surfaces revealed NaCl to adhere well to the PLA matrix, as there was no evidence of particle pullout. The strength of the bond between NaCl and PLA was also exhibited by evidence of crack front propagation shared between the NaCl particle and the surrounding matrix. The addition of MayaCrom® pigments had the effect of provoking voids within the PLA matrix which influence for the decrease in tensile strength as compared to baseline samples. Additional exploration of the benefit of combining PLA with NaCl was observed through the functionalization of jute plant fiber with aqueous NaCl. The use of palygorskite-based organo-nanoclay pigments also shows potential in playing a role in future PLA based 3D printable material systems.

Crystallinity analyses were performed on almost all materials systems to evaluate the influence of compounded PLA/ filler materials. Sodium Chloride was the filler with higher crystallinity when mixed to PLA. $MgCl_2$ did not present any crystallinity this could be due to the

high hygroscopic property of this inorganic material. Complementary melt flow tests were performed on the material systems to measure the viscosity of the materials systems. All the systems exhibited an increase on the viscosity being the compounded PLA/ salt 20% the highest value. Several aspects of this work allow the need for future study such as the increase in crystallinity observed after the addition of some filler materials. Also, the percentage decrease in strength due to raster sensibility for the PLA/ $MgCl_2$ and the tri-blend based Mayan Yellow® pigment systems.

CHAPTER 6: CRYSTALLINITY AND BIODEGRADABILITY

Approximately 4% of the world's oil and gas production is used as a feedstock for plastic production. Non- renewable petroleum based plastics remain in the environment for long periods of time after disposal. As a consequence, these types of materials are not the best choice for short time disposable products; an illustrative example is register in China in which 4 million personal computers are discarded per year [81]. With important environmental regulations over the world, plastic recycling has been used in larger scales recently. Recycling diminish the oil consumption, waste disposal and carbon dioxide emissions.

However, recycling is not an easy process, there are many types of discarded plastic that cannot recycled together due to their complexity, plastics are often in contact with external substances such as food or biological matter making them harder to recycle and undesirable for the environment[45]. Also, the facilities required for recycling are not always regulated. Rudimentary recycling methods such as: open incineration of plastics and wires, mechanical recycling of electronics, and chemical acid treatments have contributed to the release hazardous dioxins and heavy metals that have caused aquatic, air, soil and dust contamination [81]. Moreover, a high-energy consumption is required for the industrial recycling process of plastics.

On the other hand, biodegradable polymers are produced from natural resources such as corn crops or soybeans, which facilitate its degradation by organism assistance. Some of these types of polymers can help to solve the current plastic waste pollution by removing plastic products from the waste stream [45].

PLA is a sustainable alternative to petro-chemical based plastics; it has captivated significant interest for applications in different areas of our modern society such as 3D printing, medicine, packaging and consumer goods sector among others. Beyond, its excellent mechanical properties, transparency, its bio renewable profile and compostability PLA has also promised potential degradation properties [68].

As reported by Shah *et al*., [82] biodegradation is the enzymatic break down assisted by biological activity, resulting in an important change in the chemical structure of the exposed material and resulting in the production of carbon dioxide (CO_2), water (H_2O), mineral salts and new microbial components (solid biomass). Biodegradation can take place in two different conditions: aerobic in the presence of oxygen and anaerobic without oxygen.

PLA can be degraded under soil or compost conditions, this attractive characteristic could help to solve many solid contamination problems, since the final products made of this material can be disposable to composting and degrade, eventually this important characteristic could help to solve and or diminish the current plastic contamination issue. However, it is necessary to evaluate this material, such as its behavior during composting, involving the principal causes that affect the biodegradation phenomena.

6.1. Biodegradation of Poly lactic acid biopolymer

Usually, grades of commercial PLA are copolymers of poly (L-lactide) (PLLA), poly (D-lactide) (PDLA) and the equimolar poly (DL-lactide). Some physical properties of PLA such as crystallinity arrangement, molecular weight and melting properties are affected by the D- lactide content [68].

PLA is a polymer made of macromolecular chains of lactic acid. The first step to biodegrade this material is to break down the lactic chains (molecular reduction) with a hydrolysis process that is usually done with the assistance of heat and moisture. PLA contains polar oxygen linkages, which are responsible for its hydrophilic behavior resulting in increasing the rate of material decomposition if it exposed to environmental conditions (moisture and temperature). The microorganisms presented in the composting conditions then consume the resulting break down products resulting in lactic acid fragments, oligomers and other water-soluble products [83].

However, the degradation of PLA under composting conditions is affected by many factors such as crystallinity, purity, temperature, molecular weight, pH, water permeability the presence of

polar linkages and microorganisms, enzymes, or organic fillers may or may not incentive the PLA degradation. There is no way to simulate the degradation of this material using laboratory experiments. In order to determine the compostability of the material is necessary to achieve the degradation methods.

As aforementioned PLA properties are related to the presence copolymers rate. According to Pantani *et al*., [68] the degradation rate of PLA depends by the L unit content. They also related the morphology of the material on the degradation of PLLA under aqueous conditions, resulting in lower degradation for the samples with higher crystallinity order. Agreeing to Nampoothiri *et al*., [84] the high crystallinity of PLA presents a challenge in reducing its application as biodegradable bio-plastic material.

6.2. Experimental Details

The aim of the presented work was to test the PLA matrix and PLA materials systems degradation under composting conditions. Two specimens of each system were printed in order to compare between annealed and not annealed samples this with the end of test how crystallinity affects the biodegradation rate of the materials systems under certain composting conditions, complementary data from Chapter 5 (X- Ray Diffraction and Tensile tests data).

Before performing X-Ray diffraction analysis one of the two samples of each material system was annealed in an oven at 120 °C during 20 minutes. According to Nature Works technical sheet data, optimum crystallization temperatures depend on the grade, for this specific grade chosen with low D isomer content, the material can be crystallized at 100- 110 °C [85].

6.3. Controlled Compost

Biodegradation studies were performed in a homemade compost facility provided by Dr. Steven Stafford. Compost conditions were selected by following the ASTM standard D5338 test for biodegradation and other external research literature. The speed of degradation depends on;

temperature, humidity, number and type of microbes, morphology of the materials system, molecular weight and the possible influence of the fillers in to the PLA matrix material.

- Initially, the compost was watering before the samples were placed on the ground
- The PLA samples (16 annealed and 16 not annealed) will be placed on the compost and completely covered
- The samples were buried approximately at 12- 20 inches above the ground
- The compost was watered on top after the samples were buried
- Buried for 5 weeks (Feb 29th-April 5th)

External atmosphere parameters such as temperature, relative humidity, and solar radiation may affect the performance of the composting process were also recorded.

Figure 6.1 The annealed samples were marked with a pink tag in order to be able to differentiate them.

6.4. External Environmental Parameters

During the time of the samples were grounded on the compost pile, external weather conditions were monitored to have approximate ideal conditions for the degradation to occur. The composting pile was watered regularly in order to maintain a high percentage of moisture and to allow the microorganisms to act. Data on the mean daily air temperature and the amount of rainfall

during the experimental period (March 2016) were obtained from the meteorological National Weather service web site.

El Paso is located in the Chihuahuan Desert of exciting western Texas, along the Rio Grande River. It connects both the state of New Mexico and the country of Mexico with the Franklin Mountains.

Figure 6.2 El Paso Location [86]

El Paso has a dry climate due to its location and enjoys clear sunny days most of the year. However, El Paso also has a cold desert climate. The report used for this research includes average data collected by the International Airport at El Paso TX weather station from March 1974 to 2012. Results are shown on the following tables [87].

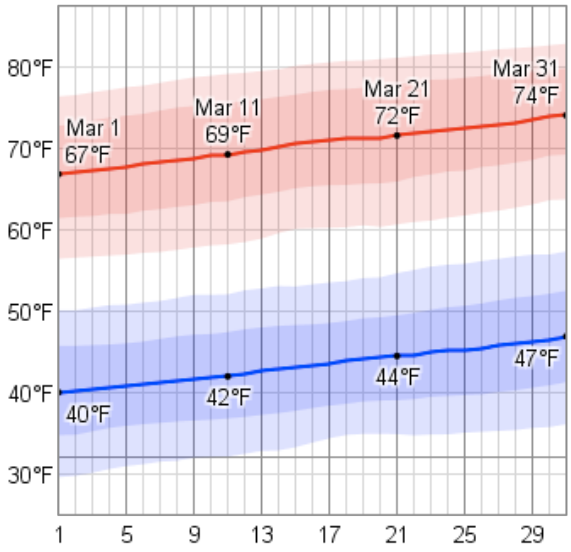

Figure 6.3 Daily low average temperatures are indicated with the blue color and high average temperatures are indicated with red [87]

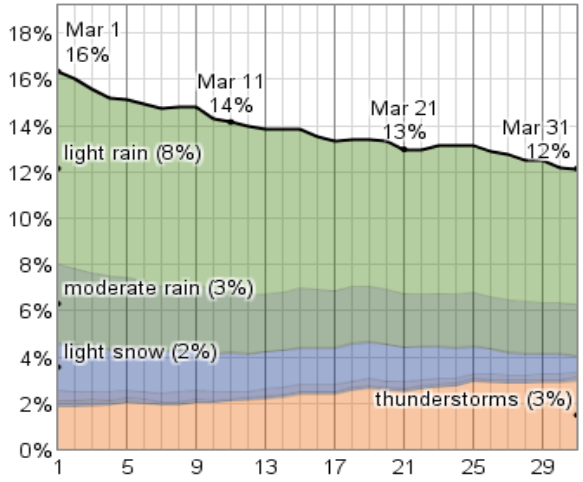

Figure 6.4 The probability that precipitation will be detected at this location fluctuates throughout the month. Precipitation is most likely around March 1, occurring in 16% of days. Precipitation is least expected around March 31, occurring in 12% of days [87]

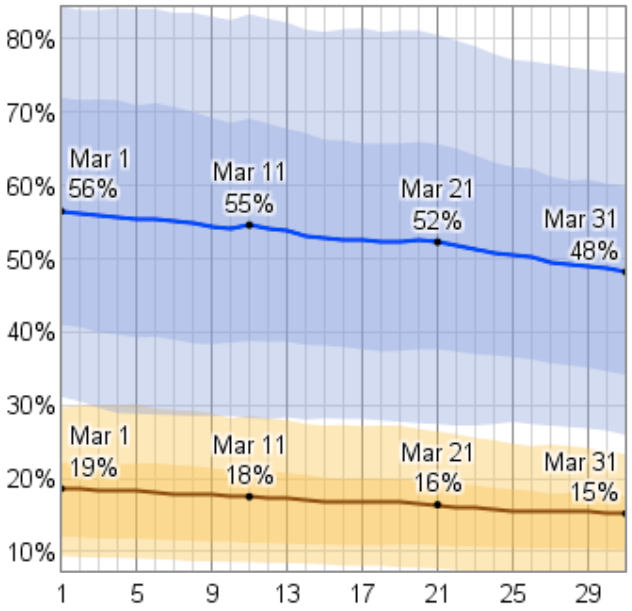

Figure 6.5 Average daily high (blue) and low (brown) relative humidity with percentile bands [87]

6.5. Mechanical Properties

The different behavior of the PLA baseline and the other materials systems to biodegradation in the presence of compost was supported by the mechanical properties of the materials systems. This specific study was developed with the end to compare and understand the rate of biodegradation for PLA and the created systems. Unfortunately, not all the samples could be tested during this analysis. Our assumptions are that some of the samples got lost under the compost degradation pile or even some of them actually biodegraded.

With the purpose of obtaining more reliable results the same normalization study previously explained was carried after the samples were taken from the compost facilities. Results (Table 6.1) showed that the sample tested which had the most significance changes on UTS after the degradation was the annealed salt at 15% loading presenting the highest percentage with an approximate 51% decrease in UTS values. However, data for the not annealed sample could not be obtained. It is believed that this sample was disintegrated under the compost conditions, since the rate of degradation for samples with lower crystallinity is higher. Followed by the tri-blend based on Mayan Blue with an approximate 36% decrease on UTS value was also observed for the not annealed sample, contradictory to the biodegradation crystallinity principle. However, an important change occurred as well for the non-annealed sample.

A most important change was found for the BPO_4, which had an important decrease of approximately 45% decrease on its UTS values for the not annealed sample and 26% for the annealed sample. The percentage decrease for both samples composed of PLA and BPO_4 follow the principle that posits the higher crystallinity the less biodegradability.

Apart from these systems almost all the other samples showed a decrease on their UTS values after were buried in the compost facilities, with the exception of the both systems based on MayaCrom® Yellow filler (the annealed tri-blend system and the not annealed PLA/ MayaCrom® Yellow) and the not annealed and annealed PLA/ Mayan MayaCrom® Blue, in those systems the UTS even increase after the biodegradation test.

Just as an extra point the annealed sample for the $MgCl_2$ was obtained from the compost facilities. However, the sample was extremely fragile, when its mechanical properties were intended to be measured the sample break down before any data could be obtained. Tough, it was observed a change in color, appearance and possible dimensional changes on the sample after the degradation study. Regarding the PLA baseline not annealed sample a little decrease on the UTS value was noted after the degradation study. As a result, can be concluding that our fillers are somewhat increasing the rate of biodegradation of the PLA material by itself. Most remarkable biodegradation rate can be hence with the help of sodium chloride filler at 15 percentages loadings.

Table 6.1 UTS for the samples after compost treatment, showing the percentage decrease on UTS values

	NORMALIZED UTS MPa				
Material	**BEFFORE THE ANALYSES**	**AFTER DEGRADATION**		**% DECREASE IN UTS**	
		NOT ANNEALED	**ANNEALED**	**NOT ANNEALED**	**ANNEALED**
PLA	62.84224916	62.63105063	-	-0.337210576	-
PLA/ SALT 5% NO MILL	58.26617552	48.32883343	50.85967152	-20.56193247	-12.71149845
PLA/ SALT 5%	52.67490364	-	-	-	-
PLA/ SALT 10%	52.99455518	41.93577527	49.59473898	-26.37075346	-6.41540662
PLA/ SALT 15%	47.40403252	-	23.21880624	-	-51.01934371
PLA/ SALT 20%	42.93203183	-	36.83247423	-	-14.2074748
PLA/ $MgCl_2$ 5%	44.56880149	-	-	-	-
PLA/BPO_4 5%	52.92482862	36.53276119	39.15340951	-44.86950039	-26.02071555
PLA/MAYAN YELLOW	51.80684757	53.93766736	45.00404981	3.950522698	-13.13107837
PLA MAYAN BLUE	47.09790348	47.85417644	49.87911183	1.580369795	5.905163799
PLA/JUTE FIBER 5%	46.3660629	-	-	-	-
PLA/ JUTE FIBER FUNCT. W SALT	50.09833376	46.37573641	-	-8.027036648	-
PLA- CARBON JUTE FIBER 5%	44.11161823	39.69984139	-	-11.11283241	-
PLA/FUNCT.JF W SALT/ MYW 2.5%	47.29578743	43.73539495	54.97577958	-8.140757577	16.23821608
PLA/FUNCT.JF W SALT/ MB 2.5%	50.33605449	41.93617104	32.15131715	-20.03016309	-36.12666413

The following table (Table 6.2) summarizes the data of the systems tested. It was expected to have a bigger change on the PLA by itself however the decrease in UTS was just 0.33%. The systems that behave under the principle of higher crystallinity the less biodegradation were: the PLA/ salt 5% system without particle pre-processing, the PLA/ salt 10% after particle processing and the boron phosphate systems. The systems that exclude the principle of higher crystallinity lower biodegradation were: PLA/ Mayan Yellow, the PLA/ MayanCrom Blue and both the tri-blend systems. Overall in almost all the systems there were changes in the UTS values on the tested

materials systems. But, there some results that had a different impact that was expected even increasing their UTS values after the degradation conditions they were: both binary blends of PLA with the MayaCrom® pigments and the tri-blend based on MayaCrom® yellow.

Table 6.2 Summary of the expected results and the results obtained after the biodegradation study

% CHANGES IN UTS AFTER BIODEGRADATION (NORMALIZED DATA)

Decrease in MP after BD	*Higher crystallinity the less BD*	*Crystallinity not influence in BD*	*Increase on MP after BD*
PLA BASELINE	PLA/ SALT 5% NO MILL	PLA/MAYAN YELLOW	PLA/MAYAN YELLOW (NOT ANNEALED)
PLA/ SALT 5% NO MILL	PLA/ SALT 10%	PLA/MAYAN BLUE	PLA MAYAN BLUE
PLA/ SALT 10%	PLA/BPO_4 5%	TRI-BLEND MY	TRI-BLEND MY (ANNEALED)
PLA/BPO4 5%		TRI-BLEND MB	
PLA/ SALT 15%			
PLA/ SALT 20%			
PLA/MAYAN YELLOW			
PLA/ JUTE FIBER FUNCT. W SALT			
PLA- CARBON JUTE FIBER 5%			
TRI-BLEND MY (NOT ANNEALED)			
TRI-BLEND MB			

6.6. Discussion and Conclusion

One of the most interesting of features of PLA is the fact that can be biodegradable in soil or compost and the products made by this material at the completion of their life cycle can be diverted from landfill to composting. However, the literature survey showed that very little is known about the degradation of PLA under composting conditions.

Chemical and biological changes during composting depend on different factors such as: moisture percentage, number and type of microorganisms, molecular weight of the material used, degree of crystallinity, and the shape and dimensions of the tested samples. Overall, after the mechanical tests of the PLA matrix and the other material systems showed a decrease in the UTS values was recorded for almost all the systems available to test. Unexpectedly, the both binary

systems based on MayaCrom® pigments fillers and the tri-blend based MayaCrom® Yellow, showed a percentage increase on the UTS values after the biodegradation test. Regarding the PLA/ BPO_4 an important decrease on the UTS of the material was recorded for both not annealed and annealed samples after the degradation study. Remarkably, this was also the system with the higher UTS before the degradation test overall other materials filler systems. According to Moffat *et al.*, [88] boron phosphate is highly used in the industry as dehydration catalyst mainly for organic synthesis. The catalytic activity of the inorganic material depends on different characteristics and conditions such as: the surface area, the available acid sites in the molecule, the number of available acid sites and the processing temperatures of the material. As a result, the degradation of the PLA may have hence by the help of the BPO_4 filler. However, two possible parameters could affect the complete degradation of this system: the temperatures were not high enough to enhance the activity of the catalyst or the time was not long enough to be decomposed under the used compost conditions.

Due to lack of availability to measure the internal conditions that may affect the compost used, the possible low percentage of moisture in the atmosphere, the fact that not all the samples could be tested and the lack of information of microorganisms presented on the compost as well the CO_2 fixation; we were not able to prove the higher degradation for materials with low-molecular weights (low percentage of crystallinity). However, we may have an important discover on the BPO_4 inorganic material which accelerate de biodegradation of all materials even when was also the material with better mechanical properties in conjunction to PLA before the crystallinity and degradation tests.

Other possible assumption could be that the printed samples of the systems with lower UTS had a decrease in strength due to a bad printing and the presence of air on the matrix of each material system.

CHAPTER 7: CONCLUIDING COMMENTS AND FUTURE WORK

The work presented here reviews one of the biggest challenges facing ME3DP technologies the limitation of the range of materials used by this technique. Acrylonitrile butadiene styrene (ABS) and poly-lactic acid (PLA) are currently the most common thermoplastics materials used in ME3DP. Due to the perceived health hazards of ABS and the increasing environmental problem of the constant increasing amount of plastics in oceans, landfills and the severe disruption of the ecosystems, the 3D printing community has the concern to create polymeric materials more environmentally sustainable. PLA offers an eco-friendly solution for polymeric 3D printing.

The purpose of this investigation was to alter the physical properties of PLA with sustainable additives in order to improve the end use products from this material. During the first four Chapters an analysis and evaluation of the possible effects of four filler/ fiber composites (analytical grade NaCl, MayaCrom® yellow, BPO_4 and jute fibers) on the PLA matrix was done by an established method from the selection and processing of the materials, to the evaluation, testing and analysis of the final parts. Viscoelastic, moisture, mechanical and fracture analyses were performed on these systems. During the viscoelastic analysis the system compounded with the sodium chloride demonstrates an improvement of the viscoelastic behavior of the PLA material by itself, the MayaCrom® pigments decrease the viscosity of the PLA matrix, which could be an important benefit to ME3DP. Most remarkable results of fracture results showed that the salt particles showed a very good attachment to the PLA matrix and that the jute fiber and the MayaCrom® Yellow created voids on the matrix. During the moisture analysis an increase on the mechanical properties for PLA and PLA/ Jute fiber system was recorded, which is backwards of what is usually reported on the literature.

This combination of materials was more deeply investigated in Chapter 5, the same materials were tested varying the wt. percentages and with the change of the particle size for NaCl in order to test how the particle size influence on the mechanical properties of the matrix. Previous mechanical results showed a high percentage of elongation at break. However; the ultimate tensile test was very

low, for this reason a functionalization study by an aqueous ionic solution was performed, at the same time a functionalization process using chemicals was performed in order to compare between the eco-friendly and not eco-friendly process and how both affect the fiber attachment on the matrix and the UTS of the final systems. The jute fibers functionalized with the help of silanes showed the higher UTS result in comparison of those functionalized with the salt. Yet, the difference on these results was not very noticeable. Deeper analysis of the jute fiber was performed with a thermal treatment on the fibers, resulting on the best UTS results of the fibers into the matrix. All the systems tested presented a decrease on the mechanical properties of the matrix materials. Being the inorganic BPO_4 filler the one that did not had a big impact on the UTS of the PLA. However, a possible chemical bonding could take place between the PLA molecule and the boron and phosphate molecules. The creation of the tri-blend systems showed a decrease on the UTS values for the tri-blend based on MayaCrom Yellow compared to the previous UTS results recorded for binary PLA/ MayaCrom Yellow system. As a result, assumptions on the percentage air on the final fabricated parts were made.

In order to have more reliable results normalization analyses were carried out, in which it could prove that the decrease in UTS values for the final fabricated systems were primarily due to the presence of air gaps. Under a perfect scenario with a 100% infill density on the samples the UTS values of the PLA by itself could have been improved with the addition of the salt particles at 5% (unmilled and milled) salt 10% and salt 20% loadings. And the tri-blend system based on the MayaCrom® Yellow. Yet, these systems presented the higher percentage of air on the final fabricated parts. Future material evaluations in ME3DP still requires more precision during the building of the parts, a deeper analysis of the required parameters such as the infill density and how the temperature affects each specific material has to be adapted, taking care of minimal defects in the final fabricated part. On this chapter an extra tensile analysis of the final parts and the evaluation of the resulting anisotropy showed promising results for the inorganic $MgCl_2$ and the tri-blend system based on the MayaCrom® yellow, these results demonstrates a tendency in favor of the

combination of these materials with very low anisotropy. These systems could benefit in one of the most popular barriers presented on 3D printing.

During Chapter 6 a biodegradation study was performed on compost in order to know how crystallinity affects the rate of biodegradation of PLA and the other materials systems. Due to lack data and possible defects during the 3D printing (infill lower than 100%) no all the systems could be tested. However, a very important result was observed for the PLA/ BPO_4 system, which actually degraded after test, more shocking is the fact that this material was first registered to have the higher UTS value in comparison of the other fifteen systems. This correlates with the hypothesis of the possible chemical change was induced into the PLA molecule.

This work presented fifteen sustainable novel material systems based on the biopolymer PLA maintaining the compatibility to the 3D platforms avoiding the hazards fumes released by the most common materials used in 3D printing. Also, these systems promise important characteristics in the different evaluated methods used.

The PLA biopolymer in conjunction with sustainable fillers specially the inorganic BPO_4 and the systems with the ionic filler at different loadings need a deeper study that can help to degrade the plastic under normal compost conditions, with the lower effort possible, and the minimal environmental impact. This work offers a solution for the most demanded area of plastic production: packaging. The presented PLA/ BPO_4 system material can be an important environmental solution that will help to diminish the amount of plastics in oceans, landfills, etc. Still, more work is needed in order to understand the influence of the BPO_4 filler in the chemical and physical properties of the PLA material as well as a more detailed control on the compost parameters.

REFERENCES

[1] A. R. Torrado, ""“Defeating Anisotropy in Materials extrusion 3D printing via developing”," 2015.

[2] A. J. M. van Wijk and I. van Wijk. 3D Printing with Biomaterials: Towards a Sustainable and Circular Economy 2015Available: https://books.google.com/books?id=tEAoBgAAQBAJ.

[3] B. Imre, K. Renner and B. Pukánszky. Interactions, structure and properties in poly (lactic acid)/thermoplastic polymer blends. Express Polymer Letters 8(1), 2014.

[4] T. Hoffman. “3D printing: What you need to know”. PCmag. Com 2011. Available: http://www.pcmag.com/article2/0,2817,2394722,00.asp.

[5] D. Chang and B. Huang. Studies on profile error and extruding aperture for the RP parts using the fused deposition modeling process. The International Journal of Advanced Manufacturing Technology 53(9-12), pp. 1027-1037. 2011. Available: http://dx.doi.org/10.1007/s00170-010-2882-1. DOI: 10.1007/s00170-010-2882-1.

[6] Rohan, M. 2013. “3D Printing Materials Market Worth $408.5 Million by 2018.” December 6. http://www.prnewswire.com/news-releases/3d-printing-materials-market-worth-4085-million-by-2018-234728411.html.

[8] Sheppard, Kimberly. 2012. 3D Printing -Unabridged Guide. Emereo Publishing. http://www.ebookmall.com/ebook/3d-printing-unabridged-guide/kimberly-sheppard/9781486198726.

[9] Belter, Joseph T., and Aaron M. Dollar. "Strengthening of 3D printed fused deposition manufactured parts using the fill compositing technique." PloS one10, no. 4 (2015): e0122915.

[10] C. R. Rocha, A. R. Torrado Perez, D. A. Roberson, C. M. Shemelya, E. MacDonald and R. B. Wicker. Novel ABS-based binary and ternary polymer blends for material extrusion 3D printing. J. Mater. Res. 29(17), pp. 1859-1866. 2014.

[11] J. W. Nicholson, "Polymer chemistry," in The Chemistry of Polymers, Springer, Ed. 2006, pp. 1-22.

[12] Lever, L.L. 2000. ¨Crystallinity¨. Polymer Crystallinity.

http://faculty.uscupstate.edu/llever/Polymer%20Resources/Crystalline.htm#crystalshttp://www.pslc.ws/macrog/crystal.html.

[13] A. L. Andrady and M. A. Neal. Applications and societal benefits of plastics. Philosophical Transactions of the Royal Society of London B: Biological Sciences 364(1526), pp. 1977-1984. 2009. . DOI: 10.1098/rstb.2008.0304.

[14] A. C. S. (ASC). (March 31, 2016). Bakelite the World First Syntetic Plastic. Available: http://www.acs.org/content/acs/en/education/whatischemistry/landmarks/bakelite.html.

[15] R. Klein. Material properties of plastics. Laser Welding of Plastics: Materials, Processes and Industrial Applications pp. 3-69.

[16] C. K. Narula, J. E. Allison, D. R. Bauer and H. S. Gandhi. Materials chemistry issues related to advanced materials applications in the automotive industry. Chem. Mater. 8(5), pp. 984-1003. 1996. Available: http://dx.doi.org/10.1021/cm950588m. DOI: 10.1021/cm950588m.

[17] N. E. Dowling. Mechanical Behavior of Materials: Engineering Methods for Deformation, Fracture and Fatigue (3rd ed.) 2007.

[18] G. E. Village. (2/25/2015). Advantages of Plastic over Metal - Custom Plastics, Inc.

[19] B. Wood, ""“Plastics Industry enters 2015 on a high note, numbers that matters”", 2015.

[20] Grand View Research. (June 2015). Plastic Compounding Market Size | Industry Report, 2022.

[21] C. R. Álvarez-Chávez, S. Edwards, R. Moure-Eraso and K. Geiser. Sustainability of bio-based

plastics: General comparative analysis and recommendations for improvement. J. Clean. Prod. 23(1), pp. 47-56. 2012. DOI: http://dx.doi.org/10.1016/j.jclepro.2011.10.003.

[22] Oon, Hock Leong, Ang, Edmund Joon Aik, Khoo, Lian Ee.,. Chemistry Expression: An Inquiry Approach.2007.

[23] Plastics Europe, "Plastics- champions of sustainable growth and innovation in europe," Plastics Europe, Brussels, Belgium, 2012.

[24] D. K. A. Barnes, F. Galgani, R. C. Thompson and M. Barlaz. Accumulation and fragmentation of plastic debris in global environments. Philos Trans R Soc Lond B Biol Sci 364(1526), pp. 1985-1998. 2009. DOI: 10.1098/rstb.2008.0205.

[25] J. Knoblauch. Plastic not-so-fantastic: How the versatile material harms the environment and human health. 2009. Available: http://www.scientificamerican.com/article/plastic-not-so-fantastic/.

[26] D. Crowley, A. Staines, C. Collins, J. Bracken, M. Bruen, J. Fry, V. Hrymak, D. Malone, B. Magette and M. Ryan. Health and environmental effects of landfilling and incineration of waste-A literature review. 2003.

[27] M. Allsopp, A. Walters, D. Santillo and P. Johnston. (2005). Plastic Debris in the World´s Oceans.

[28] C. Michael. (2014-05-06T11:34:48+00:00). Microplastics in the Environment - Bio-based News - The portal for bio-based economy and industrial biotechnology.

[29] M. Sesini. The garbage patch in the oceans: The problem and possible solutions. 2011.

[30] Le Guern, Claire. 2009. “Plastic Pollution.” Plastic-Pollution.org. http://plastic-pollution.org/.

[31] U.S Department Commerce. 2016. “| OR&R’s Marine Debris Program.” Great Pacific Garbage Patch. April 8. http://marinedebris.noaa.gov/info/patch.html. [32] P. Kershaw, S. Katsuhiko, S. Lee, J. Samseth and D. Woodring. Plastic debris in the ocean.

[32] Schuyler, Qamar, Britta Denise Hardesty, Chris Wilcox, and Kathy Townsend. 2012. “To Eat or Not to Eat? Debris Selectivity by Marine Turtles.” Edited by Graeme Clive Hays. PLoS ONE 7 (7): e40884. doi:10.1371/journal.pone.0040884.

[33] M. Niaounakis. "2 - definitions and assessment of (bio) degradation," in Biopolymers Reuse, Recycling, and Disposal, M. Niaounakis, Ed. 2013, . DOI: http://dx.doi.org/10.1016/B978-1-4557-3145-9.00002-6.

[34] F. Esposito. «Despite its history, bioplastics remains a niche industry,» plastics news, 6 august 2014. 2014.

[35] Y. Tokiwa, B. P. Calabia, C. U. Ugwu and S. Aiba. Biodegradability of plastics. 10(9), pp. 3722-3742. 2009. DOI: 10.3390/ijms10093722.

[36] M. M. Reddy, S. Vivekanandhan, M. Misra, S. K. Bhatia and A. K. Mohanty. Biobased plastics and bionanocomposites: Current status and future opportunities. Progress in Polymer Science 38(10–11), pp. 1653-1689. 2013. . DOI: http://dx.doi.org/10.1016/j.progpolymsci.2013.05.006.

[37] H. M. Koch and A. M. Calafat. Human body burdens of chemicals used in plastic manufacture. Philosophical Transactions of the Royal Society of London B: Biological Sciences 364(1526), pp. 2063-2078. 2009. Available: http://rstb.royalsocietypublishing.org/content/364/1526/2063.abstract.

[38] J. D. Meeker, S. Sathyanarayana and S. H. Swan. Phthalates and other additives in plastics: Human exposure and associated health outcomes. Philosophical Transactions of the Royal Society of London B: Biological Sciences 364(1526), pp. 2097-2113. 2009. Available: http://rstb.royalsocietypublishing.org/content/364/1526/2097.abstract.

[39] J. Oehlmann, U. Schulte-Oehlmann, W. Kloas, O. Jagnytsch, I. Lutz, K. O. Kusk, L. Wollenberger, E. M. Santos, G. C. Paull, Van Look, Katrien J. W. and C. R. Tyler. A critical analysis of the biological

impacts of plasticizers on wildlife. Philosophical Transactions of the Royal Society of London B: Biological Sciences 364(1526), pp. 2047-2062. 2009. Available: http://rstb.royalsocietypublishing.org/content/364/1526/2047.abstract.

[40] C. E. Talsness, A. J. M. Andrade, S. N. Kuriyama, J. A. Taylor and F. S. vom Saal. Components of plastic: Experimental studies in animals and relevance for human health. Philosophical Transactions of the Royal Society of London B: Biological Sciences 364(1526), pp. 2079-2096. 2009. Available: http://rstb.royalsocietypublishing.org/content/364/1526/2079.abstract.

[41] R. C. Thompson, C. J. Moore, F. S. vom Saal and S. H. Swan. Plastics, the environment and human health: Current consensus and future trends. Philosophical Transactions of the Royal Society of London B: Biological Sciences 364(1526), pp. 2153-2166. 2009. Available: http://rstb.royalsocietypublishing.org/content/364/1526/2153.abstract.

[42] J. V. Rutkowski and B. C. Levin. Acrylonitrile–butadiene–styrene copolymers (ABS): Pyrolysis and combustion products and their toxicity—a review of the literature. Fire Mater. 10(3- 4), pp. 93-105. 1986.

[43] B. Stephens, P. Azimi, Z. El Orch and T. Ramos. Ultrafine particle emissions from desktop 3D printers. Atmos. Environ. 79(0), pp. 334-339.2013. DOI: http://dx.doi.org/10.1016/j.atmosenv.2013.06.050.

[44] K.-L. G. Ho, A. L. Pometto, A. Gadea-Rivas, J. A. Briceño, and A. Rojas. Degradation of polylactic acid (PLA) plastic in Costa Rican soil and Iowa state university compost rows. Journal of Polymers and the Environment vol. 7, no. 4(- 4), pp. 173-177. 1999. DOI: - 10.1023/A:1022874530586.

[45] R. A. Gross and B. Kalra. Biodegradable polymers for the environment. 297(5582), pp. 803-807. 2002. DOI: 10.1126/science.297.5582.803.

[46] I. Tyler. (August 2013). The many faces of bioplastics | The Chemical Institute of Canada.

[47] E. T. H. Vink, K. R. Rábago, D. A. Glassner and P. R. Gruber. Applications of life cycle assessment to NatureWorks™ polylactide (PLA) production. Polym. Degrad. Stab. 80(3), pp. 403-419. 2003. . DOI: http://dx.doi.org/10.1016/S0141-3910(02)00372-5.

[48] M. A. Huneault and H. Li. Morphology and properties of compatibilized polylactide/thermoplastic starch blends. Polymer 48(1), pp. 270-280. 2007.

[49] K. Marsh and B. Bugusu. Food packaging—roles, materials, and environmental issues. J. Food Sci. 72(3), pp. R39-R55. 2007.

[50] C. Bach, X. Dauchy, M. Chagnon and S. Etienne. Chemical compounds and toxicological assessments of drinking water stored in polyethylene terephthalate (PET) bottles: A source of controversy reviewed. Water Res. 46(3), pp. 571-583. 2012. . DOI: http://dx.doi.org/10.1016/j.watres.2011.11.062.

[51] C. M. B. - Gonçalves, J. A. P. - Coutinho and I. M. - Marrucho. - Optical properties. pp. - 97. . DOI: - 10.1002/9780470649848.ch8.

[52] J. Kaiser. The dirt on ocean garbage patches. Science 328(5985), pp. 1506. 2010. DOI: 10.1126/science.328.5985.1506 [doi]

[53] S. Morét-Ferguson, K. L. Law, G. Proskurowski, E. K. Murphy, E. E. Peacock and C. M. Reddy. The size, mass, and composition of plastic debris in the western North Atlantic Ocean. Mar. Pollut. Bull. 60(10), pp. 1873-1878. 2010.

[54] S. L. Dautel. Transoceanic trash: International and United States strategies for the great pacific garbage patch. Golden Gate University Environmental Law Journal 3(1), pp. 8. 2010.

[55] K. J. McDermid and T. L. McMullen. Quantitative analysis of small-plastic debris on beaches in the hawaiian archipelago. Mar. Pollut. Bull. 48(7–8), pp. 790-794. 2004. . DOI: http://dx.doi.org/10.1016/j.marpolbul.2003.10.017.

[56] J. G. B. Derraik. The pollution of the marine environment by plastic debris: A review. Mar. Pollut. Bull. 44(9), pp. 842-852. 2002. . DOI: http://dx.doi.org/10.1016/S0025-326X(02)00220-5.

[57] P. G. Ryan, C. J. Moore, J. A. van Franeker and C. L. Moloney. Monitoring the abundance of plastic debris in the marine environment. Philos. Trans. R. Soc. Lond. B. Biol. Sci. 364(1526), pp. 1999-2012. 2009. DOI: 10.1098/rstb.2008.0207.

[58] H. Hirai, H. Takada, Y. Ogata, R. Yamashita, K. Mizukawa, M. Saha, C. Kwan, C. Moore, H. Gray and D. Laursen. Organic micropollutants in marine plastics debris from the open ocean and remote and urban beaches. Mar. Pollut. Bull. 62(8), pp. 1683-1692. 2011.

[59] A. Drizo and J. Pegna. Environmental impacts of rapid prototyping: An overview of research to date. Rapid Prototyping Journal 12(2), pp. 64-71. 2006.

[60] L. A. Niewold and A. R. Caro. High Strength Polymer Compositions Containing Hybrid Organic/Inorganic Pigments 2009.

[61] E. Stellrecht, B. Han and M. G. Pecht. Characterization of hygroscopic swelling behavior of mold compounds and plastic packages. Components and Packaging Technologies, IEEE Transactions On 27(3), pp. 499-506. 2004. DOI: 10.1109/TCAPT.2004.831777.

[62] N. Peelman, P. Ragaert, B. De Meulenaer, D. Adons, R. Peeters, L. Cardon, F. Van Impe and F. Devlieghere. Application of bioplastics for food packaging. Trends Food Sci. Technol. 32(2), pp. 128-141. 2013. . DOI: http://dx.doi.org/10.1016/j.tifs.2013.06.003.

[63] Perkin Elmer, "Dynamical Mechanical Analysis (DMA), "A begginers guide", 2008.

[64] W. Wang, M. Sain and P. A. Cooper. Study of moisture absorption in natural fiber plastic composites. Composites Sci. Technol. 66(3–4), pp. 379-386. 2006. DOI: http://dx.doi.org/10.1016/j.compscitech.2005.07.027.

[65] Umetani, Nobuyuki, and Ryan Schmidt. "Cross-sectional structural analysis for 3d printing optimization." SIGGRAPH Asia 5 (2013): 1-4.

[66] A. R. Torrado, C. M. Shemelya, J. D. English, Y. Lin, R. B. Wicker and D. A. Roberson. Characterizing the effect of additives to ABS on the mechanical property anisotropy of specimens fabricated by material extrusion 3D printing. Additive Manufacturing 6pp. 16-29. 2015.

[67] A. R. T. Perez, D. A. Roberson and R. B. Wicker. Fracture surface analysis of 3D-printed tensile specimens of novel ABS-based materials. Journal of Failure Analysis and Prevention 14(3), pp. 343-353. 2014.

[68] R. Pantani and A. Sorrentino. Influence of crystallinity on the biodegradation rate of injection-moulded poly(lactic acid) samples in controlled composting conditions. Polymer Degradation and Stability 98(5), pp. 1089-1096. 2013. . DOI: 10.1016/j.polymdegradstab.2013.01.005.

[69] H. Ma and C. W. Joo. Structure and mechanical properties of jute-polylactic acid biodegradable composites. J. Composite Mater. pp. 0021998310382316. 2010.

[70] J. Gassan and A. K. Bledzki. Thermal degradation of flax and jute fibers. J Appl Polym Sci 82(6), pp. 1417-1422. 2001.

[71] M. M. Kabir, H. Wang, K. T. Lau and F. Cardona. Chemical treatments on plant-based natural fibre reinforced polymer composites: An overview. Composites Part B: Engineering 43(7), pp. 2883-2892. 2012. DOI: http://dx.doi.org/10.1016/j.compositesb.2012.04.053.

[72] N. Sharmin, A. J. Parsons, C. D. Rudd and I. Ahmed. Effect of boron oxide addition on fibre drawing, mechanical properties and dissolution behaviour of phosphate-based glass fibres with fixed 40, 45 and 50 mol % P2O5. J. Biomater. Appl. 29(5), pp. 639-653. 2014. DOI: 10.1177/0885328214539824 [doi].

[73] L. Lim, R. Auras and M. Rubino. Processing technologies for poly (lactic acid). Progress in Polymer

Science 33(8), pp. 820-852. 2008.

[74] Lampman, Steve. Characterization and failure analysis of plastics. ASM International, 2003.

[75] D. A. Roberson, C. R. Rocha and M. Piñon. 2015. Evaluation of 3D printable sustainable composites. Conference paper.

[76] J. A. Castillo, D. E. Borchmann, A. Y. Cheng, Y. Wang, C. Hu, A. J. García and M. Weck. Well-defined poly (lactic acid) s containing poly (ethylene glycol) side chains. Macromolecules 45(1), pp. 62-69. 2011.

[77] Tabi, T., I. E. Sajó, F. Szabó, A. S. Luyt, and J. G. Kovács. "Crystalline structure of annealed polylactic acid and its relation to processing." Express Polym Lett 4, no. 10 (2010): 659-668.

[78] M. Kabir, H. Wang, T. Aravinthan, F. Cardona and K. Lau. Effects of natural fibre surface on composite properties: A review. Presented at Proceedings of the 1st International Postgraduate Conference on Engineering, Designing and Developing the Built Environment for Sustainable Wellbeing (eddBE2011). 2011, .

[79] Z. Zhang, X. Lu, F. Pan, Y. Wang and S. Yang. Preparation of anhydrous magnesium chloride from magnesium chloride hexahydrate. Metallurgical and Materials Transactions B 44(2), pp. 354-358. 2013.

[80] Tiniuos Olsen, (August 2012). Melt Flow Indexer- MP 1200 Specifications. Available: http://www.tiniusolsen.com/list-of-products/mp-1200.

[81] G. H. Xing, J. K. Y. Chan, A. O. W. Leung, S. C. Wu and M. H. Wong. Environmental impact and human exposure to PCBs in guiyu, an electronic waste recycling site in china. Environment International 35(1), pp. 76-82. 2009. DOI: 10.1016/j.envint.2008.07.025.

[82] A. A. Shah, F. Hasan, A. Hameed and S. Ahmed. Biological degradation of plastics: A comprehensive review. Biotechnol. Adv. 26(3), pp. 246-265. 2008.

[83] A. Subhani. Influence of the processes parameters on the properties of the polylactides based bio and eco-biomaterials. 2011.

[84] K. Madhavan Nampoothiri, N. R. Nair and R. P. John. An overview of the recent developments in polylactide (PLA) research. Bioresource Technology 101(22), pp. 8493-8501. 2010. . DOI: 10.1016/j.biortech.2010.05.092.

[85] NatureWorks, "Ingeo TM biopolymer 4043D technical data sheet." NatureWorks LLC, USA, Tech. Rep. NW4043D_051815V1, 2002.

[86] Weather Spark (21 March 2016). The Weather Channel El Paso TX March 2016. Available: https://weather.com/weather/weekend/l/USTX0413:1:US.

[87] Weather Spark (From 1974 to 2012). Average Weather in March for El Paso TX, USA. Available: https://weatherspark.com/averages/30173/3/El-Paso-Texas-United-States.

[88] J. Moffat and H. Goltz. Surface chemistry and catalytic properties of boron phosphate: 1. Surface area and acidity. Canadian Journal of Chemistry 43(6), pp. 1680-1688. 1965.

CAMBRIDGE UNIVERSITY PRESS LICENSE TERMS AND CONDITIONS

May 02, 2016

This Agreement between Carmen R Rocha ("You") and Cambridge University Press ("Cambridge University Press") consists of your license details and the terms and conditions provided by Cambridge University Press and Copyright Clearance Center.

License Number	3846020846496
License date	Apr 11, 2016
Licensed Content Publisher	Cambridge University Press
Licensed Content Publication	Journal of Materials Research
Licensed Content Title	Novel ABS-based binary and ternary polymer blends for material extrusion 3D printing
Licensed Content Author	Carmen R. Rocha, Angel R. Torrado Perez, David A. Roberson, Corey M. Shemelya, Eric MacDonald and Ryan B. Wicker
Licensed Content Date	Jul 28, 2014
Licensed Content Volume Number	29
Licensed Content Issue Number	17
Start page	1859
End page	1866
Type of Use	Dissertation/Thesis
Requestor type	Author
Portion	Full article
Author of this Cambridge University Press article	Yes
Author / editor of the new work	Yes
Order reference number	None
Territory for reuse	World
Title of your thesis / dissertation	Improving the Engineering properties of PLA for 3D printing and beyond
Expected completion date	Apr 2016
Estimated size(pages)	93
Requestor Location	Carmen R Rocha 200 N. Mesa Hills Dr. APT 1708 EL PASO, TX 79912 United States Attn: Carmen R Rocha

Billing Type	Invoice
Billing Address	Carmen R Rocha 200 N. Mesa Hills Dr. APT 1708 EL PASO, TX 79912 United States Attn: Carmen R Rocha
Total	0.00 USD

Terms and Conditions

TERMS & CONDITIONS

Cambridge University Press grants the Licensee permission on a non-exclusive non-transferable basis to reproduce, make available or otherwise use the Licensed content 'Content' in the named territory 'Territory' for the purpose listed 'the Use' on Page 1 of this Agreement subject to the following terms and conditions.

1. The License is limited to the permission granted and the Content detailed herein and does not extend to any other permission or content.
2. Cambridge gives no warranty or indemnity in respect of any third-party copyright material included in the Content, for which the Licensee should seek separate permission clearance.
3. The integrity of the Content must be ensured.
4. The License does extend to any edition published specifically for the use of handicapped or reading-impaired individuals.
5. The Licensee shall provide a prominent acknowledgement in the following format: author/s, title of article, name of journal, volume number, issue number, page references, , reproduced with permission.

Other terms and conditions:
v1.0

Questions? customercare@copyright.com or +1-855-239-3415 (toll free in the US) or +1-978-646-2777.

Novel ABS-based binary and ternary polymer blends for material extrusion 3D printing

Carmen R. Rocha, Angel R. Torrado Perez, and David A. Roberson[a)]
W.M. Keck Center for 3D Innovation, The University of Texas at El Paso, El Paso, TX 79968, USA; and Department of Metallurgical and Materials Engineering, The University of Texas at El Paso, El Paso, TX 79968, USA

Corey M. Shemelya and Eric MacDonald
W.M. Keck Center for 3D Innovation, The University of Texas at El Paso, El Paso, TX 79968, USA; and Department of Electrical and Computer Engineering, The University of Texas at El Paso, El Paso, TX 79968, USA

Ryan B. Wicker
W.M. Keck Center for 3D Innovation, The University of Texas at El Paso, El Paso, TX 79968, USA; and Department of Mechanical Engineering, The University of Texas at El Paso, El Paso, TX 79968, USA

(Received 8 April 2014; accepted 13 June 2014)

Material extrusion 3D printing (ME3DP) based on fused deposition modeling (FDM) technology is currently the most commonly used additive manufacturing method. However, ME3DP suffers from a limitation of compatible materials and typically relies upon amorphous thermoplastics, such as acrylonitrile butadiene styrene (ABS). The work presented here demonstrates the development and implementation of binary and ternary polymeric blends for ME3DP. Multiple blends of acrylonitrile butadiene styrene (ABS), styrene ethylene butadiene styrene (SEBS), and ultrahigh molecular weight polyethylene (UHMWPE) were created through a twin screw compounding process to produce novel polymer blends compatible with ME3DP platforms. Mechanical testing and fractography were used to characterize the different physical properties of these new blends. Though the new blends possessed different physical properties, compatibility with ME3DP platforms was maintained. Also, a decrease in surface roughness of a standard test piece was observed for some blends as compared with ABS.

I. INTRODUCTION

Material extrusion 3D printing (ME3DP) is a technology which relies upon the extrusion of a thermoplastic monofilament through a heated nozzle.[1,2] Originally trademarked as fused deposition modeling (FDM™), there has been a dramatic increase in the use of this technology with rapid growth in the form of desktop models of various grades[3] and do-it-yourself (DIY) kits due to the expiration of the original patents on the technology in 2009.[4] As is the case with other 3D printing technologies, ME3DP presents many advantages over traditional manufacturing techniques, most notably direct computer aided design (CAD) to final part fabrication, the capability to print unique and complex geometries, and short design to product cycle time. The flexibility of ME3DP makes it an attractive manufacturing platform; however, the greatest limitation to this technology is a dependence on amorphous polymeric materials as a feedstock, limiting the amount of printable materials. The lack of a large variety of compatible materials limits the applicability of parts fabricated from ME3DP and inhibits the overall growth of this technology. Currently, two of the most common polymers used by ME3DP are acrylonitrile butadiene styrene (ABS) and polylactic acid (PLA).

One method to increase the variety of materials compatible with ME3DP is the creation of polymer matrix composites (PMCs) where the matrix material is a printable material such as ABS. Indeed, several examples of the creation of printable PMCs can be found in the literature.[5–8] However, in this work, we utilize another strategy to increase the number of ME3DP-compatible materials, the use of polymer blends. While there is not a large body of work in literature performing research on printable polymer blends, there are commercially available amorphous polymer blends such as PC ABS (polycarbonate and ABS) and Ultem 9085 (polycarbonate and polyetherimide), which are both marketed by Stratasys.

The work presented here demonstrates the development of new ABS-based polymeric blends which are compatible with ME3DP, yet have physical properties that are different than pure ABS. The lynchpin of the experiments presented here was the use of the styrene ethylene butadiene styrene (SEBS) copolymer as both a blend with ABS and a compatibilizer agent in the

[a)]Address all correspondence to this author.
e-mail: droberson@utep.edu
DOI: 10.1557/jmr.2014.158

blending of ABS with ultrahigh molecular weight polyethylene (UHMWPE)—a material that is semicrystalline and neither extrudable (without specialized equipment) nor compatible with ME3DP platforms. The use of SEBS as a compatibilizer for blends of polystyrene (PS) and high density polyethylene (HDPE) has been demonstrated in the literature[9] and our work here sought to utilize the copolymer block to blend the similar materials ABS and UHMWPE. SEBS has also been widely used as a "rubber toughening" agent for several polymer systems including nylon and polyethylene terephthalate (PET) among others[10–12]; and our efforts here strived to achieve a toughened, rubberized ABS which was compatible with ME3DP platforms.

The polymer blending process has several advantages over synthesizing new printable polymers: i) by using known, printable materials as a base, the new blended material will also be compatible with ME3DP platforms; and ii) polymer blending can be done away from large-scale production facilities using small-batch polymer extruders, providing an expanding area for the development of new materials that meets the customer demand for personal 3D printers. This work is focused on altering the physical properties of printable base polymers (in this case ABS) for use in 3D printing through the addition of UHMWPE and the thermoplastic elastomer SEBS. Utilizing and optimizing these three polymeric materials can create unique combinations of properties, based on the individual constituents. For example, ABS is based on three monomers (acrylonitrile, butadiene, and styrene). Of particular interest are the acrylonitrile and butadiene groups, the former is responsible for forming polar bonding between the chains (producing a stronger material) and the latter provides better mechanical resilience.[13] Likewise UHMWPE offers high toughness, wear and abrasion resistance, and impact strength.[14] However, as mentioned before UHMWPE is not compatible with most extrusion equipment and therefore, must be blended with other polymers for 3D printing, as it lacks the melt flow capability required for printing, even above the melting temperature.

In comparison, polymeric elastomers such as SEBS have properties including low melt viscosity, low process temperature, and low distortion during extrusion.[15] Also, SEBS has demonstrated high impact strength and high elongation at break.[16] For these reasons, our work introduced a blended system of SEBS and ABS to increase the elastomeric properties and toughness of ABS. Also, by incorporating a combination of SEBS and UHMWPE to ABS, it was believed possible to achieve the benefits of UHMWPE (toughness) with the properties of ABS and SEBS (printability and relatively low process temperature). To this end, two blend types were fabricated (ABS SEBS and ABS SEBS UHMWPE) to take advantage of these properties and alter one of the most common 3D printing materials (ABS).

II. EXPERIMENTAL

A. ABS/SEBS blends

In this study, the ABS used was a CYCOLAC resin MG37CR produced by Sabic (Pittsfield, MA). The SEBS used was a powdered Kraton (Houston, TX, USA) A1536 HU SEBS polymer [Fig. 1(a)] in the form of globular chunks roughly 0.5 mm in diameter. Different blends of ABS were made with varying weight percentages of SEBS: 5, 10, 20, and 50% (in terms of ABS:SEBS ratio 95:5, 90:10, 80:20, and 50:50) and compared with baseline samples created from ABS. The ABS/SEBS blends were pre-mixed and then oven dried. The oven drying process entailed a drying cycle at 100 °C for 14 h followed by a ramp to 110 °C for 1 h and a ramp down to room temperature for an additional 1 h. The mixture was fed to a twin screw extruder/compounder (Dr. Collin Model ZK 25T, Dr. Collin GmbH, Ebersberg, Germany) operating at a temperature of 165 °C, under a pressure of 45 bar, and a screw rate of 70 rpm. The extrusion process was used to create a monofilament of 1.75 mm in diameter which is the standard diameter used by most ME3DP systems.

B. ABS/UHMWPE/SEBS blends

Blends of UHMWPE with ABS using SEBS as a compatibilizer were made using GUR® 1020 UHMWPE (Celeanese, Irving, TX) blended with the same ABS and SEBS materials mentioned above. The UHMWPE was in powder form with a size distribution [Figs. 1(b) and 1(c)] of 92.6 ± 45 μm. The ternary blends tested in this study were based on mass ratios of ABS:UHMWPE:SEBS (90:10:10 and 75:25:10). We found that we were unable to successfully create a printable monofilament when the weight percent of UHMWPE was greater than 25% compared with the ABS base (greater than an ABS:UHMWPE ratio of 75:25). The mixtures were fed to the same twin screw extruder/compounder; however, the operating parameters used for these blends were at a temperature of 195 °C, under a pressure of 72 bar, and a screw rate of 40 rpm. In contrast to both blend systems, the pure ABS filament was created using extrusion parameters of temperature of 175 °C, under a pressure of 54 bar, and a screw rate of 50 rpm. All extrusion parameters for the various blends are shown in Table I and it should be noted that the difference in physical properties necessitated different extrusion parameters which we determined empirically.

C. Materials testing and characterization

The blended materials underwent tensile testing following the ASTM Standard D638-10 using the Type V dimensions.[17] To verify commercial printability, these samples were printed using a MakerBot Replicator (MakerBot Industries, Brooklyn, NY) material extrusion

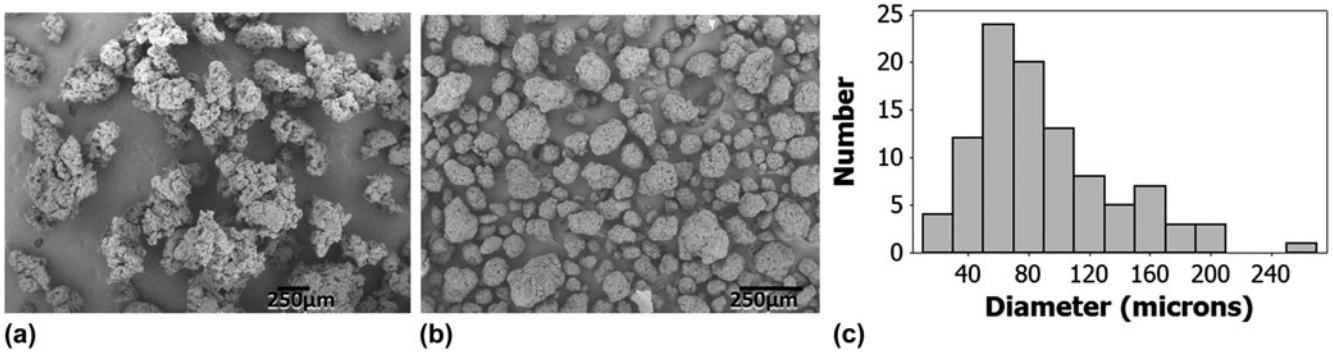

FIG. 1. SEM image of the (a) SEBS and (b) UHMWPE polymer before compounding. The size distribution of the UHMWPE polymer (c) was measured to be 92.6 ± 45 μm.

TABLE I. Extrusion parameters for the blended materials.

Material	*T* zone 1 (°C)	*T* zone 2 (°C)	*T* zone 3 (°C)	*T* zone 4 (°C)	*T* zone 5 (°C)	RPM main screw	RPM feed screw (% main)	Pressure (P) main screws (bar)	Load (%)
ABS:SEBS									
1:0	170	182	187	187	187	35	6	100	72
95:5	170	182	187	187	187	35	6	100	72
90:10	170	182	187	187	187	35	6	92	68
80:20	165	170	170	170	170	55	6	73	64
50:50	160	165	165	165	165	70	6	45	61
ABS:UHMWPE:SEBS									
75:25:10	155	185	185	185	185	40	6	80	62
90:10:10	155	195	195	195	190	40	6	72	60

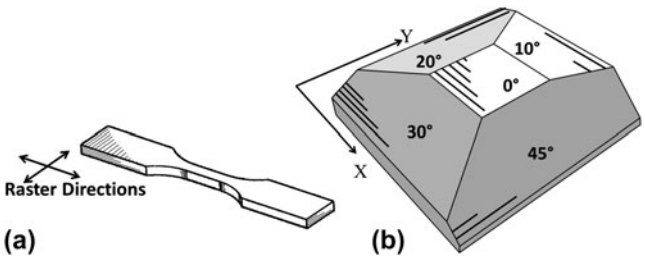

FIG. 2. (a) Type V tensile test specimen where the raster direction is designated by arrows and hash marks. (b) The structure designed to test surface roughness with surface angles at 10°, 15°, 30°, and 45° with respect to the surface normal.

3D printer. The print direction of the dog-bone structures was in the *XYZ* direction [Fig. 2(a)] with a raster height of 0.4 mm and a raster width of 0.4 mm. The raster path was set to produce a maximum filling percentage. A slight modification was made to the MakerBot Replicator; the stock drive gear was replaced with a "hyena" gear as we found this gear to work better with the blended polymer filaments. Additionally, a modified nozzle with a diameter of 0.8 mm was used to print some of the blends as seen in Table II. Machine printing parameters used for each material are listed in Table II and, as was the case with the extrusion process, the 3D printing process demanded different properties based on the material type. The tensile test specimens were subjected to loading using an Instron® 5866 (Instron, Norwood, MA) tensile tester, and the resulting stress, strain, and average Young's modulus were recorded.

Fracture surfaces of representative specimens from each sample pool were analyzed with a Hitachi TM-1000 scanning electron microscope (SEM; Hitachi High-Technologies Europe GmbH, Germany) operating at a 15 kV accelerating potential and equipped with a backscatter electron (BSE) detector. SEM imaging allowed fracture surface morphology observations of the blended structures to identify common failure modes within these new material systems. As the goal of this paper was to demonstrate the development of new polymeric blends, a test to measure the printability of the material beyond the printing of mechanical testing specimens was developed. A test structure designed to test the ability to print an inclined plane was developed with surface angles at 10°, 15°, 30°, and 45° with respect to the normal surface of the *XY* plane [Fig. 2(b)]. The specific angles were chosen based on precedence set in the literature.[18] Surface roughness measurements were taken using a Mitutoyo surface roughness tester (model SJ-201P Mitutoyo America Corp., Aurora, IL) and were also made on the flat top surface and bottom surface of the test piece (0° top and 0° bottom in the *x* and *y* direction).

TABLE II. MakerBot print parameters for all materials.

Material	Object infill (%)	Layer height (mm)	Number of shells	Feedrate (mm/s)	Travel feedrate (mm/s)	Print temperature (°C)	Filament diameter (mm)	G-code nozzle diameter (mm)	Actual nozzle diameter (mm)	Raft
ABS:SEBS										
1:0	100	0.27	1	40	55	230	1.9	0.4	0.4	No
95:5	100	0.27	1	40	55	230	1.9	0.4	0.4	No
90:10	100	0.27	1	40	55	240	1.9	0.6	0.8	No
80:20	100	0.20	1	40	55	240	1.9	0.6	0.8	No
50:50	100	0.20	1	40	55	240	1.9	0.6	0.8	No
ABS:UHMWPE:SEBS										
75:25:10	100	0.20	1	40	55	230	1.9	0.6	0.8	No
90:10:10	100	0.20	1	40	55	230	1.9	0.6	0.8	No

TABLE III. Mechanical testing data for all materials tested in this study.

Material	UTS (MPa)	Elongation at break (%)
ABS:SEBS		
1:0	34.0 ± 1.74	8.6 ± 3.3
95:5	25.5 ± 2.3	3.6 ± 0.7
90:10	26.2 ± 2.5	4.0 ± 1.1
80:20	25.2 ± 1.8	11.9 ± 2.1
50:50	18.0 ± 0.03	47.6 ± 5.0
ABS:UHMWPE:SEBS		
75:25:10	14.7 ± 0.7	5.7 ± 0.7
90:10:10	23.1 ± 0.8	8.4 ± 1.0

Sample size, $n = 5$.

III. RESULTS AND DISCUSSIONS

A. ABS/SEBS blends

The results of the mechanical testing data are shown in Table III. As can be seen, blends that were 5% and 10% by weight SEBS (the 95:5 and 90:10 ABS:SEBS blends) do not exhibit an improvement in mechanical properties and suffered from a slight decrease in ultimate tensile strength (UTS) of 25.5 ± 2.3 and 26.2 ± 2.5 MPa for 5% and 10% SEBS as compared with UTS of 34.0 ± 1.74 MPa for the baseline ABS samples. The blends with 20% and 50% by weight SEBS (the 80:20 and 50:50 ABS:SEBS blends) also displayed a lower UTS (18.0 ± 0.03 MPa); however, there was a dramatic increase in the percentage of elongation at the breaking strength where the 20% SEBS blend 50% SEBS blend displayed elongation percentage values of 11.9 ± 2.1% and 47.6 ± 5.0% compared with 8.6 ± 3.3% for the baseline ABS specimens. The increase in plastic deformation before fracture is indicative of an increase in toughness over the original ABS base resin. The stress–strain data for all blends are represented graphically in Fig. 3. Each stress–strain curve is a composite curve of every tested sample for a given blend. The data compiling to generate the curves was achieved by a process described in the study of Torrado et al.[19] where a MatLab®-based program was used. By comparing the elongation percentage before failure, it is possible to observe the difference in toughness for the new polymeric blends as compared with the base ABS resin. It is important to note that though there were differences in the mechanical properties of the blends, the materials were still compatible with our ME3DP platform.

Scanning electron microanalysis of the fracture surfaces from representative specimens from each blend sample pool revealed different characteristics based on the weight percentage of SEBS in the blend. In general, the fracture surface of the tensile specimens is indicative of craze cracking which propagated normal to the direction of applied stress as has also been demonstrated in the literature.[19,20] The prominent features of the fracture

surface for the 5% and 10% by weight SEBS blends is the presence of fibrils (indicated by arrows in Fig. 4). These fibrils appear to have torn out of the surrounding matrix, and they decrease in number as the concentration of SEBS increases. In terms of miscibility, this may indicate that ABS is miscible in SEBS because an increase in SEBS concentration corresponds to a decrease in fibrils present.

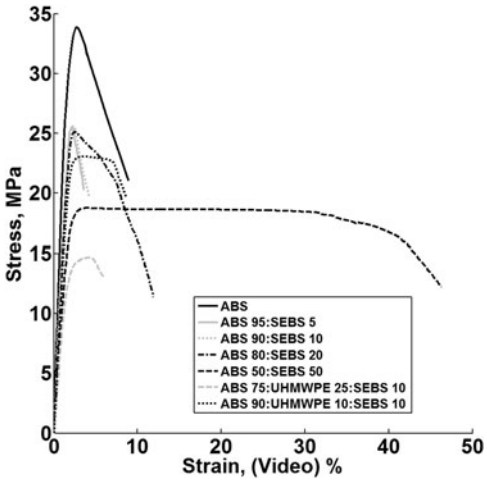

FIG. 3. Composite stress–strain diagrams generated from tensile test data for all material systems tested in this study. Note the difference in mechanical properties as compared with the base ABS resin. Most notable is the drastic increase in toughness for the 50% by weight SEBS blend.

Also, an increase in SEBS concentration causes a shift in the mechanical behavior of the tensile specimens toward a material which is more elastic than ABS alone.

The ABS blends with a concentration of 20% and 50% SEBS were qualitatively different in terms of surface smoothness than the samples printed from pure ABS. These two SEBS blends were subjected to surface roughness testing utilizing the printed test piece discussed above [Fig. 2(b)] and the results are shown in Table IV. As can be seen in the table, the 50% SEBS blend led to the printing of smoother 45° and 30° degree surfaces as compared with the sample printed from ABS. The reason for the improvement in surface roughness for inclined planes is due to the unique characteristics in the way the material is deposited during the printing process which is influenced by the rheological differences between the material systems. As is seen in the SEM images of cross sections from samples printed from selected blends in this study (Fig. 5), the filament shape is still discernable for the sample printed from ABS while the 50:50 ABS:SEBS blend deposits differently. The difference in deposition morphology allows for the creation of smoother inclined planes. The other surfaces of the ABS test piece were comparable for the blends tested.

B. ABS/UHMWPE/SEBS blends

Mechanical testing data for the two ternary blends tested here are listed in Table III. In both blended cases,

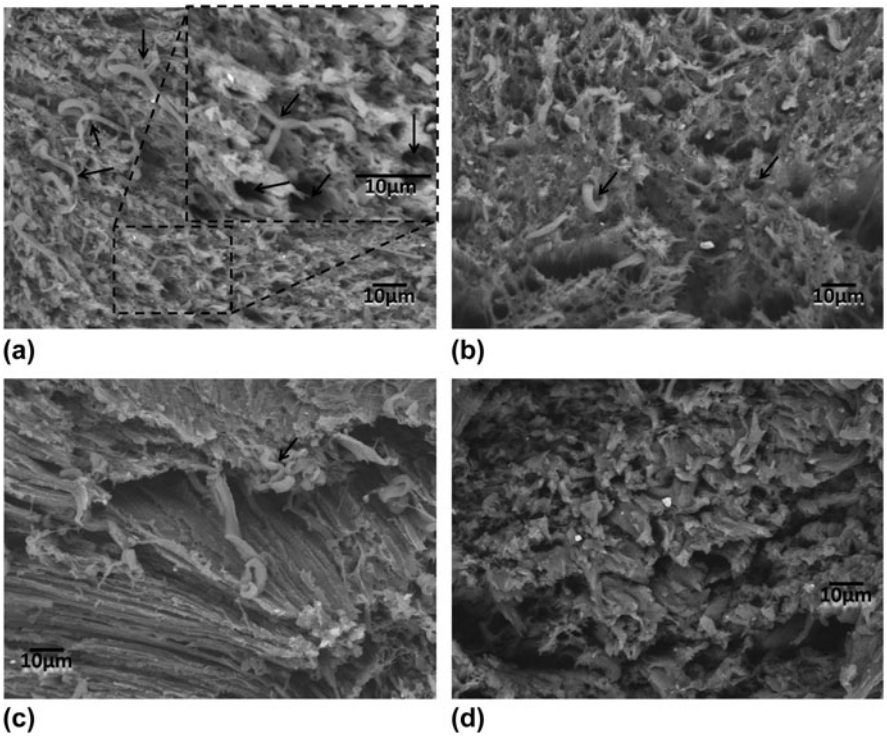

FIG. 4. Micrographs of ABS:SEBS blends (a) 95:5, (b) 90:10, (c) 80:20, (d) 50:50. The fracture surfaces of the tensile specimens are indicative of craze cracking, and all fracture surfaces prominently display fibrils, highlighted by black arrows in (a), (b), and (c).

TABLE IV. Surface roughness measurements (Ra in μm) for selected materials.

	Surface							
Material	45°	30°	15°	10°	0° top *x*	0° top *y*	0° bottom *x*	0° bottom *y*
ABS:SEBS								
1:0	47.2 ± 8.6	49.8 ± 5.4	62.9 ± 3.6	50.7 ± 5.8	9.7 ± 2.7	33.9 ± 4.3	1.06 ± 0.2	5.56 ± 5.8
80:20	44.8 ± 2.4	49.0 ± 1.7	59.4 ± 2.6	47.6 ± 12.4	13.0 ± 4.0	17.1 ± 7.3	1.8 ± 1.3	1.8 ± 0.7
50:50	35.9 ± 0.7	38.8 ± 4.7	64.5 ± 1.4	52.2 ± 13.3	11.3 ± 3.0	16.9 ± 5.9	1.5 ± 0.5	2.8 ± 1.8
ABS:UHMWPE:SEBS								
75:25:10	29.7 ± 6.0	47.0 ± 7.6	40.9 ± 10.1	36.0 ± 11.3	18.5 ± 6.7	34.0 ± 4.1	20.4 ± 5.4	23.8 ± 6.8
90:10:10	47.9 ± 9.9	40.2 ± 5.2	44.5 ± 2.9	29.9 ± 4.7	13.3 ± 2.9	28.6 ± 4.3	3.8 ± 0.9	3.9 ± 1.5

Sample size, $n = 5$.

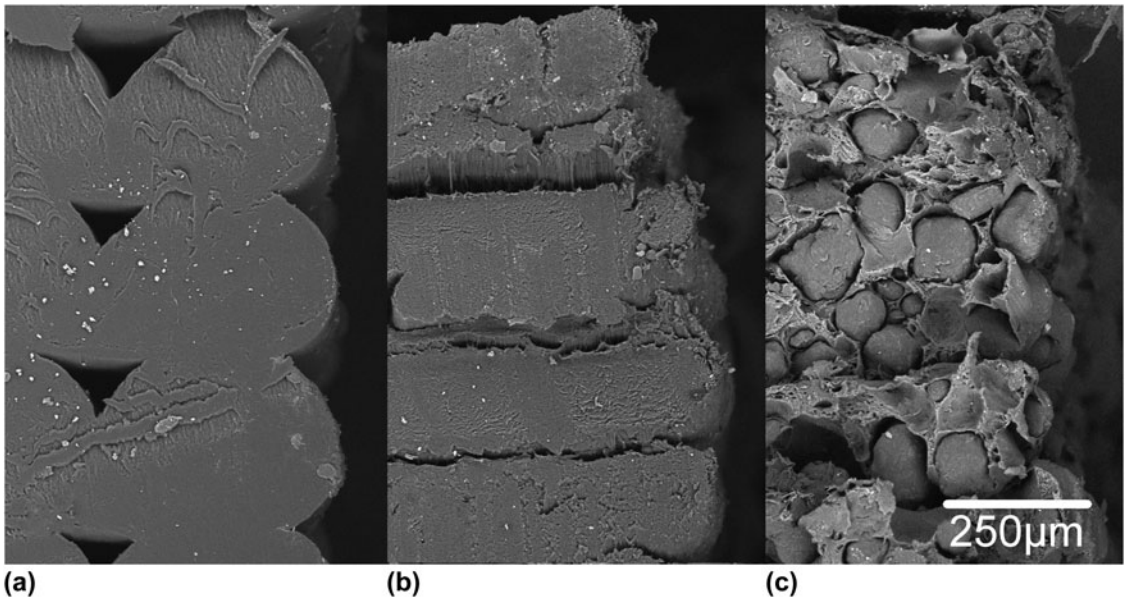

FIG. 5. SEM micrographs comparing (a) ABS, (b) the 50:50 ABS:SEBS blend, and (c) the 75:25:10 ABS:SEBS:UHMWPE ternary blend. Note that the ternary blend has a propensity to blend raster layers leading to an overall smoother surface finish for inclined planes.

the material's UTS was weaker than ABS. The average UTS for the ABS:UHMWPE:SEBS (75:25:10) blend was 14.7 ± 0.7 MPa while the ABS:UHMWPE:SEBS (90:10:10) blend produced samples with an average UTS of 23.1 ± 0.8 MPa, as compared with 34.0 ± 1.74 MPa for the baseline ABS samples.

The electron micrographs of the fracture surfaces of representative samples for the two ternary blends (ABS:UHMWPE:SEBS—75:25:10 and 90:10:10) examined in this study are shown in Fig. 6. Analysis of the micrographs confirmed prominent globules of the material in both ternary blends. Comparing the size of the globules to the size distribution of the UHMWPE powder confirms that the globules are most-likely undissolved UHMWPE particles. The surface features of the globules are much smoother than the original powder and are most likely due to particle melt during the extrusion process as the process was above the melting temperature (T_m ~130 °C) of UHMWPE. The particles also appear to pull out of the matrix as there are several cavities and free-to-move particles on the fracture surface. The fracture morphology of the matrix material is more brittle than even the comparable mixtures of ABS and SEBS meaning that it is possible that some of the UHMWPE did dissolve into the ABS matrix or that the SEBS mixed with the UHMWPE as the fracture surface of the matrix resembles the fracture surface of pure ABS (Fig. 7). Also present in the fracture surface of both ternary blends are fibrils and voids where the fibrils pulled out of (highlighted by black arrows in Fig. 6). The mechanics of the fibril tear out is more prominent here than in the ABS:SEBS blend images and may point to a threshold of miscibility between SEBS and ABS.

Surface roughness measurements (Table IV) show that for inclined surfaces, the 75:25:10 ternary blend produced the smoothest surfaces of all materials tested in this

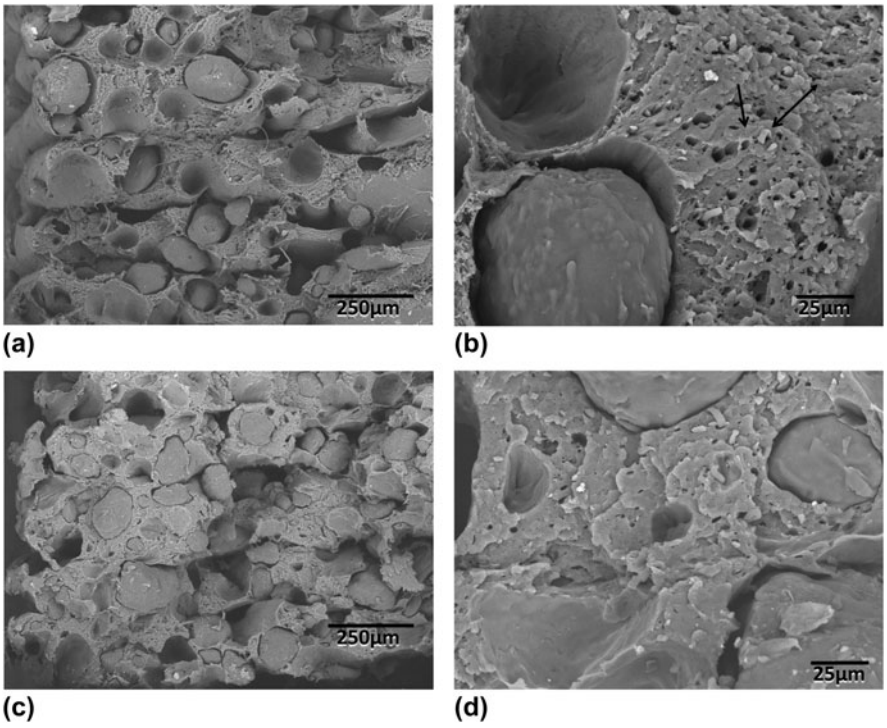

FIG. 6. Micrographs of ABS:SEBS:UHMWPE (a), (b) 90:10:10 and (c), (d) 75:25:10. Large globules are of consistent in size with undissolved UHMWPE. At higher magnifications (b), (d) the undissolved UHMWPE appear to be pulled out of the composite matrix and free-to-move after testing, in addition to have undergone melting.

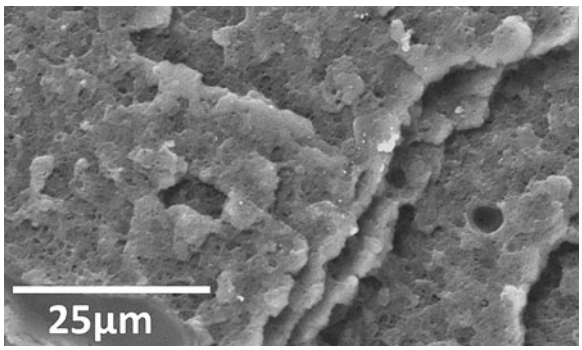

FIG. 7. Representative fracture surface of a tensile specimen printed from ABS.

study whereas the flat surfaces were among the roughest tested here. As was the case with the 50:50 ABS:SEBS blend, one reason for the smoother inclined planes may be the rheological differences for this blend as compared with the others. Figure 5 compares the print rasters near the edges of specimens for ABS [Fig. 5(a)], the 50% SEBS blend [Fig. 5(b)], and the 75:25:10 ternary blend [Fig. 5(c)]. From the images, it can be seen that the ternary blend has the propensity to deposit in a more spread out fashion than the other blends to the point that it is difficult or impossible to discern the deposition layers. In all cases, the roughness in the *x* direction was less than that in the *y* direction due to the fact that in the *y* direction the test probe traveled against the print raster direction while measurements in the *x* direction were parallel with the print raster direction. Once again, though the material displayed different mechanical properties as compared with ABS, we were still able to use it as the feedstock on our ME3DP platform.

IV. CONCLUSION

The work presented here had the goal of demonstrating the development of new polymeric blends for material extrusion 3D printing platforms through characterization of mechanical properties, phase morphology, and 3D printer compatibility of novel copolymer blend systems (ABS:SEBS and ABS:UHMWPE:SEBS), each having different physical and chemical characteristics. Toward this goal, the 3D printability of novel binary and ternary polymer blends of varying constituent concentrations was determined by printing standard tensile test specimens and a roughness testing piece with multi-angled inclined planes using a commercially available MakerBot Replicator. In terms of roughness, the 50:50 ABS:SEBS provided smoother flat surfaces and the 75:25:10 ABS:UHMWPE:SEBS blend provided the smoothest sloped surfaces due to the rheological differences as compared with ABS and the other blends in this study. However,

we were unable to create a filament when the amount of UHMWPE was increased above 25%. Mechanical testing was also performed on all printable copolymer blends. Through this testing, we observed that blending any amount of SEBS and UHMWPE into an ABS matrix lowered the UTS of printed tensile specimens. Yet, it was also observed when SEBS copolymer blends were loaded greater than 20%, the elongation percentage values (amount of plastic deformation endured by the material prior to failure) increased where tensile test samples printed from the 50:50 ABS:SEBS blend displayed elongation percentage values approaching 50% which is indicative of an increase in toughness of the material.

Characterization of the ABS:UHMWPE:SEBS and ABS:SEBS blends via SEM microanalysis revealed an insolubility of UHMWPE within the ABS matrix as for the ternary blends as well as a solubility threshold between ABS and SEBS for the binary blends. In all cases, ABS blends with altered physical properties were created and demonstrated to be compatible with a desktop grade material extrusion 3D printer. In the case of the binary ABS:SEBS blend, manipulation of the percentage of elongation at break was achieved by changing the ABS:SEBS ratio. While the addition of UHMWPE was detrimental UTS, the result was a 3D printable material capable of printing smoother inclined planes than the ABS base material alone. The work here demonstrates the ability to create 3D printer compatible materials with tailorable physical properties which can be customized for a given application.

ACKNOWLEDGMENTS

The work presented here was supported by a grant from the Intelligence Community Postdoctoral Research Fellowship Program through funding from the Office of the Director of National Intelligence under Grant No. 2012-12071000005. All statements of fact, opinion, or analysis expressed are those of the author and do not reflect the official positions or views of the Intelligence Community or any other U.S. Government agency. Nothing in the contents should be construed as asserting or implying U.S. Government authentication of information or Intelligence Community endorsement of the author's views. Additional support came from the National Aeronautics and Space Administration (NASA) under Grant No. 282002-8784. The facilities of the W.M. Keck Center for 3D Innovation and the Department of Metallurgical and Materials Engineering located at The University of Texas at El Paso were used for fabrication, SEM imaging, and material testing throughout this research project.

REFERENCES

1. D-Y. Chang and B-H Huang: Studies on profile error and extruding aperture for the RP parts using the fused deposition modeling process. *Int. J. Adv. Manuf. Technol.* **53**, 1027–1037 (2011).
2. ASTM Standard F2792-12a: *Standard Terminology for Additive Manufacturing Technologies* (ASTM International, West Conshohocken, PA, 2012).
3. D.A. Roberson, D. Espalin, and R.B. Wicker: 3D printer selection: A decision-making evaluation and ranking model. *Virtual Phys. Prototyping* **8**, 201–212 (2013).
4. S.S. Crump: The fused deposition modeling (FDM). U.S. Patent Nos. 5,121,329 and 5,340,433, 1988.
5. S. Masood and W. Song: Development of new metal/polymer materials for rapid tooling using fused deposition modelling. *Mater. Des.* **25**, 587–594 (2004).
6. M. Nikzad, S.H. Masood, and I. Sbarski: Thermo-mechanical properties of a highly filled polymeric composites for fused deposition modeling. *Mater. Des.* **32**, 3448–3456 (2011).
7. A. Safari and E.K. Akdogan: Rapid prototyping of novel piezoelectric composites. *Ferroelectrics* **331**, 153–179 (2006).
8. M.L. Shofner, K. Lozano, F.J. Rodríguez-Macías, and E.V. Barrera: Nanofiber-reinforced polymers prepared by fused deposition modeling. *J. Appl. Polym. Sci.* **89**, 3081–3090 (2003).
9. Ž. Jelčić, N. Vranješ, and V. Rek: Long-range processing correlation and morphological fractality of compatibilized blends of PS/HDPE/SEBS block copolymer. *Macromol. Symp.* **290**, 1–14 (2010).
10. J.J. Huang, H. Keskkula, and D.R. Paul: Rubber toughening of an amorphous polyamide by functionalized SEBS copolymers: Morphology and Izod impact behavior. *Polymer* **45**, 4203–4215 (2004).
11. A.J. Oshinski, H. Keskkula, and D.R. Paul: Rubber toughening of polyamides with functionalized block copolymers: 1. Nylon-6. *Polymer* **33**, 268–283 (1992).
12. V. Tanrattanakul, A. Hiltner, E. Baer, W. G. Perkins, F.L. Massey, and A. Moet, "Toughening PET by blending with a functionalized SEBS block copolymer," *Polymer*, **38**(9), 2191–2200 (1997).
13. E. Charles and Carraher Jr.: *Introduction to Polymer Chemistry*, 3rd ed. (CRC Press, Boca Raton, Florida, December 4, 2012), p. 298.
14. K.L.K. Lim, Z.A.M. Ishak, U.S. Ishiaku, A.M.Y. Fuad, A.H. Yusof, T. Czigany, B. Pukanszky, and D.S. Ogunniyi, "High-density polyethylene/ultrahigh-molecular-weight polyethylene blend. I. The processing, thermal, and mechanical properties," *J. Appl. Polym. Sci.*, vol. **97**, no. 1, pp. 413–425, Jul. 2005.
15. A.K. Gupta and S.N. Purwar: Melt rheological properties of polypropylene/SEBS (styrene–ethylene butylene–styrene block copolymer) blends. *J. Appl. Polym. Sci.* **29**, 1079–1093 (1984).
16. F. Stricker, Y. Thomann, and R. Mülhaupt: Influence of rubber particle size on mechanical properties of polypropylene–SEBS blends. *J. Appl. Polym. Sci.* **68**, 1891–1901 (1998).
17. ASTM Standard D638: *Standard Test Method for Tensile Properties of Plastics* (ASTM International, West Conshohocken, PA 2010).
18. P.M. Pandey, N. Venkata Reddy, and S.G. Dhande: Improvement of surface finish by staircase machining in fused deposition modeling. *J. Mater. Process. Technol.* **132**, 323–331 (2003).
19. A.R.T. Perez, D.A. Roberson, and R.B. Wicker: Fracture surface analysis of 3D-Printed tensile specimens of novel ABS-based materials. *J. Fail. Anal. Prev.* 1–11 (2014) doi:10.1007/s11668-014-9803-9.
20. L. Engel, H. Klingele, G.W. Ehrenstein, and H. Schaper: *An Atlas of Polymer Damage: Surface Examination by Scanning Electron Microscope* (Prentice-Hall, Inc., Englewood Cliffs, New Jersey, 1981).

SPRINGER LICENSE
TERMS AND CONDITIONS

May 02, 2016

This Agreement between Carmen R Rocha ("You") and Springer ("Springer") consists of your license details and the terms and conditions provided by Springer and Copyright Clearance Center.

License Number	3846011221648
License date	Apr 11, 2016
Licensed Content Publisher	Springer
Licensed Content Publication	Journal of Electronic Materials
Licensed Content Title	Mechanical, Electromagnetic, and X-ray Shielding Characterization of a 3D Printable Tungsten–Polycarbonate Polymer Matrix Composite for Space-Based Applications
Licensed Content Author	Corey M. Shemelya
Licensed Content Date	Jan 1, 2015
Licensed Content Volume Number	44
Licensed Content Issue Number	8
Type of Use	Thesis/Dissertation
Portion	Full text
Number of copies	1
Author of this Springer article	Yes and you are a contributor of the new work
Order reference number	None
Title of your thesis / dissertation	Improving the Engineering properties of PLA for 3D printing and beyond
Expected completion date	Apr 2016
Estimated size(pages)	93
Requestor Location	Carmen R Rocha 200 N. Mesa Hills Dr. APT 1708 EL PASO, TX 79912 United States Attn: Carmen R Rocha
Billing Type	Invoice
Billing Address	Carmen R Rocha 200 N. Mesa Hills Dr. APT 1708 EL PASO, TX 79912 United States Attn: Carmen R Rocha

Total	0.00 USD
Total	0.00 USD

Terms and Conditions

Introduction
The publisher for this copyrighted material is Springer. By clicking "accept" in connection with completing this licensing transaction, you agree that the following terms and conditions apply to this transaction (along with the Billing and Payment terms and conditions established by Copyright Clearance Center, Inc. ("CCC"), at the time that you opened your Rightslink account and that are available at any time at http://myaccount.copyright.com).
Limited License
With reference to your request to reuse material on which Springer controls the copyright, permission is granted for the use indicated in your enquiry under the following conditions:
- Licenses are for one-time use only with a maximum distribution equal to the number stated in your request.
- Springer material represents original material which does not carry references to other sources. If the material in question appears with a credit to another source, this permission is not valid and authorization has to be obtained from the original copyright holder.
- This permission
• is non-exclusive
• is only valid if no personal rights, trademarks, or competitive products are infringed.
• explicitly excludes the right for derivatives.
- Springer does not supply original artwork or content.
- According to the format which you have selected, the following conditions apply accordingly:
• **Print and Electronic:** This License include use in electronic form provided it is password protected, on intranet, or CD-Rom/DVD or E-book/E-journal. It may not be republished in electronic open access.
• **Print:** This License excludes use in electronic form.
• **Electronic:** This License only pertains to use in electronic form provided it is password protected, on intranet, or CD-Rom/DVD or E-book/E-journal. It may not be republished in electronic open access.
For any electronic use not mentioned, please contact Springer at permissions.springer@spi-global.com.
- Although Springer controls the copyright to the material and is entitled to negotiate on rights, this license is only valid subject to courtesy information to the author (address is given in the article/chapter).
- If you are an STM Signatory or your work will be published by an STM Signatory and you are requesting to reuse figures/tables/illustrations or single text extracts, permission is granted according to STM Permissions Guidelines: http://www.stm-assoc.org/permissions-guidelines/
For any electronic use not mentioned in the Guidelines, please contact Springer at permissions.springer@spi-global.com. If you request to reuse more content than stipulated in the STM Permissions Guidelines, you will be charged a permission fee for the excess content.
Permission is valid upon payment of the fee as indicated in the licensing process. If permission is granted free of charge on this occasion, that does not prejudice any rights we might have to charge for reproduction of our copyrighted material in the future.
-If your request is for reuse in a Thesis, permission is granted free of charge under the following conditions:

This license is valid for one-time use only for the purpose of defending your thesis and with a maximum of 100 extra copies in paper. If the thesis is going to be published, permission needs to be reobtained.

- includes use in an electronic form, provided it is an author-created version of the thesis on his/her own website and his/her university's repository, including UMI (according to the definition on the Sherpa website: http://www.sherpa.ac.uk/romeo/);
- is subject to courtesy information to the co-author or corresponding author.

Geographic Rights: Scope

Licenses may be exercised anywhere in the world.

Altering/Modifying Material: Not Permitted

Figures, tables, and illustrations may be altered minimally to serve your work. You may not alter or modify text in any manner. Abbreviations, additions, deletions and/or any other alterations shall be made only with prior written authorization of the author(s).

Reservation of Rights

Springer reserves all rights not specifically granted in the combination of (i) the license details provided by you and accepted in the course of this licensing transaction and (ii) these terms and conditions and (iii) CCC's Billing and Payment terms and conditions.

License Contingent on Payment

While you may exercise the rights licensed immediately upon issuance of the license at the end of the licensing process for the transaction, provided that you have disclosed complete and accurate details of your proposed use, no license is finally effective unless and until full payment is received from you (either by Springer or by CCC) as provided in CCC's Billing and Payment terms and conditions. If full payment is not received by the date due, then any license preliminarily granted shall be deemed automatically revoked and shall be void as if never granted. Further, in the event that you breach any of these terms and conditions or any of CCC's Billing and Payment terms and conditions, the license is automatically revoked and shall be void as if never granted. Use of materials as described in a revoked license, as well as any use of the materials beyond the scope of an unrevoked license, may constitute copyright infringement and Springer reserves the right to take any and all action to protect its copyright in the materials.

Copyright Notice: Disclaimer

You must include the following copyright and permission notice in connection with any reproduction of the licensed material:

"Springer book/journal title, chapter/article title, volume, year of publication, page, name(s) of author(s), (original copyright notice as given in the publication in which the material was originally published) "With permission of Springer"

In case of use of a graph or illustration, the caption of the graph or illustration must be included, as it is indicated in the original publication.

Warranties: None

Springer makes no representations or warranties with respect to the licensed material and adopts on its own behalf the limitations and disclaimers established by CCC on its behalf in its Billing and Payment terms and conditions for this licensing transaction.

Indemnity

You hereby indemnify and agree to hold harmless Springer and CCC, and their respective officers, directors, employees and agents, from and against any and all claims arising out of your use of the licensed material other than as specifically authorized pursuant to this license.

No Transfer of License

This license is personal to you and may not be sublicensed, assigned, or transferred by you without Springer's written permission.

No Amendment Except in Writing
This license may not be amended except in a writing signed by both parties (or, in the case of Springer, by CCC on Springer's behalf).
Objection to Contrary Terms
Springer hereby objects to any terms contained in any purchase order, acknowledgment, check endorsement or other writing prepared by you, which terms are inconsistent with these terms and conditions or CCC's Billing and Payment terms and conditions. These terms and conditions, together with CCC's Billing and Payment terms and conditions (which are incorporated herein), comprise the entire agreement between you and Springer (and CCC) concerning this licensing transaction. In the event of any conflict between your obligations established by these terms and conditions and those established by CCC's Billing and Payment terms and conditions, these terms and conditions shall control.
Jurisdiction
All disputes that may arise in connection with this present License, or the breach thereof, shall be settled exclusively by arbitration, to be held in the Federal Republic of Germany, in accordance with German law.
Other conditions:
V 12AUG2015

Questions? customercare@copyright.com or +1-855-239-3415 (toll free in the US) or +1-978-646-2777.

Journal of ELECTRONIC MATERIALS, Vol. 44, No. 8, 2015
DOI: 10.1007/s11664-015-3687-7

Mechanical, Electromagnetic, and X-ray Shielding Characterization of a 3D Printable Tungsten–Polycarbonate Polymer Matrix Composite for Space-Based Applications

COREY M. SHEMELYA,[1,2] ARMANDO RIVERA,[1] ANGEL TORRADO PEREZ,[1,3,4] CARMEN ROCHA,[1,3,4] MIN LIANG,[5] XIAOJU YU,[5] CRAIG KIEF,[6] DAVID ALEXANDER,[6] JAMES STEGEMAN,[7] HAO XIN,[5] RYAN B. WICKER,[1,8] ERIC MACDONALD,[1,2] and DAVID A. ROBERSON[1,3,4,9,10]

1.—W.M. Keck Center for 3D Innovation, The University of Texas at El Paso, El Paso, TX 79968, USA. 2.—Department of Electrical and Computer Engineering, The University of Texas at El Paso, El Paso, TX 79968, USA. 3.—Department of Metallurgical and Materials Engineering, The University of Texas at El Paso, El Paso, TX 79968, USA. 4.—Polymer Extrusion Lab, W. M. Keck Center for 3D Innovation, The University of Texas at El Paso, El Paso, TX 79968, USA. 5.—Department of Electrical and Computer Engineering, The University of Arizona, Tucson, AZ 85721, USA. 6.—COSMIAC, 2350 Alamo Avenue SE, Albuquerque, NM 87106, USA. 7.—NASA Glenn Research Center, 21000 Brookpark Rd, Cleveland, OH 44135, USA. 8.—Department of Mechanical Engineering, The University of Texas at El Paso, El Paso, TX 79968, USA. 9.—Center for Structural and Functional Materials Research and Innovation, The University of Texas at El Paso, El Paso, TX 79968, USA. 10.—e-mail: droberson@utep.edu

Material-extrusion three-dimensional (3D) printing has recently attracted much interest because of its process flexibility, rapid response to design alterations, and ability to create structures “on-the-go”. For this reason, 3D printing has possible applications in rapid creation of space-based devices, for example cube satellites (CubeSat). This work focused on fabrication and characterization of tungsten-doped polycarbonate polymer matrix composites specifically designed for x-ray radiation-shielding applications. The polycarbonate–tungsten polymer composite obtained intentionally utilizes low loading levels to provide x-ray shielding while limiting effects on other properties of the material, for example weight, electromagnetic functionality, and mechanical strength. The fabrication process, from tungsten functionalization to filament extrusion and material characterization, is described, including printability, determination of x-ray attenuation, tensile strength, impact resistance, and gigahertz permittivity, and failure analysis. The proposed materials are uniquely advantageous when implemented in 3D printed structures, because even a small volume fraction of tungsten has been shown to substantially alter the properties of the resulting composite.

Key words: Polymer composites, material testing, fracture analysis, mechanical properties, 3D printing

INTRODUCTION

There has recently been a substantial increase in interest in commercial and industrial applications of material-extrusion three-dimensional printing (ME3DP) based on fused deposition modeling (FDM) technology. The ability to design a structure by computer aided drafting (CAD) and immediately fabricate the design may prove to be revolutionary for rapid prototyping processes by reducing time to market for specific low-volume items.[1–3] Specifically,

(Received December 17, 2014; accepted February 5, 2015; published online March 6, 2015)

thermoplastic-based ME3DP can now incorporate additional functionality, for example electrical interconnects and components, directly during the build process.[4–21] Component integration is possible because of integration of pauses and cavities at specific positions in the layer-by-layer building process of ME3DP.[19] Electrical interconnects can also be integrated within these layers by use of a variety of embedding processes. When the 3D printing build sequence is complete, the resulting structure will be fully formed with integrated electronic functionality.[4,17,19] Combination of three-dimensional (3D) printing with such deposition methods as direct write and wire embedding gives rise to 3D printed structural electronics.[8,17,21] Although significant progress has been made in this type of 3D printing, it is hindered by a lack of printable materials with different physical properties.[8,20] There has been interest in utilizing the inherent flexibility of 3D printing to design and fabricate ME3DP structures for applications ranging from antennas and sensing to space-based cube satellites (CubeSats).[1,4,13,18,19]

For many of these potential applications, for example CubeSats, electromagnetic and radiation-sensitive components must be inserted within the ME3DP structure without compromising the mechanical strength. On integration of polymer matrix composite (PMC) thermoplastics into 3D printed structures, the mechanical advantages and/or disadvantages of both materials (in this case tungsten and polycarbonate) in a single filament can be combined.[22] For this reason, a PMC material was designed with the specific objective of increasing the x-ray radiation shielding of a polycarbonate (PC) 3D printable monofilament while simultaneously minimizing the effect on such mechanical properties as ultimate tensile strength (UTS) and impact resistance. Classically, a composite can utilize the physical properties of two or more material systems; an example of this effect can be shown in terms of yield strength, Eq. 1:

$$\sigma_c = V_{fm}\sigma_c + V_{fr}\sigma_r \tag{1}$$

where σ_c is the composite yield strength, V_{fm} is the volume fraction of the polymer, V_{fr}, is the volume fraction of the reinforcing agent (in this case an x-ray shielding particle), σ_m is the ultimate tensile strength of the polymer, and σ_r is the ultimate tensile strength of the reinforcing agent.[22]

In this work, addition of a radiation-blocking microparticle was expected to interrupt the polymer matrix and reduce such mechanical properties as tensile strength; the matrix deformation effect could be worse in the mechanical elastic region.[23,24] According to Eq. 1, however, a low volume fraction of compositing agent would not, in theory, be expected to affect composite yield strength properties. However, marked improvement in x-ray shielding capabilities was hypothesized, owing to Eq. 2, which describes the transmission of an x-ray through a material:

$$I_l = I_o e^{-\left(\frac{\mu}{\rho}\right)_m \rho_c l} \tag{2}$$

where I_o is the intensity of the x-rays before passing through the material, μ is the linear attenuation coefficient, l is the material thickness, and ρ is the density of the material.[25] Specifically, the mass absorption coefficient of the mixture $\left(\frac{\mu}{\rho}\right)_m$ will directly affect the x-ray absorption. In a PMC, the mass absorption coefficient can be expressed by Eq. 3:

$$\left(\frac{\mu}{\rho}\right)_m = x_1\left(\frac{\mu}{\rho}\right)_1 + x_2\left(\frac{\mu}{\rho}\right)_2 \tag{3}$$

where x_1 and x_2 are the mass fractions of substances 1 and 2.[25] Also, because of the constant volume of a 3D printer monofilament, filament mass will be directly related to filament density. Consequently, the density of a PMC can be approximated on the basis of the attenuation coefficient and mass fractions, as shown in Eq. 4.

$$\rho_c = x_1\rho_1 + x_2\rho_2 \tag{4}$$

Therefore, Eq. 2 becomes Eq. 5:

$$I_l = I_o e^{-\left(x_1\left(\frac{\mu}{\rho}\right)_1 + x_2\left(\frac{\mu}{\rho}\right)_2\right)(x_1\rho_1 + x_2\rho_2)l} \tag{5}$$

Equation 5 illustrates that radiation attenuation by a PMC is highly dependent on mass fraction, and not volume fraction.[25] As such, with the correct choice in additive, one can limit the effect on mechanical properties of a high volumetric loading while still providing large radiation attenuation by use of larger mass loading.

Because these structures were primarily designed for space-based applications, for which weight requirements are high-priority, initial testing was limited to materials with a five percent increase by mass as a result of the additive. Tungsten (W) was chosen as an additive, because of its high density (19.3 g/cm^3), known x-ray shielding capabilities, and non-reactivity during chemical functionalization and at extrusion temperatures. As an added benefit of tungsten's high density, low percentage loadings were expected to provide increased radiation shielding without greatly affecting the mechanical properties (because of the low volumetric loading, as explained by Eq. 1).

EXPERIMENTAL

In the work presented in this paper we examined and fully defined the effect of tungsten micro-particles on the physical properties of 3D-printed polycarbonate structures. The evaluation consisted of five specific tests:

1. Dynamic mechanical analysis (DMA);
2. Mechanical tensile testing;
3. Izod impact testing;

4. X-ray transmission (40 keV to 120 keV); and
5. Characterization of gigahertz (GHz) permittivity and loss tangent.

The results were also compared with theoretical values, where available, and the fracture surfaces were analyzed by use of scanning electron microscopy (SEM).

Polycarbonate base resin (Lexan FXD171R; Sabic, Pittsfield, MA, USA) was compounded with tungsten micro-particles (12 μm particle size, Sigma–Aldrich part number 267511) to create a metal-loaded PMC. The compounding process was preceded by a tungsten silane (Xiameter OFS-6032; Dow Corning) functionalization process to improve tungsten dispersion within and bonding with the polycarbonate resin.[26–28] The functionalized tungsten micro-particles were masterbatched with polycarbonate resin, by use of a Carver hot press, and manually kneaded to achieve full particle encapsulation. The PC–W masterbatch material was granulated by use of a polymer granulator (Granu-Grinder; Brabender, Hakensack, NJ, USA) then manually mixed with pure polycarbonate resin to furnish distinct batches containing 1%, 3%, and 5% tungsten by mass (0.1%, 0.2%, and 0.3% by volume) which were then fed to a polymer extruder.

The polycarbonate–tungsten mixture was extruded by use of a Dr Collin (Ebersberg, Germany) ZK 25T twin-screw extruder system equipped with co-rotating, intermeshing screws. All four extruded filaments were produced using the same extrusion conditions: 200°C melt zone in the screw (Dr Collin zones 1–4), no melt pump (Dr Collin zone 5), 198°C tip temperature (Dr Collin zone 6), a tip pressure of 86 bar, extruder screws set to 50 rpm, room humidity of $<40\%$, and a water bath temperature of 18°C. Before extrusion, the masterbatch material was dried in a circulating oven at 120°C for 19 h, and the polycarbonate base resin was dried for 3 h at 120°C by use of a compressed air dryer (Mini 10-CFM; Dri-Air Industries, East Winsor, CT, USA). The resulting filament ($\sim$1.72 mm diameter $\pm$ 0.05 mm) was analyzed by ASTM standard D792-13 specific gravity testing to accurately determine the tungsten volumetric loading; the loadings and specific gravities are listed in Table I.[29]

Table I. Specific gravity calculated by use of ASTM standard D792-13 and the volumetric loading (*W*) of each filament, on the basis of specific gravity measurements

Material	Specific gravity (g/cm^3 – STD 0.003)	*W* (%)
PC – FXD 171R	1.199 (MSDS[a] – 1.20)	–
PC – W	1.214	0.08
PC – W	1.241	0.23
PC – W	1.258	0.33

[a]Lexan FXD171 Technical Data Sheet, Saudi Basic Industries Corporation, 2014.

RESULTS AND DISCUSSION

Material Properties and Print Quality

Initial test specimens were printed with a MakerBot Replicator desktop 3D printer (MakerBot Industries, Brooklyn, NY, USA) and a TA Instruments Q800 dynamic mechanical analysis (DMA) system (TA Instruments, New Castle, DE, USA). The filament was printed into a rectangle (59.74 mm $\times$ 12.85 mm $\times$ 3.14 mm) by use of a 0.6 mm printing tip and a print temperature of 270°C. The resulting DMA samples were frequency cycled (1 Hz to 100 Hz) and temperature ramped (35°C to 180°C) with a dual cantilever sample stage, the results are summarized in Table II.

DMA analysis enables measurement of a wide range of material properties. Of specific interest in this work were complex viscosity, storage modulus, and glass transition temperature (T_g). The glass transition temperature seemed to change by $\sim$4°C in this work, so was expected to have little effect on printing conditions. Storage modulus is a measure of the force necessary to move a DMA sample a specific distance (N/m^2 or Pa); it is, therefore, an estimate of the elasticity (stiffness) of the material, which typically increases as composite loading

Table II. Complex viscosity (measured at 1 Hz), storage modulus (measured at 100 Hz), and glass transition temperature (measured at 100 Hz) obtained by DMA

Material	Viscosity (45°C) (MPa s)	Stor. mod. (45°C) (MPa)	T_g (°C) (100 Hz)	Viscosity (45°C) (MPa s)
FXD 171R	66.36	1222	148.45	0.3503
W – 1%	69.67	1280	151.54	0.3742
W – 3%	70.27	1299	151.55	0.5108
W – 5%	71.42	1315	152.29	0.5569

There is a noticeable increase in storage modulus with increased material loading, implying increasing stiffness. The increase in glass transition temperature is negligible when printing; however, the increase in viscosity suggests a slightly higher print temperature may be needed to maintain print quality.

increases. Complex viscosity is a relative value enabling comparison of possible print conditions for a specific polymer. For example, high complex viscosity may require a 3D printing head to move at slow speed, or use of a higher temperature. Increased print temperature and reduced print speed are undesirable, because if the printing temperature is too high or the polymer is over-exposed to the heated print head, polymer degradation may occur.[30,31] Degradation of polycarbonate typically results in release of aromatic compounds (which is worse in an air environment), contributing to a printed structure with voiding.[30,31] Because of the low percentage volumetric loading in this work, little effect on complex viscosity was expected or observed (~5 MPa s at 40°C and ~0.2 MPa s at 170°C). Therefore, although slight variability in printing conditions was predicted, the loaded filament was expected to print sufficiently well under the conditions used to print specimens from the base resin (FXD171R). Because the test parts were produced with commercially available 3D printers, sections on testing will cover only those printing properties which could be directly controlled by the user; all other printing conditions and system configurations used were the standard settings for each tool.

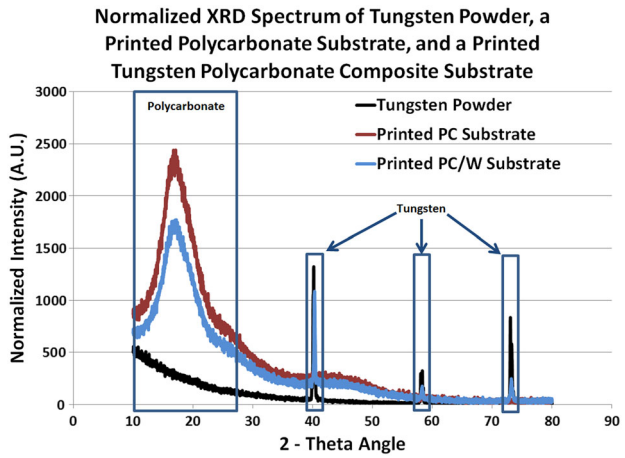

Fig. 1. X-ray diffraction measurements of tungsten powder, printed polycarbonate, and a printed PC–W PMC. The peaks highlighted show the presence of tungsten and polycarbonate. No peaks corresponding to any form of tungsten oxide were detected.

When the tungsten-loaded filament had been shown to be printable, a printed PMC specimen (5% by mass) and a sample of the base powder were analyzed by use of x-ray diffraction (XRD) with a Bruker D8 Discover equipped with a Cu K-alpha source (Bruker AXS, Billerica, MA, USA). These samples were tested to determine whether or not the functionalization/extruding/printing process oxidized the tungsten, creating WO_2 or WO_3, which could, potentially, have reduced x-ray attenuation factors.[32–34] The resulting XRD spectra are shown in Fig. 1.

As is apparent from Fig. 1, the characteristic tungsten x-ray diffraction peaks are present in both samples. A large polycarbonate diffraction peak between 2-theta values of approximately 13° to 25° is also obtained for the printed sample.[35] Because of the strength of the peak, and the lack of an identifiable tungsten oxide peak, it was concluded that our compounding process did not significantly oxidize the tungsten micro-particles.

Because of potential inconsistencies inherent in the 3D printing process (especially when comparing different filament types or printers), the physical property values reported in this work are normalized to percentage air loading (printed air gap). Air loading was determined by comparing printed part density to filament density; the results of this comparison are listed in Table III. It is worth noting that the print orientation for all mechanical test specimens was the ZXY orientation, because this direction has been found to result in the highest ultimate tensile strength (UTS) and impact resistance (when FDM-type processes are used).[2,3] The ZXY orientation values are comparable with most values reported in polymer MSDS data sets, and enable logical initial comparison between printed 3D structures. Samples of printed parts with a tungsten loading of 5% by mass are shown in Fig. 2.

X-ray Radiation Shielding

To determine attenuation of x-ray radiation, specimens (10 cm × 10 cm × 1 cm) were printed with a Stratasys (Eden Prairie, MN, USA) FDM 3000 (liquefier temperature 265°C, combined load 25, chamber temperature 75°C). The FDM 3000 allows manual control of the material feed rate and the

Table III. Percentage air fill of printed parts and the associated standard deviation

Material	FDM 3000 density (g/cm^3) (STD)	FDM 3000% air filling (STD)	400mc density (g/cm^3) (STD)	400mc % air filling (STD)
FXD 171R	0.926 (0.030)	22.83 (2.466)	0.941 (0.0125)	21.563 (1.04)
W – 5%	1.062 (0.019)	15.56 (1.486)	1.046 (0.026)	16.93 (2.095)

The results in this table were calculated by using the filament specific gravity and will be use to compare the mechanical and electromagnetic properties of the final components.

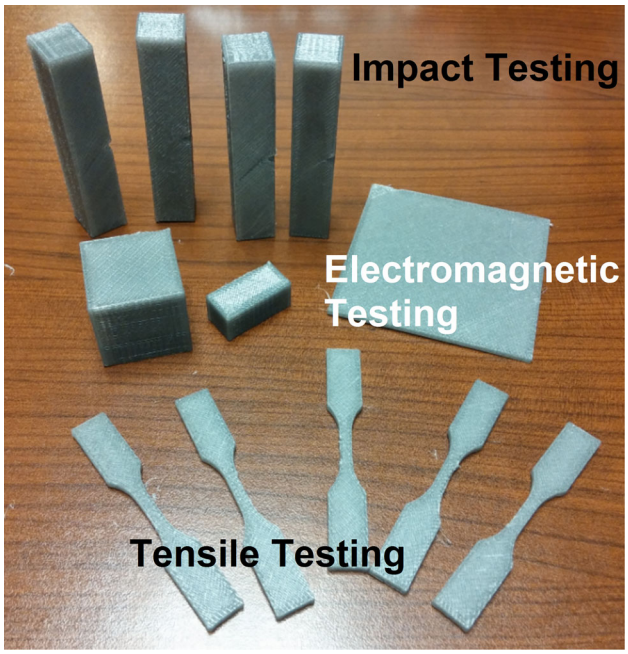

Fig. 2. Printed parts obtained by use of the PC–W PMC filament (~5% by mass). The parts shown (tensile testing, electromagnetic testing, and impact testing) were produced by use of a combination of the FDM 400mc and FDM 3000 3D printers.

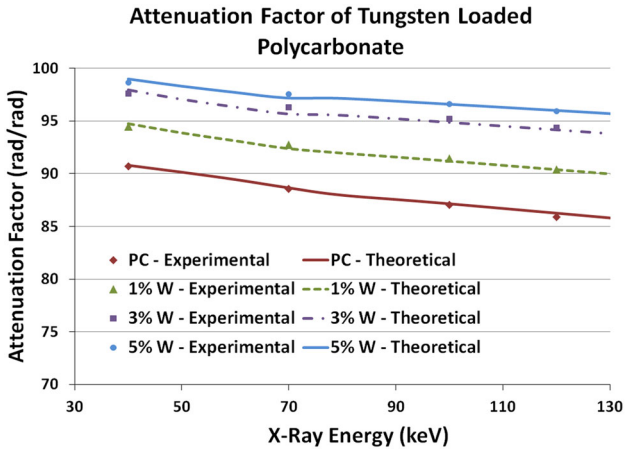

Fig. 3. Theoretical and experimental x-ray attenuation factors. The experimental results were measured at the LEXR Facility at Kirtland Airforce Base; the theoretical results were calculated by use of the Beer–Lambert law.

print head temperature, which is essential when characterizing a new 3D-printable material. This 3D printer also allows use of a temperature-controlled build envelope of 75°C. Samples were printed with approximately 1, 3, and 5% loadings of tungsten (by mass). The measured volumetric loadings are listed in Table I.

X-ray attenuation was measured at Kirtland Air Force Base by use of the low energy x-ray (LEXR) facility and a cobalt-60 source. The resulting attenuation factors are shown in Fig. 3. The expected values in Fig. 3 were determined by use of the Beer–Lambert model and the mass attenuation factors (Eq. 3) described in the Introduction.[33,34]

As is apparent from Fig. 3, the experimental x-ray attenuation follows the Beer–Lambert model. Also, the low percentage loading implemented in this study results in a dramatic increase in x-ray radiation attenuation (~10%) compared with pure polycarbonate. At low x-ray energies (40 keV to 70 keV), a volumetric loading of 0.3% results in an attenuation factor of 96 to 98 (rad/rad) for a relatively low increase in mass (~5%).

Tensile Testing

After x-ray attenuation characterization, the PC and PC–tungsten (~0.3% *v*/*v*) filaments were printed into ASTM D638-10 standard type-V dog-bone samples by use of the Stratasys FDM 3000 printer (liquefier temperature 265°C, combined load 25, chamber temperature 75°C).[36] The ASTM standard dog-bone samples (gauge section 3.18 mm × 3.2 mm) were tested by use of an Instron® (Norwood, MA, USA) 5866 tensile tester equipped with a 5 kN load cell and a strain rate of 10 mm/min, and evaluated in terms of UTS and elongation to break, as shown in Fig. 4.

These tensile testing samples(n = 6) were normalized to percentage air filling, shown in Table III, to obtain relative tensile strength values (independent of print quality) for different materials. By use of this method it is possible to compare UTS and elongation between samples with arbitrary raster filling percentages. Therefore, the changes in mechanical properties (UTS and elongation to break) become a function of fracture origin sites and the inclusion of defect points (composite loaders). The resulting mechanical performance can be directly attributed to the inclusion of loading materials and advantages and/or disadvantages of these loadings on 3D printed polymer systems.

When normalized to percentage air filling, tungsten-loaded polycarbonate does not seem to alter the UTS compared with that of the base polycarbonate resin. By use of the Tukey–Kramer honestly significant difference (HSD) test (q = 2.22813, alpha = 0.05) it was shown that the UTS data were not statistically significantly different among the data sets. As already mentioned, composite yield strength is a function of volumetric loading, so this result is expected for low loading of tungsten (~0.3% by volume). However, the DMA data in Table II shows a noticeable increase in storage modulus (~7.6%), implying an increase in material stiffness. These data were not corroborated by a Tukey–Kramer HSD (q = 2.22813, alpha = 0.05) which did not indicate a statistically significant reduction in elongation until break (Fig. 4). However, such a small percentage change in elongation is within the standard deviation experienced during testing.

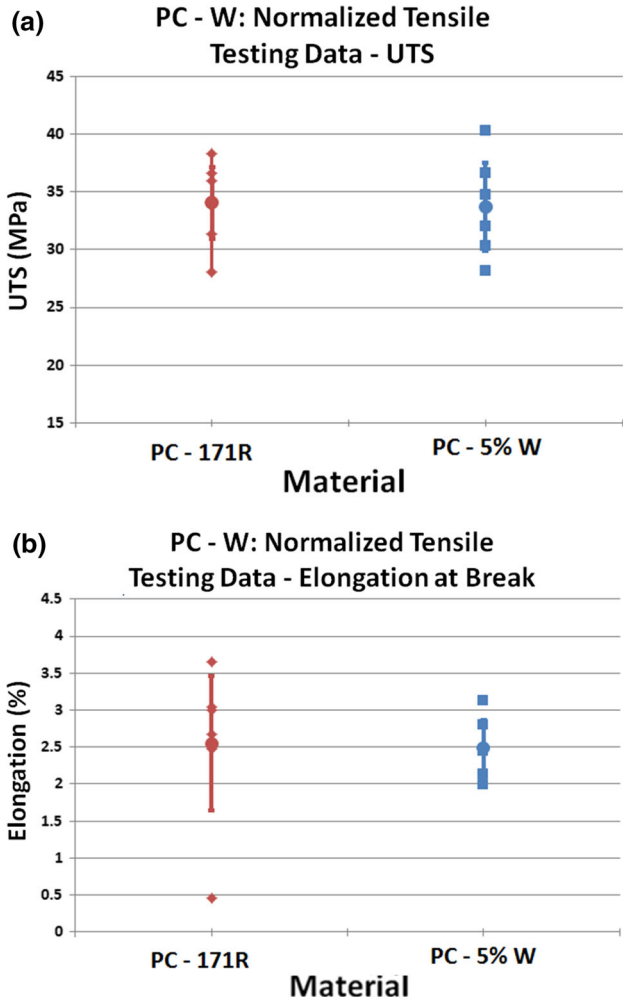

Fig. 4. ASTM standard type-V dog-bone samples tested for normalized ultimate tensile strength (a) and elongation to break (b). Individual data points are shown as small points, larger circular points depict the averages, and the standard deviation is shown as a bar through the sample points. The results were analyzed by use of the Tukey–Kramer HSD method, which revealed no statistically significant difference for UTS or elongation to break.

Impact Testing

Other samples (intended for impact testing and GHz characterization) warped severely when printed by use of the FDM 3000; as a result, PC and PC–tungsten (~0.3% by vol.) impact test specimens were printed by use of a Stratasys FDM 400mc (liquefier temperature 316°C, chamber temperature 95°C). Impact samples (12.7 mm × 12.7 mm × 63.5 mm) were printed using the ASTM D256-10 standard for Izod impact testing.[37] The notched impact test samples were measured for impact resistance (J/m) and normalized for percentage air loading as described in Table III; the resulting impact resistances are shown in Fig. 5.

As with the mechanical tensile testing samples, the impact resistance results (n = 5) were normalized to the printed percentage air fill. This enables direct comparison between material properties

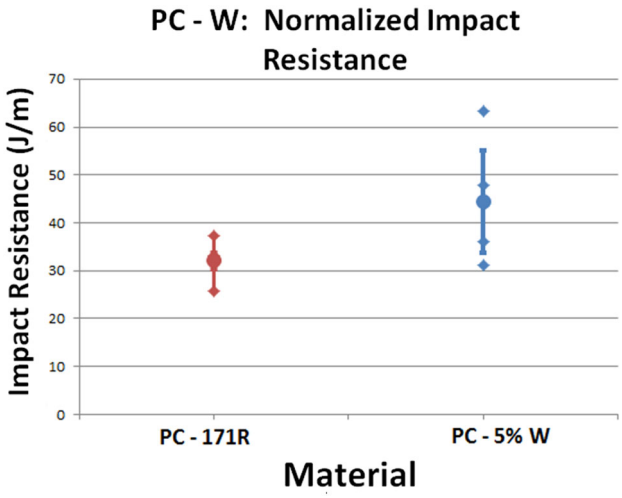

Fig. 5. Normalized impact resistances measured by use of ASTM standard notched impact specimens. Averages are marked by circular points, individual measurements are represented by diamond shapes, and the standard deviations are represented by a bar through the data sets. Tukey–Kramer analysis revealed the data sets were not statistically significantly different.

while neglecting the effects of increased air gaps obtained during the printing process. The resulting impact resistances imply the possibility of increased impact resistance with addition of tungsten nano-particles. A slight improvement in impact resistance could have been expected, because of the increased storage modulus obtained during DMA testing. However, the large standard deviation, in comparison with the baseline PC, between specimens implies that at low loadings there is some print or filler variability along the fracture plane. Also, this variability in the PC–tungsten structures results in a non-statistically significant difference between the data sets when using Tukey–Kramer HSD analysis (q = 2.306, alpha = 0.05). The Tukey–Kramer HSD analysis implies that impact resistance is generally unaltered at these low tungsten loadings.

Electromagnetic Characterization

Electromagnetic characterization was performed on a waveguide vector network analyzer (VNA) from 7 to 13 GHz, by use of terahertz time domain spectroscopy (TDS) from 100 GHz to 500 GHz, and modeled by use of the effective medium theory at 10 GHz. Effective medium theory is useful when the dimensions of all mixtures are much smaller than the operating wavelength. For a two-phase mixture of a random inclusion in a homogeneous host, the effective permittivity depends on the shape and size of the inclusion, the distance between inclusion particles, the volume fraction of the inclusion, the alignment of the inclusion, and the permittivity contrast (the ratio between the permittivity of the inclusion and that of the host material). As was observed in this work, a larger-than-unity permittivity contrast (the ratio

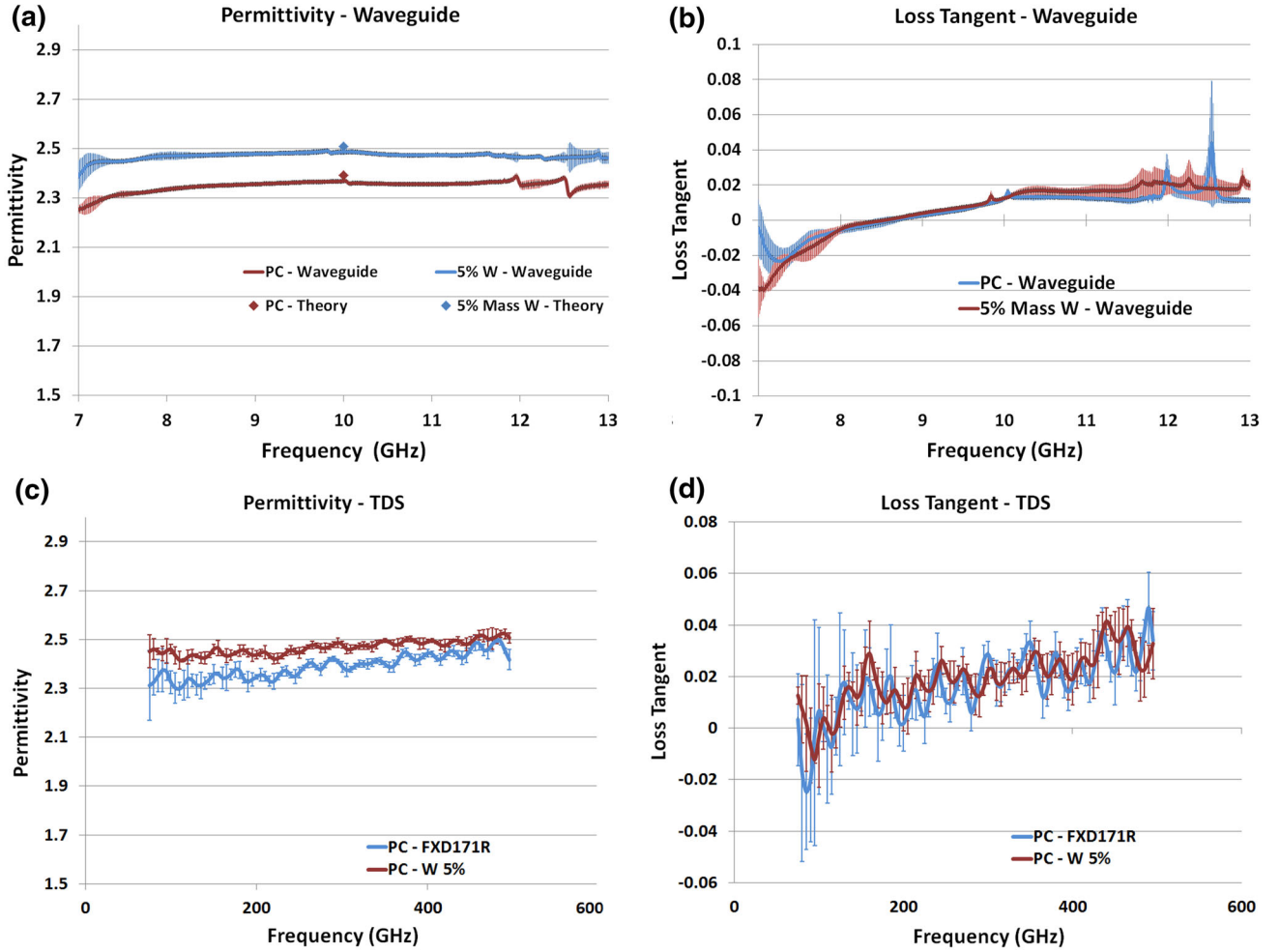

Fig. 6. Top: permittivity (a) and loss tangent (b) obtained by use of a VNA and a micro-strip waveguide; error bars are shown as shaded areas. The micro-strip permittivity (a) also shows the theoretical value expected by use of the Bruggeman effective media model. A slight increase in permittivity (∼4%) and an almost constant loss tangent are observed as a result of addition of W (5% by mass) to the polycarbonate. Bottom: permittivity (c) and loss tangent (d) obtained by use of THz TDS. A slight increase in permittivity is again observed when W is added; however, both PC and PC–W (5% by mas) have similar permittivity and loss tangents.

between the permittivity of the inclusion and that of the host material), inclusions of low volume fraction, and the existence of clusters, enables the Bruggeman model to be implemented.[38]

The permittivity and loss tangent data were measured by use of a microwave VNA in waveguide mode from 7 GHz to 13 GHz and by terahertz (THz) TDS from 100 GHz to 500 GHz. By filling the rectangular waveguides of a VNA with a slab of sample material under test and measuring the full two-port S-data, both the dielectric and magnetic properties, including loss tangents, can be extracted.[39] TDS utilizes a THz time domain signal with and without a sample, and extracts the dielectric constant and loss tangent.[40] The electromagnetic characterization samples were fabricated by use of an FDM 400mc (liquefier temperature 316°C, chamber temperature 95°C) and a sample size of 1 cm × 1.1 cm × 2.3 cm. The measured and theoretical permittivity and loss tangents are shown in Fig. 6.

Electromagnetic characterization, shown in Fig. 6, reveals an important benefit when choosing tungsten as an x-ray radiation shielding composite. The high density of tungsten has previously been shown to increase the x-ray shielding capabilities of a 3D printed structure. At GHz frequencies, however, the low percentage volume of tungsten does not seem to contribute to an increase in as printed loss tangents. This may enable 3D printed antennas to be constructed directly within a 3D printed tungsten-loaded structure without a noticeable effect on antenna performance. Also observed within tungsten–PC materials, is a slightly increased permittivity, possibly enabling future permittivity adjustment to reduce antenna physical size. It is important to note that the theoretical permittivity obtained by use of the effective media theory Bruggeman model is in agreement with the measured data at 10 GHz, shown in Fig. 6a.

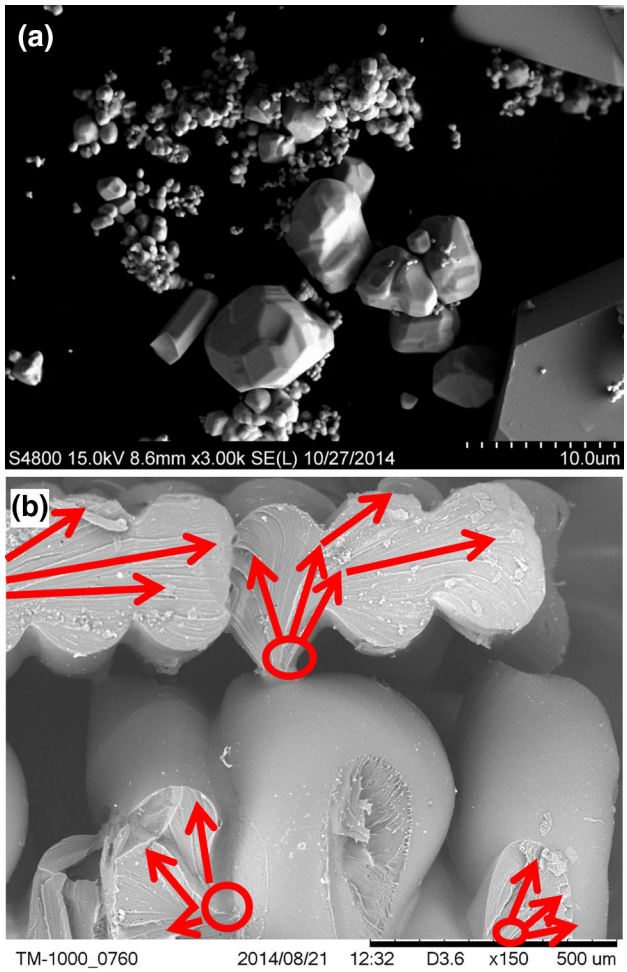

Fig. 7. Tungsten particles in a polycarbonate matrix composite (a). The fracture surface of the tensile testing specimens (b) seems to have fracture origins at the edges of printed rasters. This implies that failure occurred not at a tungsten–PC interface but at an air–PC interface.

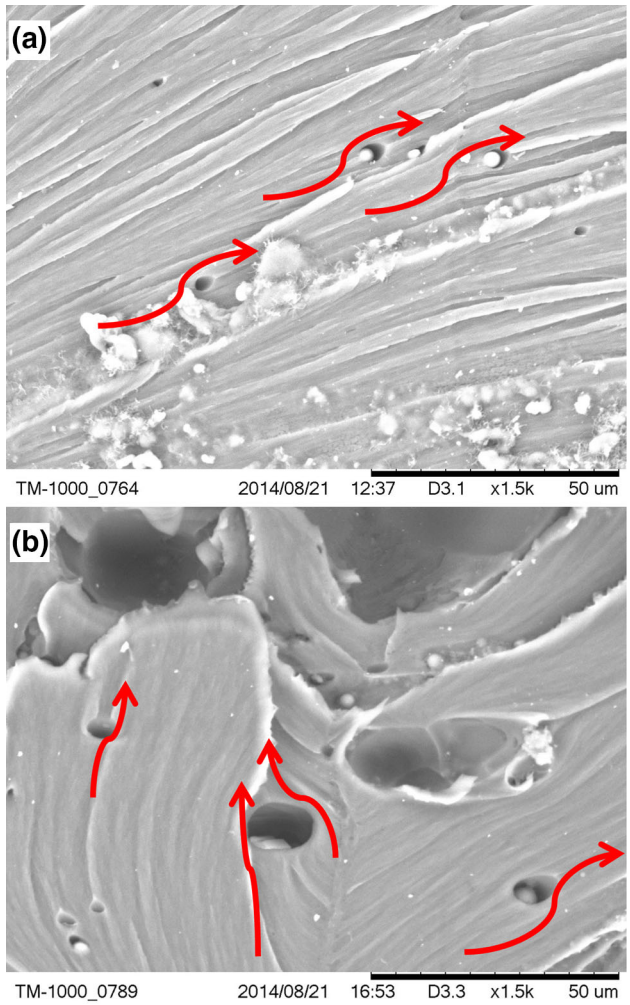

Fig. 8. High magnification of tungsten particles in a crack hackle region (a) and a region of high craze cracking (b) show that crack propagation passes around the tungsten particles without the characteristic mirror regions indicative of a crack origin site. This implies that the particles are defect sites, but not fracture origins.

Scanning Electron Microscopy

The fracture surfaces of the tensile and impact testing specimens were examined by use of both optical microscopy and an Hitachi TM-1000 scanning electron microscope (SEM) (Hitachi High-Technologies Europe, Germany) operating with a 15 kV acceleration voltage and equipped with a backscatter electron (BSE) detector. Optical microscopy enabled determination of whether print raster errors were present within the part, and SEM analysis could be used to characterize both printing error crack initiation sites; only SEM images are included in this work. If the tungsten particles, Fig. 7a, act as a failure point or stress concentrator, crack initiation will be visible under SEM at the point where the tungsten meets the polymer matrix.

Figure 7b shows a low magnification image of a tungsten composite dog-bone structure. On the fracture surface, many crack initiation sites are apparent (some examples are highlighted in red). However, these sites appear to be initiated from the edge of printed rasters. Failure occurring at the air–PC interface and not the PC–W interface implies that inclusion of the tungsten does not create points of failure within the structure. On analysis under higher magnification of a crack hackle region (Fig. 8a) and a craze cracking site (Fig. 8b), it becomes apparent that the fractures tend to propagate around the tungsten particles without the characteristic mirror and mist zones, which implies the particles act as a defect rather than a crack origin. If the tungsten particles were acting as a point of failure, one would expect the UTS to be noticeably reduced, which was not observed in this work. Therefore, as a defect, the tungsten particles should have little effect on UTS or impact resistance (because of the low percentage loading of tungsten), as was demonstrated by the tensile testing results and, to a lesser extent, the impact testing results.

CONCLUSION

Comprehensive analysis of tungsten-loaded polycarbonate 3D printing filaments is reported in this paper. The polycarbonate–tungsten polymer matrix composite was shown to be printable and resulted in marked improvement of x-ray radiation shielding (~10%), even for low-volume loadings of tungsten (~0.3% by volume). Furthermore, because of the low-volume loading, the electromagnetic properties of the polycarbonate composite were not degraded—there was no significant increase in loss tangent or change in permittivity within the GHz frequency range. These electromagnetic properties may enable antennas to be embedded within the PC–W substrates with little loss of antenna performance. The PMC will also furnish electrical components with improved x-ray shielding capability.

The mechanical properties of the tungsten PMC were also characterized. DMA, tensile testing, and impact testing were performed to determine any associated changes in mechanical properties. DMA analysis showed that increased tungsten loading increased the storage modulus and complex viscosity of the polycarbonate while maintaining a fairly constant glass transition temperature. By use of Tukey–Kramer HSD statistical analysis it was shown there was no statistically significant change in UTS, elongation to break, or impact resistance.

Fractography, by examination of SEM micrographs, led to the discovery that the vast majority of crack initiation sites originated from printed raster edges. On closer examination, the fracture surface morphology indicated that cracks propagate around the tungsten micro-particles. This propagation behavior implies that, although the tungsten particles are a defect in the material, they do not act as crack-initiation sites.

The characterization performed in this work reveals the ability of tungsten micro-particles to act as a radiation shield within a 3D printable polymer matrix composite. Addition of the tungsten has little effect on electromagnetic and mechanical properties, and the low percentage loading volumes result in a slight increase in total mass only, as is necessary for most space-based applications.

ACKNOWLEDGEMENTS

We would like to thank the Intelligence Community Postdoctoral Research Fellowship Program, The University of Texas at El Paso, the W. M. Keck Center for 3D Innovation, the University of Arizona, COSMIAC, and NASA Glenn Research Center. The research presented here was performed as a result of funding in part from The America Makes Manufacturing Initiative, the State of Texas Emerging Technology Fund, the National Aeronautics and Space Administration under grant number NNX13AB53G, AFOSR YIP under grant number FA9550-14-1-0260, the National Science Foundation under awards 0823864 and 0925220, and the state of Arizona under TRIF. This project was supported by a grant from the Intelligence Community Postdoctoral Research Fellowship Program through funding from the Office of the Director of National Intelligence. All statements of fact, opinion, or analysis expressed are those of the authors and do not reflect the official positions or views of the Intelligence Community or of any other US Government agency. Nothing in the contents should be construed as asserting or implying US Government authentication of information or Intelligence Community endorsement of the author's views.

REFERENCES

1. D. Espalin, D. Muse, E. MacDonald, and R. Wicker, *Int. J. Adv. Manuf. Technol.* 72, 963–978 (2014).
2. C. Rocha, A. Torrado-Perez, D.A. Roberson, C. Shemelya, E. MacDonald, and R. Wicker, *J. Mater. Res.* 29, 1859–1866 (2014).
3. A. Torrado-Perez, D.A. Roberson, and R.B. Wicker, *J. Fail. Anal. Prev.* 14, 343–353 (2014).
4. E. Aguilera, J. Ramos, D. Espalin, F. Cedillos, D. Muse, R. Wicker, and E. MacDonald, In *Proceedings of Solid Freeform Fabrication Symposium*, pp. 950–961 (2013).
5. A. Lopes, M. Navarrete, F. Medina, J. Palmer, E. MacDonald, and R. Wicker, In *Proceedings of 17th Solid Freeform Fabrication Symposium*, pp. 644–655 (2006).
6. R.B. Wicker, F. Medina, and C. Elkins, In *Proceedings of 15th Solid Freeform Fabrication Symposium*, pp. 754–764 (2004).
7. F. Medina, A. Lopes, A. Inamdar, R. Hennessey, J. Palmer, B. Chavez, D. Davis, P. Gallegos, and R. Wicker, In *Proceedings of 16th Solid Freeform Fabrication Symposium*, pp. 39–49 (2005).
8. A.J. Lopes, E. MacDonald, and R. Wicker, *Rapid Prototyp. J.* 18, 129–143 (2012).
9. J.A. Palmer, B. Jokiel, C.D. Nordquist, B.A. Kast, C.J. Atwood, E. Grant, F.J. Livingston, F. Medina, and R.B. Wicker, *Rapid Prototyp. J.* 12, 148–155 (2006).
10. M. Navarrete, A. Lopes, J. Acuna, R. Estrada, E. MacDonald, J. Palmer, and R. Wicker, In *Proceedings of 18th Solid Freeform Fabrication Symposium*, pp. 575–585 (2007).
11. D. Periard, E. Malone, and H. Lipson, In *Proceedings of 17th Solid Freeform Fabrication Symposium*, pp. 503–512 (2007).
12. E. DeNava, M. Navarrete, A. Lopes, M. Alawneh, M. Contreras, D. Muse, S. Castillo, E. MacDonald, and R. Wicker, In *Proceedings of 19th Solid Freeform Fabrication Symposium*, pp. 362–369 (2008).
13. C. Gutierrez, R. Salas, G. Hernandez, D. Muse, R. Olivas,E. MacDonald, M.D. Irwin, R. Wicker, M. Newton, K. Church, and B. Zufelt, In *Proceedings of 2011 IMAPS Symposium* (2012).
14. D.A. Roberson, R.B. Wicker, and E. MacDonald, *J. Electron. Mater.* 41, 2553–2566 (2012).
15. R.B. Wicker, F. Medina, E. MacDonald, D.W. Muse, and D. Espalin, U. S. Patent Pending (Application 13/343,651—3/14/2013).
16. R.B. Wicker, F. Medina, E. MacDonald, D.W. Muse, and D. Espalin, U. S. Patent Pending (Application 13/829,723—3/14/2013).
17. E. MacDonald, R. Salas, D. Espalin, M. Perez, E. Aguilera, D. Muse, and R. Wicker, *Access IEEE* 2, 1–12 (2013). doi: 10.1109/ACCESS.2014.2311810.
18. C. Shemelya, F. Cedillos, E. Aguilera, E. Maestas, D. Espalin, D. Muse, R. Wicker, and E. MacDonald, In *Proceedings of 2013 IEEE Sensing*, pp. 1–4 (2013).
19. C. Shemelya, F. Cedillos, E. Aguilera, D. Espalin, D. Muse, R. Wicker, and E. MacDonald, *IEEE Sens. J.* 15, 1280–1286 (2014). doi:10.1109/JSEN.2014.2356973.

20. D.A. Roberson, R.B. Wicker, and E. MacDonald, *Mater. Lett.* 76, 51–54 (2012).
21. R.B. Wicker and E.W. MacDonald, *Virtual Phys. Prototyp.* 7, 181–194 (2012).
22. D. Askeland, P. Fulay, and W. Wright, *The Science and Engineering of Materials*, SI ed. (Stamford: Cengage Learning, 2011), p. 661.
23. M.Z. Ronga, M.Q. Zhang, Y.X. Zheng, H.M. Zeng, R. Walter, and K. Friedrich, *Polym.* 42, 167–183 (2001).
24. C.L. Wu, M.Q. Zhang, M.Z. Rong, and K. Friedrich, *Compos. Sci. Technol.* 62, 1327–1340 (2002). doi:10.1016/S0266-3538(02)00079-9.
25. B.D. Cullity, *Elements of X-ray Diffraction*, 2nd ed. (Reading: Addison Wesley, 1978).
26. S.C. Tjong, *Mater. Sci. Eng. R* 53, 73–197 (2006).
27. Y. Xie, C.A.S. Hill, Z. Xiao, H. Militz, and C. Mai, *Compos. A* 41, 806–819 (2010).
28. S.-Y. Fu, X.-Q. Feng, B. Lauke, and Y.-W. Mai, *Compos. B* 39, 933–961 (2008).
29. ASTM Standard D792-13 (2013).
30. B.N. Jang and C.A. Wilkie, *Thermochim. Acta* 426, 73–84 (2005).
31. W. Zhoua, H. Yang, and J. Zhou, *J. Anal. Appl. Pyrolysis* 78, 413–418 (2007).
32. N.Z. Noor Azman, S.A. Siddiqui, R. Hart, and I.M. Low, *Appl. Radiat. Isot.* 71, 62–67 (2013).
33. E.B. Saloman, J.H. Hubbell, and J.H. Scofield, *Atom. Data Nucl. Data Tables* 38, 1–197 (1988).
34. J.H. Hubbell and S.M. Seltzer, Tables of x-ray mass attenuation coefficients and mass energy-absorption coefficients, version 1.4 (National Institute of *Standards and* Technology 2004), http://physics.nist.gov/xaamdi. Accessed 29 Jan 2015.
35. M.F. Garbauskas, *Handbook of Polycarbonate Science and Technology*, ed. J.T. Bendler (CRC Press, New York, 1999), p. 294.
36. ASTM Standard D638-10 (2010).
37. ASTM Standard D256-10 (2010).
38. A. Sihvola, IEEE Electromagn. Waves Ser. 47 (IEE Press, London, 1999).
39. L. Wang, R. Zhou, and H. Xin, *IEEE Trans. Microw. Theory Technol.* 56, 499–506 (2008).
40. M. Liang, Z. Wu, L. Chen, L. Song, P. Ajayan, and H. Xin, *IEEE Trans. Microw. Theory Technol.* 59, 2719–2725 (2011).

Evaluation of 3D Printable Sustainable Composites

David A. Roberson [1,2,*], Carmen R. Rocha [1,2] , Monica Piñon [1,3]

1. Polymer Extrusion Lab, W. M. Keck Center for 3D Innovation, The University of Texas at El Paso, El Paso, TX 79968
2. Department of Metallurgical and Materials Engineering, The University of Texas at El Paso, El Paso, TX 79968
3. Department of Mechanical Engineering, The University of Texas at El Paso, El Paso, TX 79968

*Corresponding Author: D. A. Roberson, droberson@utep.edu

Abstract

Polylactic acid (PLA) is rapidly becoming the mainstay material for use in desktop grade 3D printers based on FDM technology in part due to the environmental sustainability of this polymer. While biodegradability is an advantage; as compared to other materials used by FDM-type platforms, there is a lack of desirable physical attributes. The work presented here evaluates the altering of the physical properties of PLA through the addition of sustainable additives. Here, the physical properties of PLA were modified while, at the same time the two desirable aspects of 3D printer compatibility and biodegradability were retained. Rheological analysis of the material systems was performed by dynamic mechanical analysis and failure analysis of 3D printed tensile specimens was carried out through the use of scanning electron microscopy. Finally, biodegradability of the novel PLA-based material systems was assessed based on in-soil exposure testing.

Key Words: 3D Printing; Materials Characterization; Polymer Matrix Composites

Introduction

Desktop-grade additive manufacturing (AM) platforms based on Fused Deposition Modeling (FDM) technology have become a mainstay among home users, educators, and entrepreneurs. Predominantly relying on acrylonitrile butadiene styrene (ABS) or polylactic acid (PLA) as feedstock, there has been a recent trend of PLA-specific platforms such as the fifth generation MakerBot Replicator and the Printrbot Simple 3D printer. The reason for this shift in material type to PLA is debatable and could be related to perceived health detriments due to the use of ABS in 3D printing applications [1] or the environmentally friendly nature of PLA due to its biodegradability [2, 3].

PLA is a biopolymer derived from renewable resources such as corn and sugarcane and while there are examples of other polymers; namely polyethylene, which have been synthesized from the same sustainable resources, the biodegradable aspect of PLA sets it apart from other engineering plastics. The need for biodegradable polymers stems from the environmental impact of the use of polymeric waste most exemplified by the great garbage patches found in both the Atlantic and Pacific oceans [4-6].

Though PLA does have the unique aspect of being a biodegradable biopolymer; other than 3D printing, the main use of this material is food packaging and disposable utensils. To find a broader range of applicability, the physical attributes of PLA must be altered. As demonstrated by Roberson *et. al*, [7] expanding the applicability of FDM-type 3D printing also lies in the altering of the material properties of feedstock constituents. Therefore, the broadening of the physical capabilities of PLA will contribute to expanding the applicability of polymer extrusion 3D printing technologies.

Several instances of the development of 3D-printer compatible polymer matrix composites (PMC)s with specific end use applications can be found in literature. For example, Shemelya *et al*. [8] demonstrated a tunable polycarbonate matrix tungsten composite for 3D-printable radiation shielding while Masood and Song [9] demonstrated the capability to alter the heat transfer kinetics of nylon by compounding either copper or iron particles where the end goal was the creation of 3D-printable injection mold tooling.

The work presented in this paper demonstrates the altering of the physical properties of PLA while maintaining 3D printer compatibility and biodegradability. Polymer matrix composites were created from a PLA base resin where the filler materials were sustainable substances. Here, we combined PLA with NaCl, jute plant fiber and organo nanoclay pigments. Sodium chloride was chosen due to its abundance, while jute plant fiber was chosen due to examples in literature if the use of this constituent in plant fiber reinforced PMCs [10-13]. Palygorskite-based (palygorskite is an organo nanoclay) pigments, originally developed by the Mayan Culture of Mesoamerica were chosen for this study based on work demonstrating an improvement to the mechanical properties of high density polyethylene (HDPE) [14].

Experimental Procedure

For this work, Ingeo PLA, Grade 4043D (NatureWorks, LLC, Minnetonka, MN, USA) was extruded into a polymeric monofilament through the use of a twin screw extruder/compounder (Dr. Collin Model ZK 25T, Dr. Collin, Ebersberg, Germany) equipped with intermeshing co-rotating screws. Baseline PLA and composite PLA-based filaments were extruded to a target diameter of 1.75mm, one of the two standard diameters common among material extrusion 3D printers (the other being 3mm). In the case of composites, a masterbatch of concentrated material was first created by manually kneading PLA pellets with filler materials through the use of a Carver hot press (Carver, Inc., Wabash, IN, USA). The masterbatch was then granulated with a Brabender GranuGrinder (C.W. Brabender South Hackensack, NJ, USA) and subsequently combined with virgin PLA material in the extruder system.

Test specimens were fabricated according the Type V dimensions as described in the ASTM D638-10 standard by printing test specimens with a MakerBot Replicator 2X (MakerBot Industries, Brooklyn, NY, USA) or a Rostock Max Delta 3D printer (SeeMe CNC, Goshen, IN, USA) where the latter unit was modified with an E3D V6 hotend (E3D-Online Limited, Chalgrove Oxfordshire , UK). Tensile testing was carried out with an Instron® 5866 (Instron, Norwood, MA) tensile testing machine equipped with a 10kN load cell. Dynamic mechanical analysis (DMA) was also performed on all material systems with a TA Q800 (TA Instruments, New Castle, DE, USA).

Four individual filler materials were combined with PLA in the formation of sustainable 3D printable polymer matrix composites: 1) Sodium chloride (NaCl) (Sigma); 2) jute plant fiber sourced from rope purchased from Home Depot; 3) MayaCrom® Blue; and 4) MayaCrom® yellow (both from Mayan Pigments. Inc., El Paso, TX, USA). The filler materials evaluated in this study were chosen based on the perceived environmental sustainability. All additives were blended at a 5% (by weight) ratio to PLA.

Fracture surface analysis was carried out through the use of a tabletop scanning electron microscope (SEM) operating with an acceleration voltage of 15kV and equipped with a backscatter electron (BSE) detector (Hitachi, Model TM-1000,Hitachi High-Technologies Europe GmbH, Germany). To reduce charge effects within the SEM, all samples were sputter coated with a gold palladium target for 30s with a Gatan Model 682 Precision Etching Coating System (Gatan, Inc., Pleasanton, CA, USA) prior to microscopic analysis.

Results

Tensile test results (Fig. 1) revealed that the addition of jute plant fiber and MayaCrom® Blue led to tensile test specimens with lower ultimate tensile strength values lower than those printed from PLA alone. This decrease in strength may be due to the degradation of the organic components of each additive as noted in Torrado et al. [15] However, the addition of jute plant fiber increased the % elongation specimens were able to endure during the tensile test process. The addition of NaCl did not greatly affect the mechanical properties.

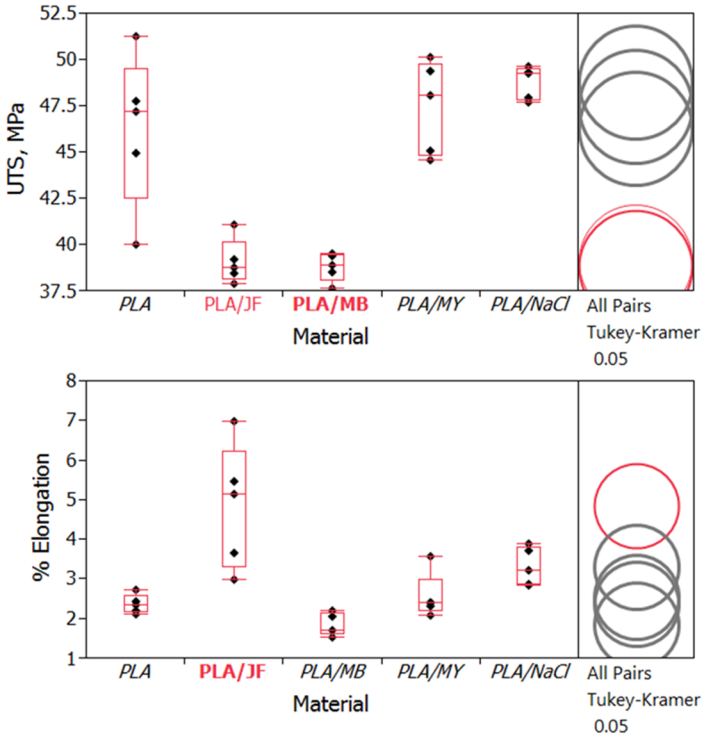

Fig. 1. Tensile test results of materials tested here.

Subjecting the material types evaluated here to DMA testing revealed differences in the thermomechanical behavior of the composite materials as compared to the baseline PLA resin. The addition of both NaCl and jute plant fiber to PLA reduced slightly the onset of glassy behavior as determined by the storage modulus curve, however the temperature at which the maximum tan δ occurred was increased, which effectively broadened the thermal window of elastic behavior as compared to baseline PLA (Table 1.) where the addition of jute increased this window by ~8.4°C. In the case of NaCl, though the temperature at which the maximum tan δ occurred was increased, the actual value of this parameter was virtually the same as PLA (1.8) meaning the elasticity was not altered. The addition of both types of MayaCrom®

pigments as well as jute plant fiber decreased the maximum tan δ indicating and increase in the elasticity of these composites as compared to the PLA base resin.

Table 1. DMA Data for the materials tested here.

Material	Storage modulus at 40 °C, MPa	Complex viscosity at 80 °C, MPa·sec	Max tan delta
PLA	2683	8.76	1.8
PLA/ MayaCrom® Blue	2162	1.052	1.166
PLA/ MayaCrom® Yellow	2146	3.58	0.8233
PLA/NaCl	2302	0.4133	1.797
PLA/Jute	2113	2.307	0.8206

Fractography (Fig. 2) of tensile test specimens printed from the composites tested here allowed for observations related to the robustness of the filler/matrix interface as wells the effect of additives to the crack surface morphology to be made. Baseline PLA tensile specimens possessed a fracture surface morphology indicative of a brittle failure mode which correlates will with the low % elongation at break values observed for the material. Fracture surface analysis revealed NaCl to adhere well to the PLA matrix. Crack propagation is evident on the surfaces (highlighted in Fig 3) of the individual particles. There is also no evidence of particle pull out nor were there any gaps between the particles and the matrix. By contrast the fracture surface of the PLA/jute plant fiber composite possessed features indicating a poor interface between the fibers and the matrix (indicated by white arrows in Fig. 1b). The addition of MayaCrom® pigments had the effect of inducing voids within the PLA matrix which accounts for the decrease in tensile strength as compared to baseline samples.

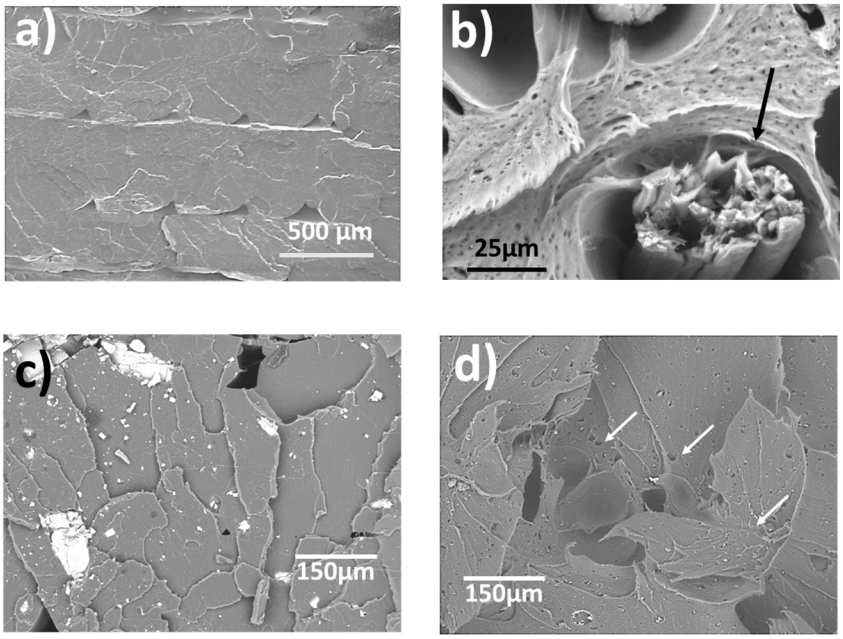

Fig. 2. SEM Micrographs of materials tested in this study: a) PLA; b) PLA/jute plant fiber; c) PLA NaCl; and d) PLA/MayaCrom® Blue.

Of the additives tested here, NaCl produced results worthy of deeper investigation. While the addition of jute plant fiber increased the glass transition window, the poor adhesion to the matrix at room temperature was a detractor to the overall performance of this composite. Since NaCl exhibited characteristics indicating a robust bond with the PLA matrix, another experiment was carried out where jute plant fiber was first functionalized in an aqueous NaCl solution prior to compounding. The result was a decrease in % elongation while the UTS remained the same (Fig. 4). Further analysis of the fracture surface via SEM (Fig. 5) revealed the presence of polymer fibrils joining the matrix to the jute fiber which formed during the tensile testing process. The presence of these fibrils indicated a robust bond had formed between the matrix and the fiber as the formation of fibrils is cause by the elongating of polymer chains under tension. The decrease in % elongation in conjunction with yield strength values similar to those of the non-functionalized samples indicates an increase in stiffness caused by an increase in the bond strength between the fiber and the matrix.

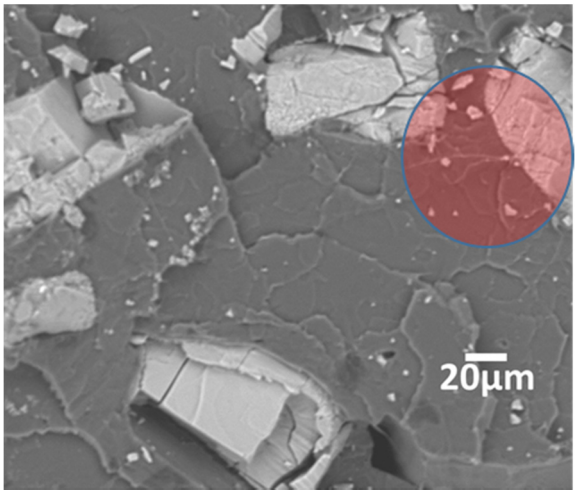

Fig. 3 NaCl adhered well to the matrix and exhibited a robust interface and shared crack propagation features with the matrix.

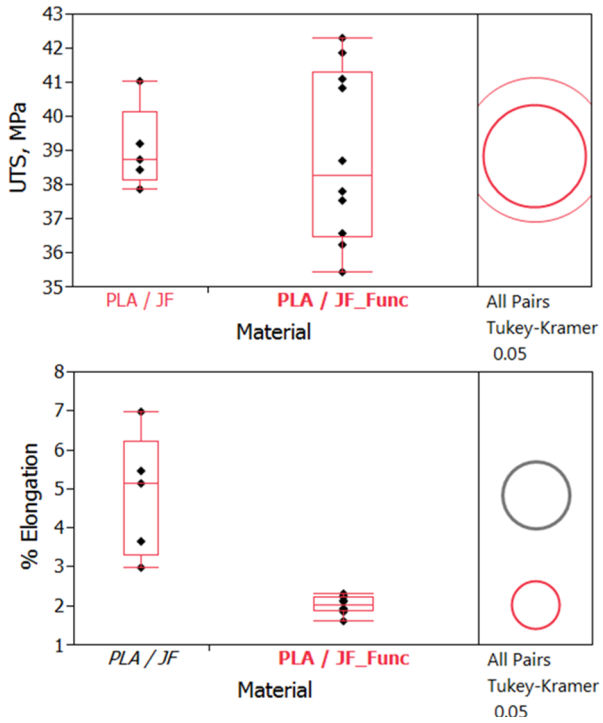

Fig. 4 The effect of NaCl functionalization of jute plant fiber on the mechanical properties of PLA/jute fiber composites.

Further analysis of the addition of NaCl to PLA on 3D printed tensile specimens entailed examining the effect of NaCl on the mechanical property sensitivity to raster orientation of 3D printed tensile test specimens. Here two raster patterns were used to print the tensile test specimens: 1) a crosshatched raster pattern where layers alternated by 90°; and 2) a transversal raster pattern where the print layers were perpendicular to the length of the tensile specimen. In the case of the transversal specimen, there was no perimeter shell and it is noted that Torrado [16] noted this print raster pattern to be equivalent in terms of UTS with tensile test specimens printed in the ZXY print orientation. Comparing the sensitivity to raster pattern between PLA and the PLA/NaCl composite revealed the addition of NaCl to reduce the difference in UTS between the

transversal and crosshatched raster pattern (Fig. 6.). More notable is that this decrease in mechanical property anisotropy did not come at the expense of overall yield strength as has been the case in work related to decreasing the anisotropy of ABS-based ternary polymeric blends as explored in Torrado *et al.* [17].

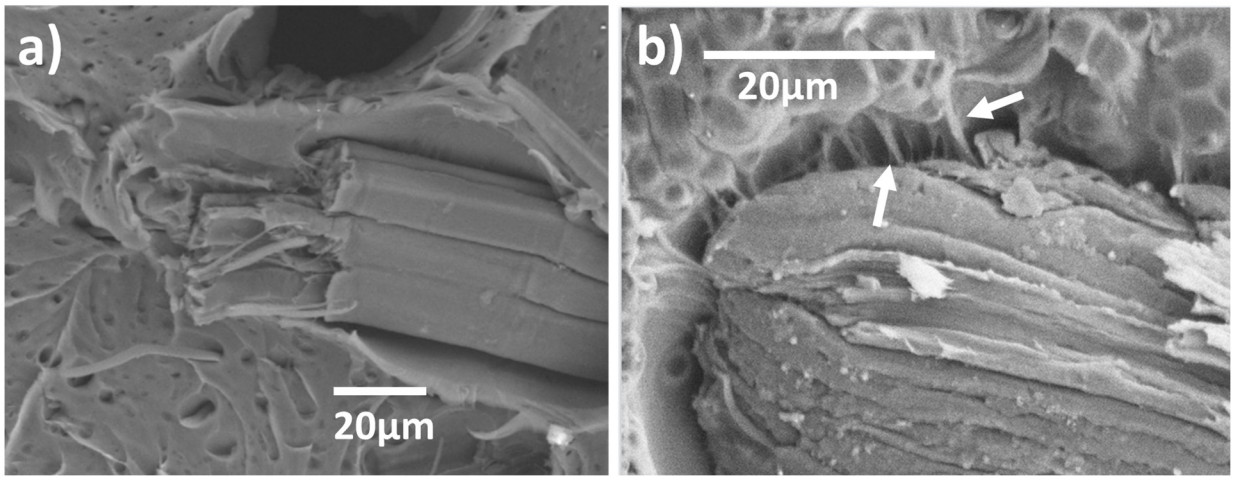

Fig. 5. a) non functionalized jute fiber and b) NaCl functionalized jute fiber. Note the presence of fibrils for the functionalized plant fibers.

Biodegradability

An attempt to assess the biodegradability of the PLA based composites evaluated in this study. Samples were buried for two and twelve weeks in topsoil which was moistened with food grade vinegar. The effect of exposure to the soil environment was assessed by tensile testing of the exposed samples as well as the monitoring of weight change before and after exposure. No observable difference to weight was observed for any of the samples buried in the soil environment for two weeks. However, after 12 weeks, PLA specimens exhibited an increase in weight, while (1.95± 0.02 g increasing to 2.03 ± 0.01 g) the PLA/NaCl composite exhibited a decrease in weight (2.49 ± 0.03 g decreasing to 2.24 ± 0.12 g). In terms of tensile strength, both PLA and the PLA/jute fiber composite exhibited an increase in tensile strength compared to non-exposed control samples while the PLA/NaCl composite exhibited a decrease in tensile strength as compared to non-exposed samples (Fig. 7.) Further exploration is needed to understand if the decrease in tensile strength and tensile strength is due to biodegradation or the effect of moisture. NaCl is water soluble and the decrease in weight and tensile strength could be due to dissolution of this substance within the PLA matrix. The increase in tensile strength and weight for PLA as

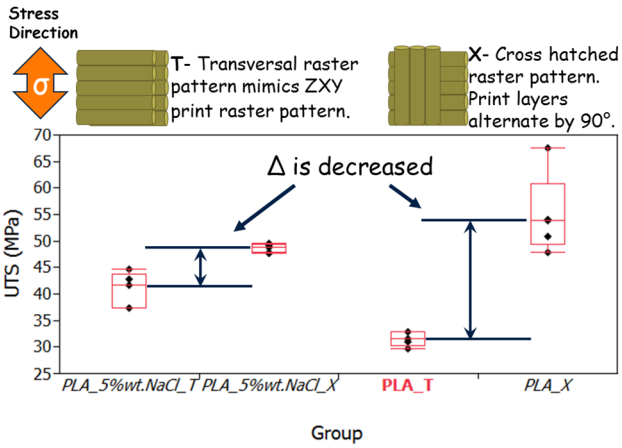

Fig. 6 The addition of NaCl to PLA decreases mechanical property sensitivity to print raster orientation.

well as the increase in tensile strength for the PLA/jute plant fiber composite is also a finding that merits further study. Future work will include subjecting samples to biodegradability testing following ASTM D6954, a standard for assessing the biodegradability of polymers.

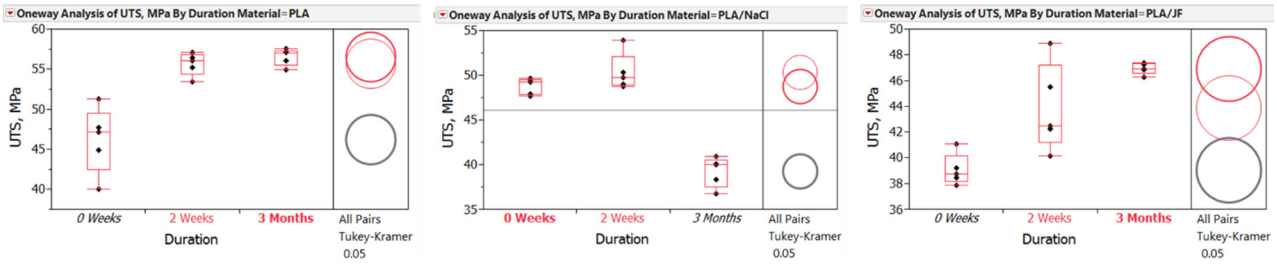

Figure 7. The effect of moist soil exposure to PLA, PLA/jute fiber composite and PLA/NaCl composites.

Conclusions

Tailoring the physical properties of the biopolymer, PLA is possible through the addition of sustainable additives. Here, when melt compounding was used to combine PLA with jute plant fiber, organo nanoclay pigments, and NaCl a discernable difference in physical properties was observed as compared to PLA alone. Explored in greatest detail was the effect of the addition of NaCl to PLA. Fractography of tensile test fracture surfaces revealed NaCl to adhere well to the PLA matrix as there was no evidence of particle pull out. The robustness of the bond between NaCl and PLA was also displayed by evidence of crack front propagation shared between the NaCl particle and the surrounding matrix. Further exploration of the benefit of combining PLA with NaCl was observed through the functionalization of jute plant fiber with aqueous NaCl. The use of palygorskite-based organonanoclay pigments also shows potential in playing a role in future PLA based 3D printable material systems. Several aspects of this work bear the need for future study such as the increase in strength observed after exposing PLA and PLA/jute plant fiber composites to a moist soil environment for durations of two and twelve weeks.

Acknowledgments

The work presented here was carried out in the W.M. Keck Center for 3D Innovation and the Department of Metallurgical and Materials Engineering, both at The University of Texas at El Paso (UTEP). The authors are grateful for funding provided through the AFOSR YIP program under grant number FA9550-14-1-0260 and the UTEP Campus Office of Undergraduate Research Initiatives (COURI).

References

[1] B. Stephens, P. Azimi, Z. El Orch, and T. Ramos, “Ultrafine particle emissions from desktop 3D printers,” *Atmospheric Environment*, vol. 79, pp. 334–339, Nov. 2013.

[2] K.-L. G. Ho, A. L. Pometto, A. Gadea-Rivas, J. A. Briceño, and A. Rojas, “Degradation of Polylactic Acid (PLA) Plastic in Costa Rican Soil and Iowa State University Compost Rows,” *Journal of Polymers and the Environment*, vol. 7, no. 4, pp. 173–177, 1999.

[3] E. T. H. Vink, K. R. Rábago, D. A. Glassner, and P. R. Gruber, “Applications of life cycle assessment to NatureWorks™ polylactide (PLA) production,” *Polymer Degradation and*

Stability, vol. 80, no. 3, pp. 403–419, 2003.
[4] J. Kaiser, "The Dirt on Ocean Garbage Patches," *Science*, vol. 328, no. 5985, pp. 1506–1506, Jun. 2010.
[5] S. Morét-Ferguson, K. L. Law, G. Proskurowski, E. K. Murphy, E. E. Peacock, and C. M. Reddy, "The size, mass, and composition of plastic debris in the western North Atlantic Ocean," *Marine Pollution Bulletin*, vol. 60, no. 10, pp. 1873–1878, Oct. 2010.
[6] S. L. Dautel, "Transoceanic Trash: International and United States Strategies for the Great Pacific Garbage Patch," *Golden Gate U. Envtl. L.J.*, vol. 3, p. 181, 2010 2009.
[7] David Roberson, Corey M Shemelya, Eric MacDonald, and Ryan Wicker, "Expanding the applicability of FDM-type technologies through materials development," *Rapid Prototyping Journal*, vol. 21, no. 2, pp. 137–143, Mar. 2015.
[8] C. M. Shemelya, A. Rivera, A. T. Perez, C. Rocha, M. Liang, X. Yu, C. Kief, D. Alexander, J. Stegeman, H. Xin, R. B. Wicker, E. MacDonald, and D. A. Roberson, "Mechanical, Electromagnetic, and X-ray Shielding Characterization of a 3D Printable Tungsten–Polycarbonate Polymer Matrix Composite for Space-Based Applications," *Journal of Elec Materi*, pp. 1–10, Mar. 2015.
[9] S. H. Masood and W. Q. Song, "Development of new metal/polymer materials for rapid tooling using Fused deposition modelling," *Materials & Design*, vol. 25, no. 7, pp. 587–594, Oct. 2004.
[10] S. K. Acharya and S. C. Mishra, "Weathering Behavior of Fly-ash Jute Polymer Composite," *Journal of Reinforced Plastics and Composites*, Jun. 2007.
[11] T.-T.-L. Doan, S.-L. Gao, and E. Mäder, "Jute/polypropylene composites I. Effect of matrix modification," *Composites Science and Technology*, vol. 66, no. 7–8, pp. 952–963, Jun. 2006.
[12] M. A. Khan, N. Haque, A. Al-Kafi, M. N. Alam, and M. Z. Abedin, "Jute Reinforced Polymer Composite by Gamma Radiation: Effect of Surface Treatment with UV Radiation," *Polymer-Plastics Technology and Engineering*, vol. 45, no. 5, pp. 607–613, Jun. 2006.
[13] D. Plackett, T. Løgstrup Andersen, W. Batsberg Pedersen, and L. Nielsen, "Biodegradable composites based on l-polylactide and jute fibres," *Composites Science and Technology*, vol. 63, no. 9, pp. 1287–1296, Jul. 2003.
[14] L. A. Niewold and A. R. Caro, 2009, *High strength polymer compositions containing hybrid organic/inorganic pigments*. U.S. Patent application No. US20110200772 A1.
[15] A. R. Torrado Perez, D. A. Roberson, and R. B. Wicker, "Fracture Surface Analysis of 3D-Printed Tensile Specimens of Novel ABS-Based Materials," *J Fail. Anal. and Preven.*, vol. 14, no. 3, pp. 343–353, Jun. 2014.
[16] Angel R. Torrado Perez, Defeating Anisotropy in Material Extrusion 3D Printing via Materials Development, Ph.D. Dissertation, The University of Texas at El Paso, 2015.
[17] A. R. Torrado, C. M. Shemelya, J. D. English, Y. Lin, R. B. Wicker, and D. A. Roberson, "Characterizing the effect of additives to ABS on the mechanical property anisotropy of specimens fabricated by material extrusion 3D printing," *Additive Manufacturing*, vol. 6, pp. 16–29, Apr. 2015.

CURRICULUM VITAE

Carmen Raquel Rocha Gutierrez was born in March 18th 1988. The youngest daughter of Edmundo Rocha and Beatriz Gutierrez. Carmen Raquel Rocha Gutierrez earned a bachelor's degree (B.S.) in Chemistry from Universidad Autonoma de Chihuahua in 2011. After the encouragement and support of her beloved father and the previous great experience of her oldest sister as a graduate student in UTEP. Dr. Rocha decided to continue her studies and moved to El Paso Texas to pursue her master and doctoral degrees in Materials Science and Engineering at The University of Texas at El Paso (UTEP). Throughout her time at UTEP, Dr. Rocha participated in different research fields. During her master's degree she worked in conjunction with the University of Guam and National Geographic to analyze strata of an abandoned underwater cave. This work was published in the Quaternary International Journal. Also, Dr. Rocha's work appears in a chapter of the book "Underwater Caves". In addition, Dr. Rocha worked as a Teacher Assistant for the Chemistry department under the supervision of Dr. Bonnie Gunn in the Fall/ Spring 2013.

After incorporating to Dr. Roberson's team Carmen specialized in the development and improvement of materials for material extrusion 3D printing and participated in the 25th annual Solid Freeform Fabrication Symposium in 2014. She is the lead author of one publication in the topic and coauthor other publications and contributions to the polymers' lab.

During her PhD program Dr. Rocha worked as a Teacher and a Research Assistant for the department of Material Science and Engineering under the supervision of Dr. David A. Roberson, who also supervised her dissertation entitled, "Improving the Engineering properties of PLA for 3D printing and beyond".

Selected Publications:

Rocha, Carmen, John A. Peterson, Andrea Jalandoni, Russel R. Chianelli, and Lin Ma. 2016. “Paleoenvironmental Investigations, Chemical Analysis and Characterization of Underwater Strata of Marigondon Cave.” Quaternary International. Accessed April 11. doi:10.1016/j.quaint.2014.04.005.

Ramos, Manuel, Luis Ortiz-Jordan, Abel Hurtado-Macias, Sergio Flores, José T. Elizalde-Galindo, **Carmen Rocha**, Brenda Torres, Maryam Zarei-Chaleshtori, and Russell R. Chianelli. "Hardness and elastic modulus on six-fold symmetry gold nanoparticles." Materials 6, no. 1 (2013): 198-205.

Peterson, John A., Andrea Jalandoni, and **Carmen Rocha.** 2014. An archaeological survey of an underwater cave in Marigondon, Philippines. The Archaeology of Underwater Caves. Ed. Peter Campbell. Oxbow Books. (In Publication)

Rocha, C. **R.**, Torrado, A. R**.**, Roberson, D. A., Shemelya, C. M., MacDonald, E, Wicker, R. B. (2014) Novel ABS-based binary and ternary polymer blends for material extrusion 3D printing. Journal of Materials Research, 29(17) 1859-1866.

Shemelya, C. M., Rivera, A., Torrado, A. R., **Rocha, C.**, Liang, M., Yu, X., Kief, C., Alexander, D., Stegeman, J., Xin, H., Wicker, R. B., MacDonald, E., Roberson, D. A., (2015). Mechanical, Electromagnetic, and X-Ray Shielding Characterization of a 3D Printable Tungsten/Polycarbonate Polymer Matrix Composite for Space Based Applications. Journal of Electronic Materials, (Accepted)

Roberson, D.A., **Rocha, C.R**. and Piñon, M., Evaluation of 3D Printable Sustainable Composites. 2015. (Conference paper)

Permanent address:

Bahía de Topolobampo #8914. Colonia Bahías Residencial

Chihuahua, Chih. Mexico

crrocha2@miners.utep.edu / carmenrochag@gmail.com

This dissertation was typed by Carmen Rocha Gutierrez.